CHANNEL-QUALITY-DRIVEN HIGH-PERFORMANCE RECEIVERS FOR NEXT GENERATION WIRELESS COMMUNICATION SYSTEMS

A Dissertation
Presented to
The Academic Faculty

By

Yiming Kong

In Partial Fulfillment
of the Requirements for the Degree
Doctor of Philosophy in the
School of Electrical and Computer Engineering

Georgia Institute of Technology

December 2019

Copyright © Yiming Kong 2019

CHANNEL-QUALITY-DRIVEN HIGH-PERFORMANCE RECEIVERS FOR NEXT GENERATION WIRELESS COMMUNICATION SYSTEMS

Approved by:

Dr. Xiaoli Ma, Advisor
School of Electrical and Computer Engineering
Georgia Institute of Technology

Dr. Gee-Kung Chang
School of Electrical and Computer Engineering
Georgia Institute of Technology

Dr. John R. Barry
School of Electrical and Computer Engineering
Georgia Institute of Technology

Dr. Mary Ann Weitnauer
School of Electrical and Computer Engineering
Georgia Institute of Technology

Dr. Ellen W. Zegura
School of Computer Science
Georgia Institute of Technology

Date Approved: August 9, 2019

To my family,

my teachers, and

those who might find it helpful.

ACKNOWLEDGEMENTS

I would like to express my deepest gratitude to my advisor, Prof. Xiaoli Ma, for her continuous support, guidance, and encouragement during my Ph.D. study. Her dedication to interesting and challenging scientific problems, rigorous pursuit to high-quality research, and generously shared wisdom about work as well as life have been and will continue to be my source of inspiration and strength. I also would like to sincerely thank my supervisor Dr. Hui Zang at FutureWei Technologies. She has taught me many invaluable things, from the importance of receiving and giving critical feedback, how to effectively conduct industry-driven research, to the art of leadership in professional careers and in life.

Next, I would like to sincerely thank my committee members, Prof. Gee-Kung Chang, Prof. John R. Barry, Prof. Mary Ann Weitnauer, and Prof. Ellen W. Zegura for serving on my committee and providing many insightful comments and feedback that greatly improved the quality of this work. I am also grateful for the financial support from Prof. Gee-Kung Chang during Summer 2018 and Prof. Chin-Hui Lee during Fall 2017.

Third, I would like to thank my colleagues/collaborators at Georgia Tech: Dr. Yiyin Wang, Dr. Jihua Lu, Dr. Qi Zhou, Dr. Zhenhua Yu, Dr. Malik M. U. Gul, Dr. Marie Shinotsuka, Dr. Kai Ying, Dr. Andrew Harper, Dr. Brian Beck, Dr. Qingsong Wen, Dr. Hyunwoo Cho, Dr. Li'an Li, Rongxin Zhang, Lei Yan, Muhammad S Omar, Chao-Han Yang, Yahya M. Alfadhli, Qi Zhou, Dr. You-Wei Chen, Shuyi Shen, for many helpful discussions and friendly support. For the same reason, I would like to thank my colleagues at FutureWei Technologies. I would also like to thank my friends: Dr. Taoran Le, Jacques Florence, Dr. Daniela Staiculescu, Prakriti Kaini, Dr. Patricia Yang, Sam Li, Shi-Rong Chang, Dr. Christine Taylor, Christine Zhao, and many more, who made this journey much more joyful. Special thanks to Yikuai Wang and You Li, for *always* having my back.

Lastly, I would like to thank my family. Specially, I would like to thank my parents, for their support and trust in me throughout the years, and for their *wonderful* love.

TABLE OF CONTENTS

LIST OF TABLES

LIST OF FIGURES

LIST OF SYMBOLS

$\mathcal{S}^n$ n-ary Cartesian power of a set $\mathcal{S}$.

$|\cdot|$ the magnitude of a number, or the cardinality of a set, depending on the context.

$\mathcal{S}_z$ the alphabet set in lattice-reduced domain.

$\leftarrow$ the assignment operator.

$\mathcal{O}(\cdot)$ Big-O notation.

$\mathbb{C}$ complex field.

$\mathcal{N}_c(a, b)$ a complex normal distribution with parameters a and b.

$CP(\cdot)$ the column pair of a vector.

δ_c the parameter of the CLLL algorithm.

$\det(\cdot)$ determinant of a matrix.

$\mathcal{H}(\cdot)$ entropy of a random variable.

$E(\cdot)$ expectation.

$\lceil \cdot \rfloor$ the round operator.

$\|\cdot\|_F$ Frobenius norm of a matrix.

$GL_n(\mathbb{Z}_j)$ the group of $n \times n$ unimodular matrices.

$\mathbb{I}(\cdot)$ the imaginary part of a number.

$\otimes$ Kronecker product.

$\| \cdot \|$ l_2-norm of a vector.

$\mathcal{L}$ a point lattice.

$(\cdot)^*$ conjugation.

$H_{m,n}$ element of matrix $\boldsymbol{H}$ at the m-th row and n-th column.

$(\cdot)^H$ Hermitian transpose of a matrix.

$(\cdot)^{-1}$ inverse of a matrix.

$(\cdot)^\dagger$ Moore-Penrose pseudoinverse of a matrix.

$(\cdot)^T$ transpose of a matrix.

$\boldsymbol{H}$ a matrix.

$\mathcal{I}(X;Y)$ mutual information between random variable X and random variable Y.

N_u number of users in the MU MIMO downlink.

L_p the packet length at the media access control layer.

$P(\cdot)$ the probability of event $(\cdot)$, with subscripts under P to denote the system configuration sometimes.

$Q(x) = (2\pi)^{-1/2} \int_x^\infty \exp(-t^2/2)dt$.

$\mathcal{Q}(\cdot)$ quantization.

$\mathbb{R}(\cdot)$ the real part of a number.

ρ_r receive correlation coefficient.

ρ_t transmit correlation coefficient.

$SA(\cdot)$ Seysen metric of a matrix.

$tr(\cdot)$ trace of a matrix.

$vec(\cdot)$ returns an $mn \times 1$ column vector whose elements are taken column-wise from matrix $(\cdot)$ of size $m \times n$.

$\boldsymbol{I}_k$ an identity matrix of size $k \times k$.

N_r number of receive antennas.

N_t number of transmit antennas.

$\mathcal{S}$ alphabet set.

$\mathbb{Z}_j$ Gaussian integer set.

$\boldsymbol{y}$ column vector.

LIST OF ABBREVIATIONS

ccdf complementary cumulative distribution function.

od orthogonality deficiency.

pdf probability density function.

ACK acknowledgment.

ARQ automatic repeat request.

AWGN additive white Gaussian noise.

BD block diagonalization.

BER bit error rate.

BIC Bayesian information criteria.

BPSK binary phase shift keying.

BS base station.

CA channel assisted.

CC channel controlled.

CLLL complex Lenstra–Lenstra–Lovász algorithm.

CRC cyclic redundancy check.

CSI channel state information.

DCLLL dual complex Lenstra–Lenstra–Lovász algorithm.

DoF degrees of freedom.

DPC dirty-paper coding.

DSP digital signal processing.

E2 exploration and exploitation.

ELR element-based lattice reduction.

FEC forward error correction.

GKw generalized Kumaraswamy distribution.

GOF goodness-of-fit.

GZI generalized zero forcing channel inversion.

HARQ hybrid automatic retransmission request.

IID independent and identically distributed.

LAS likelihood ascent search.

LD linear detector.

LE linear equalization.

LLL Lenstra–Lenstra–Lovász algorithm.

LogL log likelihood.

LoS line-of-sight.

LR lattice reduction.

MAC media access control.

MCMC Markov chain Monte Carlo.

MDP Markov decision process.

MIMO multi-input and multi-output.

MLD maximum likelihood detector.

MLE maximum likelihood equalizer.

MMSE minimum mean-squared error.

mmWave millimeter wave.

MSE mean-squared error.

MU multiuser.

MUI multiuser interference.

NACK negative acknowledgment.

OFDM orthogonal frequency division multiplexing.

PELR pairwise element-based lattice reduction.

PER packet error rate.

PHY physical.

PQR pairwise QR.

QAM quadrature amplitude modulation.

QRD QR decomposition.

RBD regularized block diagonalization.

RL reinforcement learning.

RSS residual sum of squares.

RTS reactive tabu search.

RV random variable.

SA Seysen's algorithms.

SD sphere decoding.

SDMA space division multiple access.

SDP semidefinite programming.

SIC successive interference cancellation.

SISO single-input single-output.

SM spatial multiplexing.

SMMSE successive minimum mean-squared error.

SNR signal-to-noise ratio.

STC space-time coding.

STCM space-time coded multiplexing.

THP Tomlinson-Harashima precoding.

TS tree search.

UE user equipment.

URLLC ultra-reliable low-latency communications.

VP vector perturbation.

w.r.t. with respect to.

ZF zero-forcing.

ZFE zero-forcing equalizer.

SUMMARY

The ever-growing wireless and mobile traffic constantly pushes wireless communication systems for higher data rate and better spectral efficiency. One of the key technologies to meet such demand is the multi-input multi-output (MIMO) technique. By allowing independent data streams to be transmitted and received simultaneously among multiple antennas, MIMO scales up the system capacity by the minimum of the number of transmit and receive antennas at high signal-to-noise ratio (SNR). It has been a major component in the latest wireless communication standards, such as 3GPP LTE-Advanced and 802.11ac, where MIMO systems are supported with up to eight spatial streams. With a new wave of data-rate-hungry mobile applications (e.g., high definition video streaming, virtual and augmented reality) coming, the next generation wireless communication systems are faced with even higher demand on spectral efficiency. Large MIMO has been proposed, where tens or hundreds of antennas are equipped at either or both ends of the communication link. In such cases, it becomes critical to design high-performance receivers with affordable complexity. Other than spectral efficiency, new applications such as autonomous driving and remote surgery also have stringent reliability and latency constraint. For these use cases, latency reduction and reliability improvement on existing systems are needed.

In practice, linear or successive interference cancellation (SIC) detection is often employed at the receiver in MIMO systems for its affordable complexity. However, due to their sensitivity to ill-conditioned MIMO channels, the performance of linear and SIC detectors is often far from optimal. Recent research has investigated the effect of channel quality on detection performance, and various techniques are proposed that improve channel quality before detection. The objective of this thesis is to further explore the relations between channel quality and detection performance, develop efficient high-performance detectors by improving channel quality for various large MIMO systems, and design low-latency high-reliability transmission schemes for MIMO systems.

Large MIMO systems can often be categorized into two types. Type-I large MIMO refers to the case where large number of antennas exists at both sides of the communication link. For Type-I large MIMO, several lattice reduction (LR) algorithms have been proposed to enhance channel quality and provide near-optimum bit error rate (BER) for linear and SIC detectors. In this thesis, we first study the maximum information rate of MIMO transmission with LR aided equalization. As antenna correlation becomes prominent when MIMO size grows, we also investigate the effect of spatial correlation on the complexity of LR algorithms.

Next, we apply LR techniques to improve the performance of the multiuser (MU) MIMO system. At an MU MIMO uplink where each user equipment (UE) employs Alamouti code, the MU MIMO channel possesses specific structure that has not been fully exploited by existing detectors. We develop LR aided detectors that utilize the special properties of the channel and strike a better performance-complexity-tradeoff among comparisons. For an MU MIMO downlink where each UE has multiple antennas and receives spatially multiplexed data streams, we present an LR aided linear joint transceiver design that minimizes the sum of mean-squared error. It is worth mentioning that the proposed schemes for MU MIMO work in both current and large MIMO.

LR algorithms successfully improve channel quality and performance of linear and SIC detectors, but have two problems. First, most LR algorithms are mechanism-driven and it is sometimes hard to link the quality of reductions to the performance of the MIMO systems. Second, the design of LR is detached from the channel distribution. Existing LR algorithms cannot learn from the channels they have operated on, which might limit their performance. Utilizing techniques from reinforcement learning (RL), we design RL-based LR algorithms that learn to efficiently reduce channel matrices according to pre-defined objectives. Preliminary results show that RL-based LR algorithms are more adaptive, and perform comparably to state-of-the-art LR-aided detectors with less DSP complexity.

For Type-II large MIMO (or massive MIMO), the number of antennas at one side of the

link is much greater than that at the other side. This is expected to result in better channel condition (e.g., asymptotic orthogonality between channel responses for individual terminals), which enables linear detectors (LDs) to achieve close-to-optimal performance. But in reality, two facts affect the orthogonality of massive MIMO channel. First, practical massive MIMO systems have limited numbers of antennas. Second, the behavior of the propagation channel highly depends on the frequency of electromagnetic waves. Therefore, we quantify the impact of limited number of antennas and propagation conditions on channel quality and the performance of LDs. By studying the orthogonality deficiency of the MIMO channel using an independent and identically distributed Weibull fading model, we show that if the number of receive antennas exceeds a certain number while the number of transmit antennas is fixed, the channel is in "good" quality for LDs to collect the same diversity as that of the optimal detector with high probability in practice.

Other than spectral efficiency, future wireless applications may also demand high reliability and low latency. Automatic repeat request (ARQ) has been shown to be a key technique to meet the reliability constraint but often at the cost of latency. Targeting MIMO systems with linear detection at the receiver, we propose channel assisted (CA) strategies for the ARQ process. The retransmission of a data frame is requested as soon as the receiver decides the estimated channel is "bad". By skipping detection and demodulation of data frames during "bad" channels, the receiver is able to improve its performance with reduced latency and complexity. From simulations, the proposed CA strategies dramatically decrease the latency for basic and Type-I hybrid ARQ processes at low to moderate SNR levels, while improving the reliability at high SNR regime.

CHAPTER 1
INTRODUCTION

1.1 Motivation and state-of-the-art

The great advantage of multi-input and multi-output (MIMO) over single-input single-output (SISO) transmission in channel capacity has been well established in the pioneering work such as [1, 2, 3, 4]. At high signal-to-noise ratio (SNR), MIMO technology can scale up the system capacity by the minimum of the number of transmit and receive antennas. To reap the theoretical capacity gain, extensive work has been done on space-time coding (STC) for MIMO systems (see e.g., [5, 6]), leading to a number of influential architectures such as V-BLAST [7] and the Alamouti STC [8]. They are now key components for modern wireless systems. For example, 3GPP LTE-Advanced supports up to eight layers spatial multiplexing in the downlink, and transmit diversity based on space-frequency block coding (i.e., Alamouti scheme in the space-frequency domain) [9].

With a new wave of data-rate-hungry applications (e.g., high definition video streaming, virtual and augmented reality) coming, next generation wireless communication systems are faced with even higher demand on data rate. Therefore, large MIMO has been proposed, where tens or hundreds of antennas are equipped at either or both ends of the communication link (see e.g., [10, 11, 12]). The drastic increase of antennas promises extra degrees of freedom (DoF) and energy efficiency, but also calls for efficient high performance receivers. Other than data rate, new applications such as autonomous driving and remote surgery have stringent reliability and latency constraints. For these use cases, latency reduction and reliability improvement on existing systems are desired. In the following, we will review the state-of-the-art in our problem scope.

1.1.1 Detection schemes for MIMO systems

Large MIMO systems can often be categorized into two types. Type-I large MIMO refers to the case where similar large number of antennas are equipped at both ends of the communication link [12, 13]. Type-II large MIMO, or massive MIMO, is where one side of the communication link has significantly larger number of antennas than the other. In [14], a theoretical study of the capacity lower bounds of massive MIMO is carried out with linear precoding and detection, where the imperfect channel estimation, pilot contamination, and inter-cell interference are taken into account. A real-time massive MIMO testbed with 100 base station (BS) antennas is presented in [15], and its capability to simultaneously serve up to 12 user equipments (UEs) in static indoor and outdoor scenarios is demonstrated.

Detection schemes for Type-I large MIMO systems

The detectors for MIMO system determine a vector of information symbols sent over a MIMO communication channel. As an NP-hard problem, the brute-force maximum likelihood detector (MLD) costs exponential complexity with respect to N_t, and is infeasible at even moderate MIMO size (e.g., $N_t = 10$). At the other end of the complexity spectrum, the linear detectors (LDs), such as matched filter, zero-forcing (ZF) and minimum mean-squared error (MMSE) LDs, achieve polynomial complexity but lose bit error rate (BER) diversity in general. This is due to their sensitivity to ill-conditioned MIMO channels.

Many detectors were proposed to strike a better performance-complexity-tradeoff. Among them, tree search (TS) based detectors receive a lot of attention. Sphere decoding (SD), the well-known depth-first TS detector, achieves near optimal BER with significantly lower complexity than the brute-force MLD [16, 17]. But its average complexity is still exponential for each fixed SNR and it is inefficient for large MIMO or low SNR [18]. To reduce the complexity of SD and achieve a fixed throughput, the width-first TS K-best detector [19] keeps k best candidates at each layer, and performs close to SD when k is large. The successive interference cancellation (SIC) detector [7], where symbols are successively de-

tected and canceled out from the received signal vector, can be viewed as a special case of K-best detector when $k = 1$. K-best detectors work in large MIMO since their complexity can be adjusted by varying k.

Recently, several classes of detectors are proposed for Type-I large MIMO. One class is based on local neighborhood search, where the detector iteratively updates a candidate solution by searching its neighbors [20, 21, 22]. In likelihood ascent search (LAS) [20], a candidate solution is updated by its neighbor that increases a likelihood function. Reactive tabu search (RTS) explores beyond local optima by allowing "worse" moves, and prevents cycling by making past moves as "tabu" for a (dynamically adjusted) period [21]. Although obtaining near optimal performance with binary phase shift keying (BPSK) and lower-order quadrature amplitude modulation (QAM), LAS and RTS perform poorly at higher-order QAM. Layered tabu search improves BER for higher-order QAM, but suffers higher complexity [22].

Another class of detectors is based on Bayesian inference [23, 24, 12]. The probability data association based detector models noise-plus-interference as Gaussian, and performs better with increasing MIMO dimension [23]. Belief propagation based detectors on factor graphs and Markov random fields are reported in [24, 12]. However, their performance also degrades at higher-order QAM. Interestingly, MIMO detection can also be solved with Markov chain Monte Carlo (MCMC) methods by sampling the distribution of interests. In [25], the stalling problem of conventional MCMC is handled by using randomized sampling probabilistically. To improve BER at high-order QAM, a multiple restart strategy is introduced in [26] to trade performance with complexity. With a relaxation of its problem setup, MIMO detection can be solved with semidefinite programming (SDP) [27]. The SDP relaxation based detectors ensure polynomial-worst-case complexity and collect full receive diversity with BPSK, but their design often depends on the specific constellation, and their performance degrades at higher-order QAM.

In short, the previously mentioned classes of detectors for Type-I large MIMO share

some problems: 1) detection performance degrades and/or complexity increases with the constellation size; 2) the detection process is carried out per signal vector, regardless of whether the channel is static or not; and 3) theoretical bounds such as diversity of these detectors are generally difficult to analyze, which hinders their applications in real-world.

The lattice reduction (LR) aided detectors form another important class of MIMO detectors. Inspired by the link between channel condition and linear and SIC detection performance, they set to find a reduced channel matrix of better quality through unimodular transformation. The signal detection is then performed with respect to (w.r.t.) the reduced channel and unimodular-transformed back. Various definitions of "better" lead to numerous LR algorithms, including the Seysen's algorithms (SA) [28, 29] and Lenstra–Lenstra–Lovász algorithm (LLL) [30]. The LLL and complex Lenstra–Lenstra–Lovász algorithm (CLLL) based detectors [31, 32, 33, 34] are often preferred due to the available theoretical performance bounds and average-case polynomial complexity [35, 36]. In [32, 33], CLLL aided detectors are shown to collect full receive diversity. VLSI implementations of LR algorithms further demonstrate their practicality [37, 38, 39]. To speed up the convergence of CLLL and improve its applicability in large MIMO, Wen et al. developed an efficient greedy CLLL in [40], which achieves full receive diversity and state-of-the-art performance with much lower complexity. For efficient hardware implementation, fixed-complexity CLLL is proposed in [41, 42] that explores a better column traversal strategy and termination criterion, and has significant complexity advantage in large MIMO. Targeting the direct reduction of BER for LDs, Zhou et al. proposed an element-based lattice reduction (ELR) algorithm in [43], which shows superior BER with very low complexity.

Two attractive properties of LR aided detectors are worth noting: 1) LR is carried out per channel matrix, and its complexity overhead can be very low when the channel is more or less static, and 2) the complexity of LR is independent of the constellation size.

While it is important to evaluate the diversity and complexity of MIMO equalization/detection schemes, the maximum information rate of MIMO transmission when cer-

tain equalizer is employed serves as a useful metric to measure how the receiver utilizes the channel from a theoretical standpoint [44]. Hereupon, we use the phrase "capacity of an equalizer" to denote the maximum mutual information between the transmit and receive signals when a certain equalizer is used. The capacity of zero-forcing equalizer (ZFE) is studied in [44]. In [45], Ma and Zhang showed that the capacity difference between maximum likelihood equalizer (MLE) and ZFE is linked to the orthogonality deficiency (od) of the dual of the channel matrix. Since LR aided equalizers has well established merits in complexity and diversity but unknown capacity, ***the first motivation of this thesis is to investigate the capacity of LR-aided equalizers***.

Detection and precoding schemes for MU MIMO systems

In multiuser (MU) MIMO, a multi-antenna BS serves multiple UEs simultaneously over the same spectrum, and achieves great spectral efficiency at the system level. Nowadays, two- (or multi-) antenna UEs become common. At the uplink, Alamouti space-time code can be applied at the multi-antenna UEs to enable transmit diversity. We term such systems as space-time coded multiplexing (STCM) systems. As the number of active users increases in the STCM system, efficient detectors are needed at the BS.

The existing detectors [46, 47, 48, 49] for STCM systems are often categorized as group-based or direct detection detectors. Group-based detectors use ZF and MMSE criteria to reduce the interference from other STC groups before decoding each STC group (see e.g., [46]). Direct detectors convert the STCM model into the standard form of a MIMO system and use existing MIMO detection schemes such as LD or SIC (see e.g., [47, 48]). Direct detectors usually have a lower BER but higher complexity than group-based detectors [48]. The complexity of direct LDs is reduced by utilizing the symmetric structures of the equivalent channel matrix in [49]. However, linear and SIC detectors perform poorly and lose diversity at high SNR. Directly applying LR aided detectors to the STCM systems without adaptation incurs unnecessary computational cost. An et al. proposed an LR aided

detector for STCM systems in [50], but they investigated when the number of transmit antennas equals four and only optimized the LR algorithm instead of the full detector. Thus, ***the second motivation of this thesis is to design LR aided detectors for STCM systems to strike a better tradeoff between BER and complexity at large MIMO by utilizing the specific properties of the equivalent channel***.

At the downlink of MU MIMO space division multiple access (SDMA) systems, to combat multiuser interference (MUI), exploit channel state information (CSI), and optimize system performance, the BS often uses precoding. The non-linear dirty-paper coding (DPC) [51] achieves sum-rate capacity, but is computationally prohibited. A suboptimal structure of DPC is the Tomlinson-Harashima precoding (THP) (see e.g., [52]), which employs modulo operation to reduce transmit power. Another non-linear precoding scheme that achieves near-capacity is vector perturbation (VP) [53, 54], where the signal at the transmitter is perturbed by a vector to minimize transmit power and MUI. However, the complexity of the non-linear methods can still be too high for large MU MIMO with multi-antenna UEs. Linear precoding is favorable in terms of computational complexity, but the optimum linear transceiver is difficult to obtain directly. Joint iterative algorithms are developed (e.g. based on the mean-squared error (MSE) criterion [55, 56, 57, 58]), but they can take long to converge and incur high complexity when multi-antenna UEs receive multiple data streams from the BS. Another approach is to solve the problem sub-optimally with two steps. First, a preprocessing method is used to mitigate MUI (and noise) [59, 60, 61, 62, 63, 64]. Second, the system is optimized based on certain criteria, such as mutual information rate, maximum SNR, and minimum sum of the MSEs [65]. Examples of the stepwise designs include [66, 67, 68]. LR algorithm has been used to reduce MSE for single user MIMO [65]. ***The third motivation is to develop an LR aided transceiver architecture with the goal of minimizing sum of the MSEs of the MU MIMO downlink, using the two-step process***.

Machine learning techniques for MIMO systems

LR algorithms improve channel quality and thus performance of linear detection, but have two problems. First, LR algorithms are mechanism-driven, and in many cases it is hard to link the quality of reductions to the performance of the MIMO systems. Second, the design of LR is detached from the channel distribution. Existing LR algorithms do not have the ability to learn from the channels they have seen, which might limit their performance. Recently, machine learning techniques have been applied to solve problems in MIMO systems [69, 70, 71, 72, 73, 74, 75, 76]. Reinforcement learning (RL) has been used for link adaptation in MIMO orthogonal frequency division multiplexing (OFDM) system in [77], and adaptive transmission in underwater acoustic channels in [78]. Noticing the similarities between an RL agent and LR, ***the fourth motivation of the thesis is to design RL-based LR algorithms that learn to optimize pre-defined objectives through trail-and-error interactions with the channel environment***.

Detection schemes for Type-II large MIMO (or massive MIMO) systems

The Type-II large MIMO, or massive MIMO, refers to the situation where the number of antennas at BS is much greater than the users. Massive MIMO is attractive for its dramatically increased capacity and energy efficiency and the asymptotically optimal performance of linear detection under favorable propagation environment [10, 11]. But in reality, two facts may invalid the assumption of favorable propagation and thus the optimality of the LD. First, practical massive MIMO systems have limited numbers of antennas. Second, the behavior of the propagation channel highly depends on the frequency of electromagnetic waves. Massive MIMO has been considered for both sub-6 GHz and millimeter wave (mmWave) technologies, whose basic transmission properties (e.g., diffraction and attenuation) are quite different from each other. Therefore, ***the fifth motivation is to quantify the impact of limited number of antennas and propagation conditions on the orthogonality of massive MIMO channel, and thus on the performance of LDs***.

1.1.2 Techniques for low-latency high-reliability communications

Future applications such as autonomous driving and remote surgery not only demand high data rate but also have stringent reliability and latency constraints. To support high-reliability low-latency communications, where short- and medium-size packets dominate the traffic, next generation wireless system demands re-visit of information theory for short- and medium-size packet transmissions and protocol designs that factor the overhead of metadata [79]. For existing systems, high-reliability low-latency communications require reliability improvement and latency reduction at all layers [80]. At the media access control (MAC) and physical (PHY) layers, automatic repeat request (ARQ) techniques are critical in satisfying the reliability constraints without sacrificing the bandwidth efficiency [81, 82, 83, 84]. For the downlink transmission of ultra-reliable low-latency communications (URLLC) traffic in a frequency-division-duplex based system, Anand et al. demonstrated how Type-I hybrid automatic retransmission request (HARQ) can be used to meet the reliability constraint and maximize URLLC capacity in high-load scenarios in [83].

The higher reliability introduced from ARQ comes at the price of higher latency. Recently, many schemes are proposed to directly reduce latency and complexity of ARQ process. For example, Turbo code has excellent error performance but its decoder processing has major impact on latency. Berardinelli et al. proposed a technique to predict Turbo decoder outcome before decoding happens to generate early HARQ feedback with high accuracy in SISO systems in [85]. For single-input multi-output systems, Makki et al. proposed a fast Type-II HARQ where some feedback signals and successive decoding are omitted based on the link quality in [86]. Based on achievable rates of finite-length codes, closed-form formulas for reliability, latency, and throughput are derived. Significant delay reduction is demonstrated. However, their derivation is based on a quasi-static channel model and information theoretic results on short packets transmission without considering sub-optimal factors in practical systems.

As previously mentioned, practical systems are limited by power consumption and

complexity constraints, and low-complexity LDs are often employed in reality [87]. Taking the usage of ZF LDs into account, Zhang et al. proposed a channel controlled (CC) ARQ scheme for MIMO relay networks in [88]. The CC ARQ scheme relies on channel conditions instead of error detection code to achieve joint cooperative and spatial diversity. But the proposed scheme is not adaptive to noise level and thus compromises throughput at high SNRs. On the other hand, due to the relation between channel quality and packet error performance for LDs, feedback can be returned early to improve latency and complexity. Thus, ***the sixth motivation is to propose channel assisted strategies to reduce latency and complexity for the ARQ process, targeting linear receivers in MIMO systems***.

1.2 Objectives

Now, we summarize the objectives of this dissertation. In this dissertation, we explore the relations between channel quality and detection performance, develop efficient high-performance detectors by improving channel quality for various MIMO systems, and design channel assisted strategies at receivers to reduce the latency/complexity and improve the reliability of the ARQ process. Specifically, we

1. Derive the maximum information rate of MIMO transmission with LR aided equalizers and investigate the effect of spatial correlation on the complexity of LR algorithms through simulations;

2. Design LR aided detectors that fully utilize specific structures of the STCM channel to achieve better tradeoff between BER performance and complexity;

3. Design LR aided linear joint transceiver architecture to minimize sum of MSEs for the MU MIMO downlink;

4. Design RL based LR algorithms that learn to perform reduction to optimize predefined objectives, through trial and error interactions with the environment;

5. Quantify the impact of MIMO size and propagation condition on channel orthogonality and thus the performance of LDs in massive MIMO;

6. Design channel assisted strategies to reduce latency and complexity for basic ARQ and Type-I HARQ process in MIMO systems with linear receivers.

1.3 Outline

The rest of the dissertation is organized as follows:

Chapter 2 introduces the background for MIMO system model, conventional MIMO detectors, channel quality, LR algorithms, LR aided detection, and MU MIMO systems.

Chapter 3 presents results on the maximum information rate (denote as "capacity") with LR-aided equalizers in MIMO systems. We show that the capacity gap between MLE and LR-aided ZFE is linked to the od of the dual of the lattice-reduced channel matrix. We provide the conditions when the ergodic capacity of LR-aided LEs is greater than that of LEs, as well as when their outage diversity is the same as that of MLE. We also study the effect of spatial correlation on the complexity of LR algorithms.

Chapter 4 applies LR techniques to MU MIMO systems. We present pairwise element-based lattice reduction (PELR) aided detectors for the STCM systems. By utilizing the symmetric structure of the equivalent channel matrix, the proposed PELR aided detectors approximately halve the complexity of the original ELR-aided detectors while keeping similar BER performance. They also have lower BER and similar complexity compared to other state-of-the-art detectors. Then, we present a linear joint transceiver design for downlink transmissions of MU MIMO system using lattice reduction algorithms, based on the minimum sum of the MSEs criterion and subject to a per-user power constraint. We compare the error performance and complexity of our proposed design with several existing schemes through simulations and show that our new design performs very well with low complexity especially when each user is equipped with a large number of antennas (e.g., more than three) and receives spatially multiplexed data streams.

Chapter 5 presents RL-based LR-aided detectors for MIMO systems. At the expense of off-line training and storage, the RL-based LR-aided detectors learn the optimal reduction strategies based on pre-defined objectives for various channel models. Preliminary results show that RL-based LR-aided detectors perform comparably to state-of-the-art LR-aided detectors, while offering less digital signal processing (DSP) complexity.

Chapter 6 examines od of massive MIMO channels and its relationship to performance of LDs. The Weibull distribution is adopted for modeling the fading envelopes, and various propagation channels are simulated by varying the Weibull parameters. By proposing an approximate distribution of od, we show that for various propagation channels, if the number of receive antennas exceeds a certain number while the number of transmit antennas is fixed, LDs achieve the same diversity as that of the MLD with high probability in practice.

Chapter 7 proposes channel assisted (CA) strategies at linear receivers to reduce latency for basic ARQ and Type-I HARQ processes. From simulations, the proposed CA strategies greatly decrease the latency for both ARQ processes at low to moderate SNRs, while improve the reliability at high SNR regime.

Chapter 8 summarizes the contributions, provides future research directions, and concludes this dissertation.

CHAPTER 2

BACKGROUND

In this chapter, we review the background for MIMO system model, conventional detection schemes, LR algorithms, LR aided detection, and MU MIMO systems.

2.1 MIMO systems

Consider a spatial multiplexing (SM) MIMO system with N_r receive and N_t transmit antennas. The MIMO channel between the N_r receive and N_t transmit antennas is assumed to be flat-fading and modeled by the matrix $\boldsymbol{H}$, where $H_{m,n}$ represents the random fading coefficient between the m-th receive and n-th transmit antennas. By default, we assume that $N_r \geq N_t$, $\boldsymbol{H}$ has full rank, and that CSI is known at the receiver but unknown at the transmitter. The transmit signal vector is denoted as $\boldsymbol{s}$, where the individual symbol $s_k, k = 1, \cdots, N_t$, is drawn from alphabet set $\mathcal{S} \subset \mathbb{Z}_j$, and $\boldsymbol{R}_s = E(\boldsymbol{s}\boldsymbol{s}^H) = \sigma_s^2 \boldsymbol{I}_{N_t}$. $(\cdot)^H$ denotes Hermitian transpose, $E(\cdot)$ the expectation, and $\boldsymbol{I}_k$ an identity matrix with size $k \times k$. The receive signal vector is expressed as $\boldsymbol{y}$, and the additive white Gaussian noise (AWGN) vector is denoted as $\boldsymbol{w}$, where $E(\boldsymbol{w}\boldsymbol{w}^H) = \sigma_w^2 \boldsymbol{I}_{N_r}$. The system input-output model can be written as

$$\boldsymbol{y} = \boldsymbol{H}\boldsymbol{s} + \boldsymbol{w}. \tag{2.1}$$

Note that, other than multi-antenna systems, various communication systems can be subsumed into model (2.1), such as OFDM systems [89] and single carrier block transmission systems [90].

2.2 Conventional detection schemes for MIMO systems

At the receiver, with CSI and observations of $\boldsymbol{y}$, detectors are adopted to obtain the estimated transmit symbol vector $\hat{\boldsymbol{s}}$. When the transmit symbols are equal probable, the optimal detector is the MLD (sometimes also called MLE). It is defined as

$$\hat{\boldsymbol{s}}_{mld} = \arg \min_{\hat{\boldsymbol{s}} \in \mathcal{S}^{N_t}} \|\boldsymbol{y} - \boldsymbol{H}\hat{\boldsymbol{s}}\|^2, \tag{2.2}$$

where $\mathcal{S}^n$ is the n-ary Cartesian power of the alphabet set $\mathcal{S}$, and $\|\cdot\|$ computes the l_2 norm. The computational complexity of MLD is $\mathcal{O}(|\mathcal{S}|^{N_t})$, where $|\cdot|$ denotes the cardinality of a set and $\mathcal{O}(\cdot)$ is the Big-O notation. Thus, MLD is infeasible for large N_t. A common way to mitigate inter-symbol interference is to apply linear equalization (LE). For example, ZFE completely eliminates inter-symbol interference by applying the pseudo-inverse of the channel matrix to the received signal $\boldsymbol{y}$. The ZF equalized signal becomes

$$\boldsymbol{H}^{\dagger}\boldsymbol{y} = \boldsymbol{s} + \boldsymbol{H}^{\dagger}\boldsymbol{w}, \tag{2.3}$$

where $(\cdot)^{\dagger}$ denotes the Moore-Penrose pseudoinverse. Then, the ZF LD is defined as

$$\hat{\boldsymbol{s}}_{zf} = \mathcal{Q}(\boldsymbol{H}^{\dagger}\boldsymbol{y}), \tag{2.4}$$

where $\mathcal{Q}(\cdot)$ denotes quantization. To handle the noise enhancement of ZF, the MMSE detector applies MMSE LE before quantization, and is defined as

$$\hat{\boldsymbol{s}}_{mmse} = \mathcal{Q}\left(\left(\boldsymbol{H}^H\boldsymbol{H} + \sigma_w^2\boldsymbol{R}_s^{-1}\right)^{-1}\boldsymbol{H}^H\boldsymbol{y}\right), \tag{2.5}$$

where $(\cdot)^{-1}$ denotes matrix inverse. The MMSE detector can be written in the same form as the ZF LD [45]. Thus, we mainly use ZF for our analysis. SIC detectors perform decoding and subtracting consecutively, and thus improve the effective SNR at every decoding stage

and provide better performance than LDs [91]. The ZF SIC detector is defined as

$$\begin{aligned} \boldsymbol{Q}^H\boldsymbol{y} = \boldsymbol{y}' &= \boldsymbol{R}\boldsymbol{s} + \boldsymbol{Q}^H\boldsymbol{w}, \\ \hat{s}_k &= \mathcal{Q}\left(\frac{y'_k - \sum_{l=k+1}^{N_t} R_{k,l}\hat{s}_l}{R_{k,k}}\right), k = N_t, \cdots, 1, \end{aligned} \tag{2.6}$$

where matrix $\boldsymbol{Q}$ and $\boldsymbol{R}$ are from the QR decomposition (QRD) of $\boldsymbol{H}$.

2.2.1 Performance evaluation: error rate, diversity, and capacity

Let $P(\cdot)$ computes the probability of an event and $Q(x)$ denotes the Q-function. Let us consider the pair-wise error probability (PEP) for system (2.1). When MLD is used,

$$P(\boldsymbol{s} \to \boldsymbol{s}'|\boldsymbol{H}) = Q\left(\sqrt{\frac{vec(\boldsymbol{H}^H)^H(\boldsymbol{S}-\boldsymbol{S}')(\boldsymbol{S}-\boldsymbol{S}')^H vec(\boldsymbol{H}^H)}{2\sigma_w^2}}\right), \tag{2.7}$$

where $vec(\cdot)$ returns an $mn \times 1$ column vector whose elements are taken column-wise from matrix $(\cdot)_{m\times n}$, and $\boldsymbol{S} = blockdiag\{\boldsymbol{s}, \boldsymbol{s}, \cdots, \boldsymbol{s}\} \in \mathbb{C}^{N_r N_t \times N_r}$, where $\mathbb{C}$ denotes the complex field. When $\boldsymbol{H}$ contains independent and identically distributed (IID) $\mathcal{N}_c(0,1)$ distributed entries, where $\mathcal{N}_c(a,b)$ denotes a complex normal distribution with parameters a and b, the average PEP satisfies (see [91, p. 79])

$$P(\boldsymbol{s} \to \boldsymbol{s}') \le \left(\frac{\|\boldsymbol{s}-\boldsymbol{s}'\|^2}{4\sigma_w^2}\right)^{-N_r} = \left(\frac{\|\boldsymbol{s}-\boldsymbol{s}'\|^2}{4}\right)^{-N_r}\left(\frac{1}{\sigma_w^2}\right)^{-N_r}. \tag{2.8}$$

Because of its per-symbol quantization, ZF LD effectively decomposes the MIMO channel into N_t sub-channels. As a result, the equivalent system model becomes

$$\boldsymbol{x}_{zf} = \boldsymbol{s} + \boldsymbol{\eta}, \tag{2.9}$$

where $\boldsymbol{\eta}$ is the equivalent noise vector with diagonal covariance matrix $\boldsymbol{R}_{zf}$ defined as

$$(\boldsymbol{R}_{zf})_{k,k} = \left(\sigma_w^2(\boldsymbol{H}^H\boldsymbol{H})^{-1}\right)_{k,k}, \quad k = 1, \cdots, N_t. \tag{2.10}$$

Consider the PEP for the k-th transmit symbol,

$$P(s_k \to s_k'|\boldsymbol{H}) = Q\left(\sqrt{\frac{|s_k - s_k'|^2}{2\sigma_w^2\,(\boldsymbol{R}_{zf})_{k,k}}}\right). \tag{2.11}$$

Thus the detected symbol with the largest $(\boldsymbol{R}_{zf})_{k,k}$ dominates the PEP at high SNR, and reducing the maximum of $\boldsymbol{R}_{zf}$ can decrease PEP. Since $(\boldsymbol{R}_{zf})_{k,k}^{-1}$ is Chi-squared distributed with $2(N_r - N_t + 1)$ DoF, the average PEP at high SNR is (see [92])

$$P(s_k \to s_k') \le \left(\frac{|s_k - s_k'|^2}{4}\right)^{-(N_r-N_t+1)} \left(\frac{1}{\sigma_w^2}\right)^{-(N_r-N_t+1)}. \tag{2.12}$$

Given the SIC detector in (2.6), the PEP of the N_t-th transmit symbol is

$$P(s_{N_t} \to s_{N_t}'|\boldsymbol{H}) = Q\left(\sqrt{\frac{|s_{N_t} - s_{N_t}'|^2 R_{N_t,N_t}^2}{2\sigma_w^2}}\right). \tag{2.13}$$

Because the PEP of the N_t-th symbol bounds the overall PEP, increasing R_{N_t,N_t} can decrease PEP. Since $2R_{N_t,N_t}^2$ is Chi-squared distributed with $2(N_r - N_t + 1)$ DoF, at high SNR, we have (see [91, p. 65] and [93])

$$P(s_{N_t} \to s_{N_t}') \le \left(\frac{|s_{N_t} - s_{N_t}'|^2}{8}\right)^{-(N_r-N_t+1)} \left(\frac{1}{\sigma_w^2}\right)^{-(N_r-N_t+1)}. \tag{2.14}$$

Diversity

As we have seen, when close-form expression is unavailable, error rate is described by their upper bound. Another important parameter of error rate is *diversity*:

Definition 1. *Suppose that $P(\text{error})$ is the average probability of error for a certain system*

as a function of SNR. The diversity *is defined as*

$$G_d = \lim_{SNR \to \infty} -\frac{\log P(error)}{\log(SNR)}. \tag{2.15}$$

Diversity shows how fast error rate decays with SNR. For IID complex Gaussian distributed MIMO channel, it has been proved that the diversity of LD and SIC detector is $N_r - N_t + 1$ [91, 94], and the diversity of MLD is N_r. This can also be observed from Eqs. (2.8), (2.12), (2.14).

Maximum mutual information ("Capacity")

The maximum information rate of MIMO transmission when a certain equalizer is employed shows how the receiver utilizes the channel from a theoretical standpoint [44]. Hereupon, we use the phrase "capacity of an equalizer" to denote the maximum mutual information between the transmit and receive signals when a certain equalizer is adopted. The mutual information rate with MLE at the receiver is computed as (see e.g., [3, 45])

$$\mathcal{I}(\boldsymbol{y}; \boldsymbol{s}|\boldsymbol{H}) = \mathcal{H}(\boldsymbol{y}|\boldsymbol{H}) - \mathcal{H}(\boldsymbol{y}|\boldsymbol{s}; \boldsymbol{H}) = \mathcal{H}(\boldsymbol{y}|\boldsymbol{H}) - \mathcal{H}(\boldsymbol{w}), \tag{2.16}$$

where $\mathcal{I}(X;Y)$ represents the mutual information between two random vectors and $\mathcal{H}(\cdot)$ denotes entropy. Since the noise vector $\boldsymbol{w}$ is Gaussian,

$$\mathcal{H}(\boldsymbol{w}) = \log_2 \det(\pi e \sigma_w^2 \boldsymbol{I}_{N_r}), \tag{2.17}$$

where $\det(\cdot)$ denotes the determinant of a matrix. Maximizing $\mathcal{I}(\boldsymbol{y}; \boldsymbol{s}|\boldsymbol{H})$ is the same as maximizing $\mathcal{H}(\boldsymbol{y}|\boldsymbol{H})$. Since $E(\boldsymbol{y}\boldsymbol{y}^H) = \boldsymbol{H}\boldsymbol{R}_s\boldsymbol{H}^H + \sigma_w^2 \boldsymbol{I}_{N_r}$,

$$\mathcal{H}(\boldsymbol{y}|\boldsymbol{H}) \leq \log_2 \det\left(\pi e \left(\boldsymbol{H}\boldsymbol{R}_s\boldsymbol{H}^H + \sigma_w^2 \boldsymbol{I}_{N_r}\right)\right), \tag{2.18}$$

with equality when $\boldsymbol{s}$ is Gaussian distributed. Therefore, the capacity with MLE at the receiver is:

$$C_{ml}(\boldsymbol{H}) = \log_2 \left(\det \left(\boldsymbol{R}_s \boldsymbol{R}_{ml}^{-1} + \boldsymbol{I}_{N_t} \right) \right), \tag{2.19}$$

where

$$\boldsymbol{R}_{ml} = \sigma_w^2 (\boldsymbol{H}^H \boldsymbol{H})^{-1} \tag{2.20}$$

is the equivalent noise covariance matrix for MLE.

When ZFE is adopted, the equivalent system model is expressed in (2.9). The mutual information between the transmit and receive signals is (see [44, 45])

$$\mathcal{I}(\boldsymbol{x}_{zf}; \boldsymbol{s} | \boldsymbol{H}) \leq \log_2 \frac{\det \left(\pi e \left(\boldsymbol{R}_s + \boldsymbol{R}_{zf} \right) \right)}{\det(\pi e \boldsymbol{R}_{zf})}, \tag{2.21}$$

with equality when $\boldsymbol{s}$ is Gaussian distributed. Thus, the capacity of ZFE is

$$C_{zf}(\boldsymbol{H}) = \log_2 \left(\det \left(\boldsymbol{R}_s \boldsymbol{R}_{zf}^{-1} + \boldsymbol{I}_{N_t} \right) \right). \tag{2.22}$$

At high SNR,

$$\frac{2^{C_{zf}(\boldsymbol{H})}}{2^{C_{ml}(\boldsymbol{H})}} = \frac{\det(\boldsymbol{R}_{ml})}{\det(\boldsymbol{R}_{zf})} = \frac{\det \left((\boldsymbol{H}^H \boldsymbol{H})^{-1} \right)}{\prod_{k=1}^{N_t} \left((\boldsymbol{H}^H \boldsymbol{H})^{-1} \right)_{k,k}} \leq 1, \tag{2.23}$$

which shows the capacity difference between MLE and ZFE depends on how orthogonal $(\boldsymbol{H}^\dagger)^H$ is.

2.3 Channel quality

We have seen the error rate of the ZF and SIC detector being connected to $(\boldsymbol{H}^H \boldsymbol{H})^{-1}$ and R_{N_t,N_t}, and the capacity gap between ZFE and MLE at high SNR being connected to the orthogonality of $(\boldsymbol{H}^\dagger)^H$. Now let us formally introduce two channel qualities that affect detection performance. The first channel quality is od.

Definition 2 (od). *Consider an $N_r \times N_t$ matrix $\boldsymbol{H} = [\boldsymbol{h}_1, \boldsymbol{h}_2, \cdots, \boldsymbol{h}_{N_t}]$ where $\boldsymbol{h}_k$ denotes $\boldsymbol{H}$'s k-th column. We define the od of a channel matrix $\boldsymbol{H}$ as*

$$od(\boldsymbol{H}) = 1 - \frac{\det(\boldsymbol{H}^H \boldsymbol{H})}{\prod_{k=1}^{N_t} \|\boldsymbol{h}_k\|^2}. \tag{2.24}$$

Thus, $od(\boldsymbol{H})$ is a random variable (RV) on the interval $[0, 1]$. The closer it is to 0, the more orthogonal $\boldsymbol{H}$ is. As lemma 1 shows, $od(\boldsymbol{H})$ directly relates to the diversity of LDs.

Lemma 1 ([45, Corollary 1]). *For a random channel distribution, if $od(\boldsymbol{H}) \leq \epsilon$, $\forall \boldsymbol{H}$ and $\epsilon \in [0, 1)$, then LDs collect the same diversity as MLD does.*

Also notice that the capacity gap between MLD and ZFE in (2.23) is a function of od. At high SNR,

$$\frac{2^{C_{zf}(\boldsymbol{H})}}{2^{C_{ml}(\boldsymbol{H})}} = \frac{\det\left((\boldsymbol{H}^H \boldsymbol{H})^{-1}\right)}{\prod_{k=1}^{N_t} \left((\boldsymbol{H}^H \boldsymbol{H})^{-1}\right)_{k,k}} = 1 - od\left((\boldsymbol{H}^\dagger)^H\right) \leq 1. \tag{2.25}$$

The second channel quality we introduce is the maximum equivalent noise variance.

Definition 3. *Given an $N_r \times N_t$ matrix $\boldsymbol{H}$ and noise variance σ_w^2, we define the maximum equivalent noise variance as $\max_k \sigma_w^2 \left((\boldsymbol{H}^H \boldsymbol{H})^{-1}\right)_{k,k}$.*

Looking at PEP of ZF LD in (2.12), reducing the maximum equivalent noise variance improves the performance of LDs.

2.4 LR algorithms and LR aided detectors

Seeing the impact of channel quality on performance of LDs and SIC detectors, it is natural to think of ways to improve channel quality before detection. This is the key idea behind LR algorithms. Due to the discrete nature of the transmit symbols, the channel matrix that acts on the data can be viewed as a (non-unique) basis of a lattice. In other words, the

channel matrix $\boldsymbol{H}$ spans a lattice $\mathcal{L}(\boldsymbol{H})$,

$$\mathcal{L}(\boldsymbol{H}) = \left\{ \sum_{k=1}^{N_t} x_k \boldsymbol{h}_k | x_k \in \mathbb{Z}_j \right\}, \tag{2.26}$$

where $\boldsymbol{h}_k$ is the k-th column vector of channel matrix $\boldsymbol{H} = [\boldsymbol{h}_1, \boldsymbol{h}_2, \cdots, \boldsymbol{h}_{N_t}]$. From lattice theory, we know there are multiple basis that span the same lattice. Thus, an LR algorithm sets out to find a basis $\tilde{\boldsymbol{H}}$ of better quality that spans the same lattice. This indicates that the new and original basis are connected via unimodular transformation $\boldsymbol{T}$, $\tilde{\boldsymbol{H}} = \boldsymbol{H}\boldsymbol{T}$. There are various definitions of "better quality", which leads to various LR algorithms. With LR, the system model (2.1) can be re-written as

$$\boldsymbol{y} = \boldsymbol{H}\boldsymbol{T}\boldsymbol{T}^{-1}\boldsymbol{s} + \boldsymbol{w} = \tilde{\boldsymbol{H}}\boldsymbol{z} + \boldsymbol{w}. \tag{2.27}$$

Because both $\boldsymbol{T}^{-1}$ and $\boldsymbol{s}$ have Gaussian integer entries, $\boldsymbol{z}$ also has Gaussian integers entries. The detection of $\boldsymbol{z}$ is performed using e.g., MLD, LD, and SIC. $\hat{\boldsymbol{z}}$ is then transformed to the original symbol domain, i.e., $\hat{\boldsymbol{s}} = \boldsymbol{T}\hat{\boldsymbol{z}}$. Since $\tilde{\boldsymbol{H}}$ is "better", the error probability when estimating $\boldsymbol{z}$ is generally smaller than that when estimating $\boldsymbol{s}$ directly.

Depending on the criterion of "better", various LR algorithms have been developed, such as Minkowski, Hermite Korkine Zolotareff (HKZ), Gauss [95], LLL [30], CLLL [33], dual complex Lenstra–Lenstra–Lovász algorithm (DCLLL) [96], SA [97, 28, 29], and ELR [43]. Among them, CLLL, SA, ELR are commonly used. An $N_r \times N_t$ complex matrix $\tilde{\boldsymbol{H}}$ is "CLLL reduced" if its QRD $\tilde{\boldsymbol{H}} = \tilde{\boldsymbol{Q}}\tilde{\boldsymbol{R}}$ satisfies the following conditions [33]:

$$|\mathbb{R}(\tilde{R}_{l,k})| \leq \frac{1}{2}|\tilde{R}_{l,l}|, |\mathbb{I}(\tilde{R}_{l,k})| \leq \frac{1}{2}|\tilde{R}_{l,l}|, \forall l < k, \tag{2.28}$$

$$\delta_c |\mathbb{R}(\tilde{R}_{k-1,k-1})|^2 \leq |\tilde{R}_{k,k}|^2 + |\tilde{R}_{k-1,k}|^2, \forall k \in [2, N_t], \tag{2.29}$$

where $\mathbb{R}(\cdot)$ and $\mathbb{I}(\cdot)$ takes the real and imaginary parts of a number, and δ_c is the parameter of the CLLL algorithm, shown in Table 2.1.

Table 2.1: The CLLL algorithm using MATLAB syntax [33, Table I]

Input: $\boldsymbol{H}$, δ_c, **Output:** $\tilde{\boldsymbol{Q}}$, $\tilde{\boldsymbol{R}}$, $\boldsymbol{T}$	
(S1)	$[\tilde{\boldsymbol{Q}}, \tilde{\boldsymbol{R}}] = qr(\boldsymbol{H})$;
(S2)	$m = size(\boldsymbol{H}, 2); \boldsymbol{T} = \boldsymbol{I}_m; k = 2;$
(S2)	**While** $k \leq m$
(S3)	**for** $n = k-1 : -1 : 1$
(S4)	$u = round\left(\frac{\tilde{\boldsymbol{R}}(n,k)}{\tilde{\boldsymbol{R}}(n,n)}\right)$;
(S5)	**If** $u \neq 0$
(S6)	$\tilde{\boldsymbol{R}}(1:n,k) = \tilde{\boldsymbol{R}}(1:n,k) - u\tilde{\boldsymbol{R}}(1:n,n)$;
(S7)	$\boldsymbol{T}(:,k) = \boldsymbol{T}(:,k) - u\boldsymbol{T}(:,n)$;
(S5)	**end**
(S5)	**end**
(S5)	**if** $\delta_c \lvert\tilde{\boldsymbol{R}}(k-1,k-1)\rvert^2 > \lvert\tilde{\boldsymbol{R}}(k,k)\rvert^2 + \lvert\tilde{\boldsymbol{R}}(k-1,k)\rvert^2$
(S6)	swap the $k-1$th and kth columns in $\tilde{\boldsymbol{R}}$ and $\boldsymbol{T}$
(S7)	$\Theta = [\alpha^*, \beta; -\beta, \alpha]$ where $\alpha = \frac{\tilde{\boldsymbol{R}}(k-1,k-1)}{\lVert\tilde{\boldsymbol{R}}(k-1:k,k-1)\rVert}$, and $\beta = \frac{\tilde{\boldsymbol{R}}(k,k-1)}{\lVert\tilde{\boldsymbol{R}}(k-1:k,k-1)\rVert}$
(S8)	$\tilde{\boldsymbol{R}}(k-1:k, k-1:m) = \Theta\tilde{\boldsymbol{R}}(k-1:k, k-1:m)$;
(S9)	$\tilde{\boldsymbol{Q}}(:, k-1:k) = \tilde{\boldsymbol{Q}}(:, k-1:k)\Theta^H$;
(S10)	$k = \max(k-1, 2)$;
(S11)	**else**
(S12)	$k = k+1$;
(S12)	**end**;
(S17)	**end**

Another definition of reduction is "SA reduced". Matrix $\tilde{\boldsymbol{H}}$ is "SA reduced" if the Seysen metric $SA(\cdot)$

$$SA(\tilde{\boldsymbol{H}}) = \sum_{k=1}^{N_t} \|\tilde{\boldsymbol{h}}_k\|^2 \|\tilde{\boldsymbol{\alpha}}_k^T\|^2 \tag{2.30}$$

achieves its minimum [28], where $\tilde{\boldsymbol{\alpha}}_k$ is the k-th row of $\tilde{\boldsymbol{H}}^\dagger$. Other than the above two definitions of reduction, matrix $\tilde{\boldsymbol{H}}$ is "ELR reduced" [43] if the maximum equivalent noise variance $\max_k \tilde{C}_{k,k}$ is minimized, where $\tilde{\boldsymbol{C}} = (\tilde{\boldsymbol{H}}^H \tilde{\boldsymbol{H}})^{-1}$.

But for SA and ELR, it is difficult (if not impossible) to compute the optimally reduced basis. Thus, the corresponding LR algorithm computes a suboptimal basis through a sequence of reductions. In the ELR algorithm, at the l-th step, an unimodular matrix $\boldsymbol{T}_l$ is computed, which represents a translation between two columns in $\tilde{\boldsymbol{H}}$, so that the current largest diagonal element of $\tilde{\boldsymbol{C}}$ is reduced by the largest amount. The ELR algorithm is shown in Table 2.2. $\lceil\cdot\rfloor$ is the round operation and $\leftarrow$ is the assignment operator. Note that,

an LR algorithm not necessarily reduces the channel quality defined in Section 2.3, except for ELR. This motivates us to design learning based LR algorithms in Chapter 5.

Table 2.2: ELR and ELR-SLB algorithms [43, Table I]

Input: $\boldsymbol{H}$, **Output:** $\tilde{\boldsymbol{H}}, \boldsymbol{T}$	
(S1)	$\tilde{\boldsymbol{C}} = \left(\boldsymbol{H}^H \boldsymbol{H}\right)^{-1}, \boldsymbol{T}' = \boldsymbol{I}_{N_t}$
(S2)	**Do**
(S3)	$\lambda_{l,k} \leftarrow -\left\lceil \frac{\tilde{C}_{l,k}}{\tilde{C}_{l,l}} \right\rfloor, \forall l \neq k$
(S4a)	**For the D-ELR-SLV: If** the largest element of $\tilde{\boldsymbol{C}}$ is irreducible, **goto** 11
(S4b)	**For the D-ELR-SLB: If** all $\lambda_{l,k} = 0, \forall l \neq k$, **goto** 11
(S5)	Find the largest reducible $\tilde{C}_{k,k}$
(S6)	Choose $l = \arg\max_{\tilde{l}=1,\tilde{l}\neq k}^{N_t} \Delta_{\tilde{l},k}$
(S7)	$\boldsymbol{t}'_k \leftarrow \boldsymbol{t}'_k + \lambda_{l,k} \boldsymbol{t}'_l$
(S8)	$\tilde{\boldsymbol{c}}_k \leftarrow \tilde{\boldsymbol{c}}_k + \lambda_{l,k} \tilde{\boldsymbol{c}}_l$
(S9)	$\tilde{\boldsymbol{c}}^{(k)} \leftarrow \tilde{\boldsymbol{c}}^{(k)} + \lambda^*_{l,k} \tilde{\boldsymbol{c}}^{(l)}$
(S10)	**While (true)**
(S11)	$\boldsymbol{T} = (\boldsymbol{T}'^{-1})^H, \tilde{\boldsymbol{H}} = \boldsymbol{H}\boldsymbol{T}$

2.5 MU MIMO systems

Now, we introduce two specific setups of the MU MIMO system.

2.5.1 The STCM system

Consider an STCM system of N_r receive and N_t transmit antennas, where $N_r \geq N_t/2$ (see [98]). The channel is narrowband and denoted by an $N_r \times N_t$ matrix $\boldsymbol{B} = [\boldsymbol{b}_1, \boldsymbol{b}_2, \cdots, \boldsymbol{b}_{N_t}]$, where $\boldsymbol{b}_k, k = 1, \cdots, N_t$ are column vectors of size $N_r \times 1$. The entry $B_{m,n}$ in the channel matrix $\boldsymbol{B}$ represents the channel coefficient between the n-th transmit and m-th receive antennas. Without loss of generality, we apply Alamouti space-time code on every two transmit antennas and form $N_t/2$ transmit groups. The transmitted symbols are drawn from alphabet set $\mathcal{S}$. We denote the symbols transmitted in the l-th group at the first interval as s_{2l-1} and s_{2l}, and the symbols transmitted during two intervals in the l-th block as $\boldsymbol{S}_l$,

$l = 1, \cdots, N_t/2$. Then,

$$\boldsymbol{S}_l = \begin{bmatrix} s_{2l-1} & s_{2l}^* \\ s_{2l} & -s_{2l-1}^* \end{bmatrix}, \tag{2.31}$$

where $(\cdot)^*$ denotes conjugate. The signal at the receiver is

$$\boldsymbol{Y} = \boldsymbol{B}\boldsymbol{S} + \boldsymbol{W}, \tag{2.32}$$

where $\boldsymbol{S} = [\boldsymbol{S}_1^T, \cdots, \boldsymbol{S}_{N_t/2}^T]^T$ is of size $N_t \times 2$, $(\cdot)^T$ denotes transpose, $\boldsymbol{W} = [\boldsymbol{w}_1, \boldsymbol{w}_2]$ is the complex AWGN of size $N_r \times 2$, $\boldsymbol{w}_1$ and $\boldsymbol{w}_2$ are of size $N_r \times 1$, $\boldsymbol{Y} = [\boldsymbol{y}_1, \boldsymbol{y}_2]$ is the receive matrix of size $N_r \times 2$, and $\boldsymbol{y}_1$ and $\boldsymbol{y}_2$ are of size $N_r \times 1$. The signal and noise variances are σ_s^2 and σ_w^2, respectively. We express the system model in (2.32) equivalently as

$$\boldsymbol{y} = \boldsymbol{H}\boldsymbol{s} + \boldsymbol{w}, \tag{2.33}$$

where $\boldsymbol{y} = [\boldsymbol{y}_1^T, \boldsymbol{y}_2^{*T}]^T$ is the equivalent $2N_r \times 1$ receive vector, $\boldsymbol{s} = [s_1, s_2, \cdots, s_{N_t}]^T$ and $\boldsymbol{w} = [\boldsymbol{w}_1^T, \boldsymbol{w}_2^{*T}]^T$. The equivalent channel matrix is of size $2N_r \times N_t$ and written as

$$\boldsymbol{H} = \begin{bmatrix} \boldsymbol{b}_1 & \boldsymbol{b}_2 & \cdots & \boldsymbol{b}_{N_t-1} & \boldsymbol{b}_{N_t} \\ -\boldsymbol{b}_2^* & \boldsymbol{b}_1^* & \cdots & -\boldsymbol{b}_{N_t}^* & \boldsymbol{b}_{N_t-1}^* \end{bmatrix}. \tag{2.34}$$

2.5.2 The linear precoded MU MIMO downlink

We consider an MU-MIMO system downlink with N_u UEs (see e.g., [99]). Shown in Figure 2.1, the BS has N_t transmit antennas, and the k-th UE has N_{r_k} receive antennas. $N_r = \sum_{k=1}^{N_u} N_{r_k}$ is the total number of receive antennas. The channel from the BS to the k-th UE is denoted by channel matrix $\boldsymbol{H}_k \in \mathbb{C}^{N_{r_k} \times N_t}$, and the total channel matrix is $\boldsymbol{H} = [\boldsymbol{H}_1^T, \boldsymbol{H}_2^T, \cdots, \boldsymbol{H}_{N_u}^T]^T$. We assume that BS knows $\boldsymbol{H}$ perfectly. The information symbol vector for the k-th UE is $\boldsymbol{s}_k \in \mathbb{C}^{r_k \times 1}$, where r_k is the number of transmit data streams for the k-th UE and $r_k \leq N_{r_k}$. The total number of transmit streams is $r = \sum_{k=1}^{N_u} r_k \leq N_r$. The

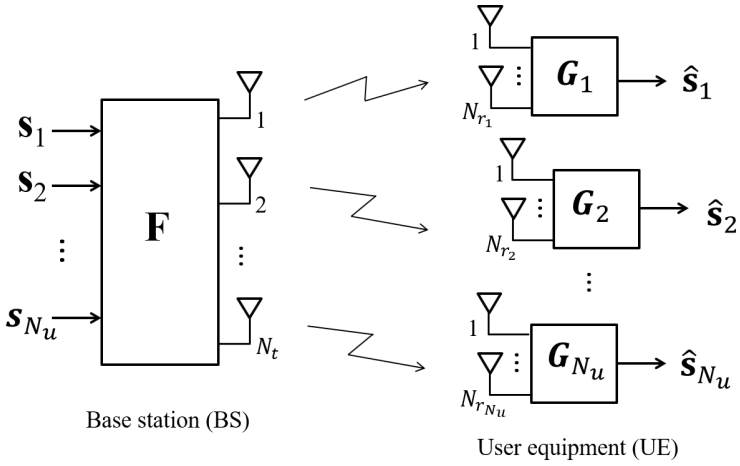

Figure 2.1: Block diagram of an MU-MIMO downlink, adopted from [99, Figure 1]

entries of $\boldsymbol{s}_k$ are drawn from alphabet set $\mathcal{S} \subset \mathbb{Z}_j$. The precoding matrix for the k-th UE is $\boldsymbol{F}_k \in \mathbb{C}^{N_t \times r_k}$. Thus, the total information symbol vector is $\boldsymbol{s} = [\boldsymbol{s}_1^T, \cdots, \boldsymbol{s}_{N_u}^T]^T \in \mathbb{C}^{r \times 1}$, where $\boldsymbol{R}_s = E(\boldsymbol{s}\boldsymbol{s}^H) = \sigma_s^2 \boldsymbol{I}_r$ and the total precoding matrix is $\boldsymbol{F} = [\boldsymbol{F}_1, \boldsymbol{F}_2, \cdots, \boldsymbol{F}_{N_u}] \in \mathbb{C}^{N_t \times r}$. The transmit signal after linear precoding is $\boldsymbol{x} = \boldsymbol{F}\boldsymbol{s}$, which is an $N_t \times 1$ vector and satisfies the transmit power constraint $tr(E(\boldsymbol{x}\boldsymbol{x}^H)) = \sigma_s^2 tr(\boldsymbol{F}\boldsymbol{F}^H) \leq P_{total}$, where P_{total} is the average transmit power for the downlink, and $tr(\cdot)$ computes the trace of a matrix.

The received signal at the k-th UE is $\boldsymbol{y}_k = \boldsymbol{H}_k \boldsymbol{F}\boldsymbol{s} + \boldsymbol{w}_k$, where $\boldsymbol{w}_k \in \mathbb{C}^{N_{r_k} \times 1}$ is the zero mean complex Gaussian noise with covariance $\sigma_w^2 \boldsymbol{I}_{r_k}$ at the k-th UE. Denoting the decoding matrix of the k-th UE as $\boldsymbol{G}_k$, the estimated symbol vector at the k-th UE becomes $\hat{\boldsymbol{s}}_k = \boldsymbol{G}_k(\boldsymbol{H}_k \boldsymbol{F}\boldsymbol{s} + \boldsymbol{n}_k)$. We can stack the estimated symbol vectors $\hat{\boldsymbol{s}}_k, k = 1, \cdots, N_u$ together to form $\hat{\boldsymbol{s}} = [\hat{\boldsymbol{s}}_1^T, \cdots, \hat{\boldsymbol{s}}_{N_u}^T]^T \in \mathbb{C}^{r \times 1}$ and express the system compactly as

$$\hat{\boldsymbol{s}} = \boldsymbol{G}(\boldsymbol{H}\boldsymbol{F}\boldsymbol{s} + \boldsymbol{w}), \tag{2.35}$$

where $\boldsymbol{w} = [\boldsymbol{w}_1^T, \cdots, \boldsymbol{w}_{N_u}^T]^T \in \mathbb{C}^{N_r \times 1}$, and $\boldsymbol{G} = blockdiag\{\boldsymbol{G}_1, \boldsymbol{G}_2, \cdots, \boldsymbol{G}_{N_u}\} \in \mathbb{C}^{r \times N_r}$.

Block diagonalization

With multi-antenna UEs, the linear block diagonalization (BD) [59, 61] can be used to completely eliminate MUI and decompose the MU MIMO downlink channel into several independent SU MIMO channels. The BD algorithm aims to find a precoding matrix $\boldsymbol{F} = [\boldsymbol{F}_1, \boldsymbol{F}_2, \cdots, \boldsymbol{F}_{N_u}]$ which eliminates the MUI completely, i.e.,

$$\boldsymbol{H}_l \boldsymbol{F}_k = \boldsymbol{0}_{N_{r_l} \times r_k}, \forall k \neq l, 1 \leq l, k \leq N_u. \tag{2.36}$$

To do so, BD algorithm utilizes SVD operations to compute the precoding matrix of each user. The columns of the k-th precoding matrix lie in the nullspace of $\bar{\boldsymbol{H}}_k$,

$$\bar{\boldsymbol{H}}_k = [\boldsymbol{H}_1^T, \cdots, \boldsymbol{H}_{k-1}^T, \boldsymbol{H}_{k+1}^T, \cdots, \boldsymbol{H}_{N_u}^T]^T. \tag{2.37}$$

Let $\bar{L}_k = \textit{rank}(\bar{\boldsymbol{H}}_k)$ and denote the SVD of $\bar{\boldsymbol{H}}_k$ as

$$\bar{\boldsymbol{H}}_k = \bar{\boldsymbol{U}}_k \bar{\boldsymbol{\Lambda}}_k \bar{\boldsymbol{V}}_k^H, \tag{2.38}$$

where $\bar{\boldsymbol{U}}_k$ is an $(N_r - N_{r_k}) \times (N_r - N_{r_k})$ unitary matrix, $\bar{\boldsymbol{\Lambda}}_k$ is an $(N_r - N_{r_k}) \times N_t$ diagonal matrix and $\bar{\boldsymbol{V}}_k = [\bar{\boldsymbol{V}}_k^{(1)}, \bar{\boldsymbol{V}}_k^{(0)}]$ is an $N_t \times N_t$ unitary matrix. The last $N_t - \bar{L}_k$ right singular vectors $\bar{\boldsymbol{V}}_k^{(0)}$ form an orthonormal basis of the nullspace of $\bar{\boldsymbol{H}}_k$. In this way, precoding matrix $\boldsymbol{F}_k$ for the k-th UE can be designed as $\boldsymbol{F}_k = \bar{\boldsymbol{V}}_k^{(0)} \boldsymbol{A}_k$, where $\boldsymbol{A}_k$ is an $(N_t - \bar{L}_k) \times r_k$ matrix that is designed alone by some optimization criteria, and this type of design satisfies the zero MUI constraint in (2.36). The received signal after BD at the k-th UE becomes

$$\boldsymbol{y}_k = \boldsymbol{H}_k \bar{\boldsymbol{V}}_k^{(0)} \boldsymbol{A}_k \boldsymbol{s}_k + \boldsymbol{w}_k, k = 1, \cdots, N_u. \tag{2.39}$$

Generalized zero forcing channel inversion

To further reduce the complexity of BD, the generalized zero forcing channel inversion (GZI) is proposed in [64], which uses matrix inversion and QRD to equivalently eliminate MUI. First, the pseudo-inverse of channel matrix $\boldsymbol{H}$ is computed as

$$\boldsymbol{H}^{\dagger} = \boldsymbol{H}^{H}(\boldsymbol{H}\boldsymbol{H}^{H})^{-1} = [\hat{\boldsymbol{H}}_1, \hat{\boldsymbol{H}}_2, \cdots, \hat{\boldsymbol{H}}_{N_u}]. \tag{2.40}$$

Then, we perform QRD on $\hat{\boldsymbol{H}}_k$,

$$\hat{\boldsymbol{H}}_k = \boldsymbol{Q}_k\boldsymbol{R}_k, k = 1, 2, \cdots, N_u, \tag{2.41}$$

where $\boldsymbol{Q}_k$ is an $N_t \times N_{r_k}$ unitary matrix and $\boldsymbol{R}_k$ is an $N_{r_k} \times N_{r_k}$ upper triangular matrix. It can be seen that $\boldsymbol{H}_l\hat{\boldsymbol{H}}_k = \boldsymbol{H}_l\boldsymbol{Q}_k\boldsymbol{R}_k = \boldsymbol{0}_{N_{r_l}\times N_{r_k}}, \forall\ k \neq l$. Because $\boldsymbol{R}_k$ is invertible, we have $\boldsymbol{H}_l\boldsymbol{Q}_k = \boldsymbol{0}_{N_{r_l}\times N_{r_k}}, \forall k \neq l$. Thus by designing the k-th UE's precoding matrix as $\boldsymbol{F}_k = \boldsymbol{Q}_k\boldsymbol{A}_k$, where in this case $\boldsymbol{A}_k$ is an $N_{r_k} \times r_k$ matrix that is designed alone by some optimization criteria, zero MUI constraint in (2.36) is also satisfied. The received signal after GZI at the k-th UE becomes

$$\boldsymbol{y}_k = \boldsymbol{H}_k\boldsymbol{Q}_k\boldsymbol{A}_k\boldsymbol{s}_k + \boldsymbol{w}_k, k = 1, \cdots, N_u. \tag{2.42}$$

To summarize, both BD and GZI effectively decompose an MU-MIMO system into K parallel SU MIMO systems. But note that the matrix $\boldsymbol{A}_k$ left for further design is different in dimension for BD and GZI, and this will result in different performance and complexity between BD-based design and GZI-based design.

With the background reviewed, we derive the capacity of LR-aided equalizers in the next chapter.

CHAPTER 3

LR-AIDED EQUALIZATION: CAPACITY AND COMPLEXITY

In this chapter, we derive the capacity of LR aided equalizers in MIMO systems. We also study the complexity of LR algorithms against spatial correlation. The content of this chapter is adopted from our publications [100, 101].

3.1 Channel model

We adopt the system model described in (2.1). Kronecker correlation model [102, 103] is used to describe the correlations between the faded envelopes of the MIMO sub-channels

$$\boldsymbol{H} = \boldsymbol{R}_r{}^{1/2} \boldsymbol{H}_w \boldsymbol{R}_t{}^{T/2}, \tag{3.1}$$

where the $N_r \times N_t$ matrix $\boldsymbol{H}_w$ has IID complex Gaussian distributed entries with zero mean and unit variance, the $N_t \times N_t$ matrix $\boldsymbol{R}_t$ and $N_r \times N_r$ matrix $\boldsymbol{R}_r$ are transmit and receive correlation matrix, respectively, and represent the correlation of transmit/receive signals across the elements of antenna array. Their relationship with channel correlation matrix $E(\boldsymbol{h}\boldsymbol{h}^H)$ is given by $E(\boldsymbol{h}\boldsymbol{h}^H) = \boldsymbol{R}_t \otimes \boldsymbol{R}_r$, where $\boldsymbol{h} = vec(\boldsymbol{H})$, and $\otimes$ denotes the Kronecker product. It is assumed that $\boldsymbol{R}_t$, $\boldsymbol{R}_r$, $E(\boldsymbol{h}\boldsymbol{h}^H)$ all have full rank. Correlation coefficient is defined as the normalized correlation of signals across two neighboring antenna elements. Transmit correlation coefficient and receive correlation coefficient are denoted as ρ_t and ρ_r, respectively.

3.2 Capacity of LR-aided equalizers in MIMO systems

3.2.1 Instantaneous capacity

The steps to derive the capacity of a certain equalizer is as follows: 1) identify if the noise statistics is changed by equalization and detection process; and 2) build the equivalent model between input signal vector and un-quantized output of the equalizer. Now, let us derive the capacity of LR-aid MLE. Given the system model in (2.27), LR-aided MLE is defined as

$$\hat{\boldsymbol{z}}_{lrml} = \arg \min_{\hat{\boldsymbol{z}} \in \mathcal{S}_z^{N_t}} \|\boldsymbol{y} - \tilde{\boldsymbol{H}}\hat{\boldsymbol{z}}\|^2, \tag{3.2}$$

and $\hat{\boldsymbol{s}}_{lrml} = \boldsymbol{T}\hat{\boldsymbol{z}}_{lrml}$. $\mathcal{S}_z$ is the alphabet set in LR domain by transforming $\mathcal{S}$ with $\boldsymbol{T}^{-1}$. Since the statistics of noise is not changed, LR-aided MLE performs the same as MLE (see [100]). Thus,

$$C_{ml}^{LR}(\boldsymbol{H}) = C_{ml}(\boldsymbol{H}) = \log_2 \left(\det \left(\boldsymbol{R}_s \boldsymbol{R}_{ml}^{-1} + \boldsymbol{I}_{N_t}\right)\right). \tag{3.3}$$

Now let us derive the capacity of LR-aided LEs. Given the model in (2.27) and definition of ZFE in (2.4), the equivalent transmission model becomes

$$\boldsymbol{x}_{lrzf} = \boldsymbol{z} + \boldsymbol{\xi} = \boldsymbol{T}^{-1}\boldsymbol{s} + \boldsymbol{\xi}, \tag{3.4}$$

where $\boldsymbol{\xi}$ is the equivalent noise vector. Due to the symbol-by-symbol detection of ZFE, the covariance matrix $\boldsymbol{R}_\xi$ of $\boldsymbol{\xi}$ in Eq. (3.4) is *diagonal* and is defined as

$$(\boldsymbol{R}_\xi)_{k,k} = \left(\sigma_w^2 (\tilde{\boldsymbol{H}}^H \tilde{\boldsymbol{H}})^{-1}\right)_{k,k}, \quad k = 1, ..., N_t. \tag{3.5}$$

The mutual information when LR-aided ZFE is used is

$$\mathcal{I}(\boldsymbol{x}_{lrzf}; \boldsymbol{s}|\boldsymbol{H}) = \mathcal{H}(\boldsymbol{x}_{lrzf}|\boldsymbol{H}) - \mathcal{H}(\boldsymbol{\xi}|\boldsymbol{H}). \tag{3.6}$$

Since $\boldsymbol{\xi}$ is Gaussian,

$$\mathcal{I}(\boldsymbol{x}_{lrzf}; \boldsymbol{s}|\boldsymbol{H}) \leq \log_2 \frac{\det\left(\pi e\left(\boldsymbol{T}^{-1}\boldsymbol{R}_s(\boldsymbol{T}^{-1})^H + \boldsymbol{R}_\xi\right)\right)}{\det(\pi e \boldsymbol{R}_\xi)}, \tag{3.7}$$

with equality when $\boldsymbol{s}$ is Gaussian. Therefore,

$$C_{zf}^{LR}(\boldsymbol{H}) = \log_2\left(\det\left(\boldsymbol{R}_s\boldsymbol{R}_{lrzf}^{-1} + \boldsymbol{I}_{N_t}\right)\right), \tag{3.8}$$

where $\boldsymbol{R}_{lrzf} := \boldsymbol{T}\boldsymbol{R}_\xi\boldsymbol{T}^H$ is the effective noise covariance matrix for LR-aided ZFE.

When SNR is high, we have

$$C_{ml}^{LR}(\boldsymbol{H}) \approx \log_2\left(\det\left(\boldsymbol{R}_s\boldsymbol{R}_{ml}^{-1}\right)\right), \tag{3.9}$$

$$C_{zf}^{LR}(\boldsymbol{H}) \approx \log_2\left(\det\left(\boldsymbol{R}_s\boldsymbol{R}_{\xi}^{-1}\right)\right), \tag{3.10}$$

since $\det(\boldsymbol{T}^H\boldsymbol{T}) = 1$. We summarize our first proposition as follows.

Proposition 1. *Given the MIMO system model in* (2.27)*, the instantaneous capacity when LR-aided MLE is used is the same as that when MLE is used. Also, the instantaneous capacity when LR-aided LEs are used is less than or equal to that when LR-aided MLE is used. i.e.,*

$$C_{zf}^{LR}(\boldsymbol{H}) \leq C_{ml}^{LR}(\boldsymbol{H}) = C_{ml}(\boldsymbol{H}).$$

Proof: See Appendix A.1. ■

At high SNR, we quantify the gap between $C_{zf}^{LR}(\boldsymbol{H})$ and $C_{ml}^{LR}(\boldsymbol{H})$ as

$$C_{ml}^{LR}(\boldsymbol{H}) - C_{zf}^{LR}(\boldsymbol{H}) = -\log_2\left(1 - od(\tilde{\boldsymbol{H}}(\tilde{\boldsymbol{H}}^H\tilde{\boldsymbol{H}})^{-1})\right). \tag{3.11}$$

As $od((\tilde{\boldsymbol{H}}^\dagger)^H)$ decreases, the capacity gap between LR-aided MLE and LR-aided ZFE

narrows. Meanwhile,

$$C_{zf}^{LR}(\boldsymbol{H}) - C_{zf}(\boldsymbol{H}) = \log_2 \frac{1 - od((\tilde{\boldsymbol{H}}^{\dagger})^H)}{1 - od((\boldsymbol{H}^{\dagger})^H)}. \tag{3.12}$$

This result implies that LR algorithms that aim to reduce the od of the dual channel matrix will provide larger improvement of instantaneous capacity than those that do not.

3.2.2 Ergodic capacity

For a fading channel with CSI at the receiver, the ergodic capacity is obtained by taking expectation of the instantaneous capacity, i.e., $C_{ergodic} = E_{\boldsymbol{H}}\left(C(\boldsymbol{H})\right)$, From Proposition 1, we have

$$E_{\boldsymbol{H}}\left(C_{zf}^{LR}(\boldsymbol{H})\right) \leq E_{\boldsymbol{H}}\left(C_{ml}^{LR}(\boldsymbol{H})\right) = E_{\boldsymbol{H}}\left(C_{ml}(\boldsymbol{H})\right). \tag{3.13}$$

Proposition 2. *The ergodic capacity of LR aided LEs is greater than that of LEs at high SNR if*

$$E_{\boldsymbol{H}}\left(\frac{1 - od((\boldsymbol{H}^{\dagger})^H)}{1 - od((\tilde{\boldsymbol{H}}^{\dagger})^H)}\right) \leq 1. \tag{3.14}$$

Thus, the ergodic capacity of the dual ELR aided LEs [43] is greater than that of the LEs.

Proof: See Appendix A.2. ■

Figure 3.1 shows the ergodic capacity of various equalizers. The ergodic capacity of MLE is greater than that of LR aided ZFE, and the ergodic capacity of LR aided ZFE is greater than that of ZFE. Moreover, CLLL-aided ZFE has larger ergodic capacity gap to MLE compared to other LR aided ZFEs. This is because CLLL does not attempt to reduce the size of dual basis, and thus the od of the dual basis may be quite large.

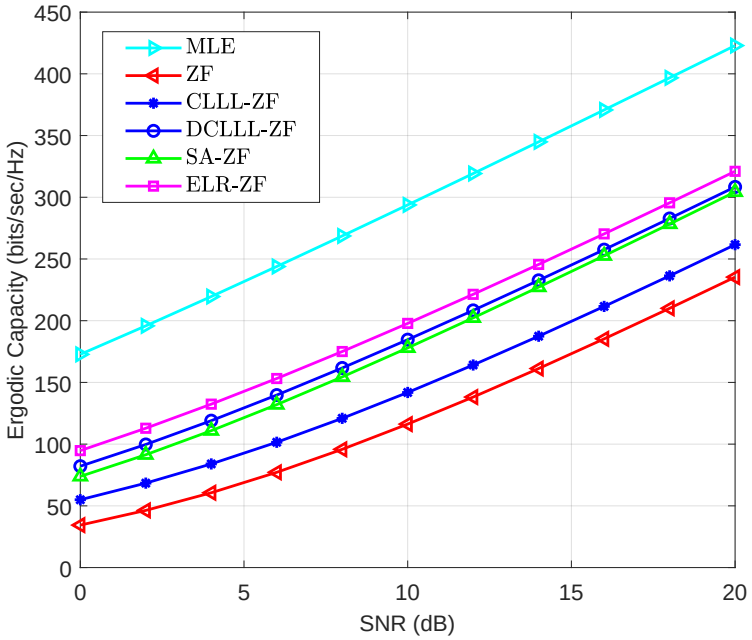

Figure 3.1: Ergodic capacity of various equalizers for 40×40 MIMO.

3.2.3 Outage capacity

For a certain system, the probability that instantaneous capacity is smaller than a threshold is denoted as $P(C < C_{th})$. The outage diversity order G_o is defined as (see [45])

$$G_o = \lim_{SNR \to \infty} -\frac{\log P(C < C_{th})}{\log(\text{SNR})}. \tag{3.15}$$

Proposition 3. *The outage diversity of LR aided MLE is the same as that of MLE. The outage diversity of the LR aided LEs is the same as that of MLE when the* od *of the reduced channel matrix is bounded by a number less than one.*

Proof: See Appendix A.3. ■

In Figure 3.2, the outage diversity orders of different equalizers are plotted. First we look at the solid lines. MLE achieves full outage diversity. ZFE loses outage diversity, since $od(\boldsymbol{H})$ does not have a bound smaller than one. ELR also does not have $od(\tilde{\boldsymbol{H}})$ bounded by a number smaller than one [43], and thus ELR aided ZFE loses outage diversity. CLLL and DCLLL are able to bound $od(\tilde{\boldsymbol{H}})$ and $od((\tilde{\boldsymbol{H}}^{\dagger})^{H})$ by a number smaller than one [33], thus

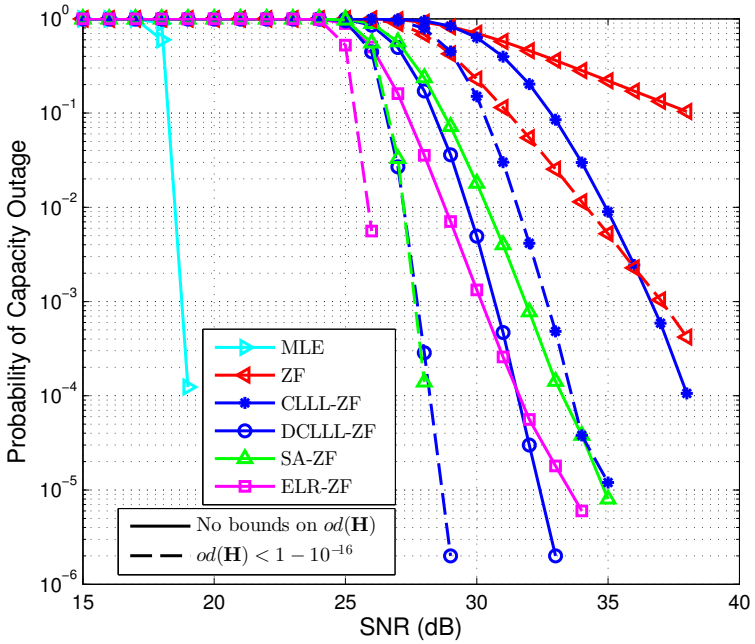

Figure 3.2: Outage diversity of various equalizers for 40×40 MIMO.

CLLL-aided ZFE and DCLLL-aided ZFE are able to collect full outage diversity. It is also noticed that although the curves of the ergodic capacity of DCLLL-, SA-, and ELR aided ZFE are close in Figure 3.1, their outage probabilities here are different. The reason is that different LR algorithms might produce different reduced channel matrices, so that the distributions of the instantaneous capacity are different for different LR aided ZFEs. Then we look at the dashed lines. The dashed lines are produced by enforcing a smaller-than-one bound on $od(\boldsymbol{H})$. Now we see that ZFE collects full outage diversity. Also since $od(\boldsymbol{H})$ are bounded by $\epsilon_1 < 1$, CLLL, DCLLL, and ELR are able to bound $od(\tilde{\boldsymbol{H}})$ by $\epsilon_2 < 1$. Thus, CLLL-, DCLLL-, and ELR aided ZFEs are able to collect full outage diversity.

3.3 Complexity of LR algorithms under spatial correlation

3.3.1 Equal transmit and receive correlation

To see how correlation affect the complexity of LR, we measure the complexity of LR algorithms as the number of complex arithmetics divided by the number of receive antennas. Figure 3.3 shows the complexity of various LR algorithms as both transmit and receive

correlation coefficient increases, for 20×20 MIMO, 64QAM. Complexity of LR($\bar{\boldsymbol{H}}$) does not vary too much when $\rho_r = \rho_t \leq 0.6$. When $\rho_r = \rho_t \geq 0.7$, except for ELR, complexity increases. But when SNR is low, the ratio of increase is lower, because the complexity of LR($\bar{\boldsymbol{H}}$) is dominated by the scaled identity matrix when $\rho_r = \rho_t$ is large.

3.3.2 Transmit or receive correlation

Now we examine how transmit (receive) correlation alone affects the complexity of LR algorithms. Figure 3.4 shows the average complexity of LR($\bar{\boldsymbol{H}}$) with different MIMO sizes ($N_r = N_t$) and different (ρ_r, ρ_t) pairs. As observed, ELR has the lowest average complexity while SA has the highest. The average complexity of DCLLL and CLLL are in between that of ELR and SA, with DCLLL having lower complexity than CLLL. Also, the average complexity of LR algorithms increases as ρ_r or ρ_t increases. Moreover, when the correlation coefficient is small, receive correlation costs LR algorithm more in terms of average complexity than transmit correlation. But when both the MIMO size and the correlation coefficient is large, we notice that transmit correlation costs LR algorithm more in terms of average complexity than receive correlation.

3.4 Chapter summary

In this chapter, first, we have studied the capacity of LR-aided equalizers. It has been shown that the instantaneous capacity gap between MLE and LR-aided ZFE is greater than or equal to zero and increases with $od((\tilde{\boldsymbol{H}}^{\dagger})^H)$, and that between LR-aided ZFE and ZFE increases with $\left(1 - od((\tilde{\boldsymbol{H}}^{\dagger})^H)\right) / \left(1 - od((\boldsymbol{H}^{\dagger})^H)\right)$. For outage capacity, LR-aided LEs collect the same outage diversity as MLE does if od of the reduced channel matrix is bounded by a number smaller than one. Second, we studied the complexity of LR-aided detectors when the MIMO channel is spatially correlated. We showed through simulations that transmit correlation costs LR algorithms more in terms of complexity compared to receive correlation when MIMO size and correlation coefficient are large.

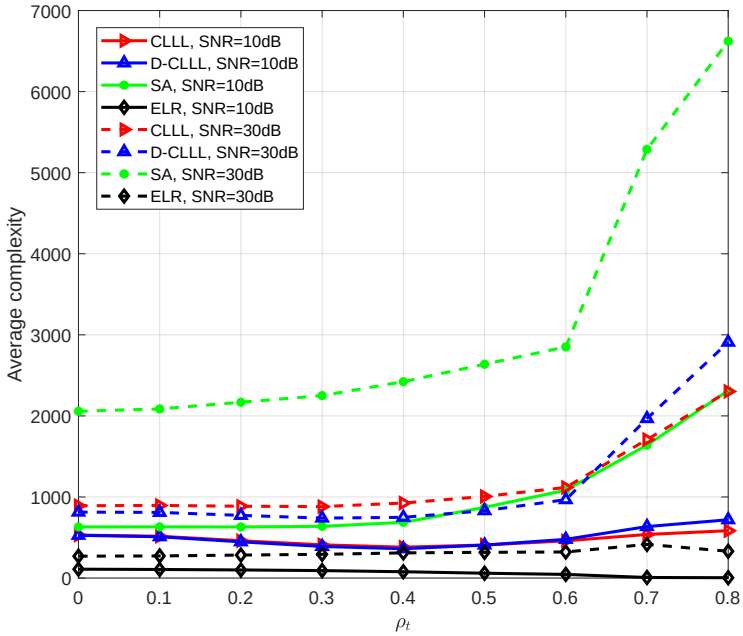

Figure 3.3: Average complexity of LR($\bar{\boldsymbol{H}}$) for 20×20 MIMO systems, SNR = 10dB or 30dB, 64QAM.

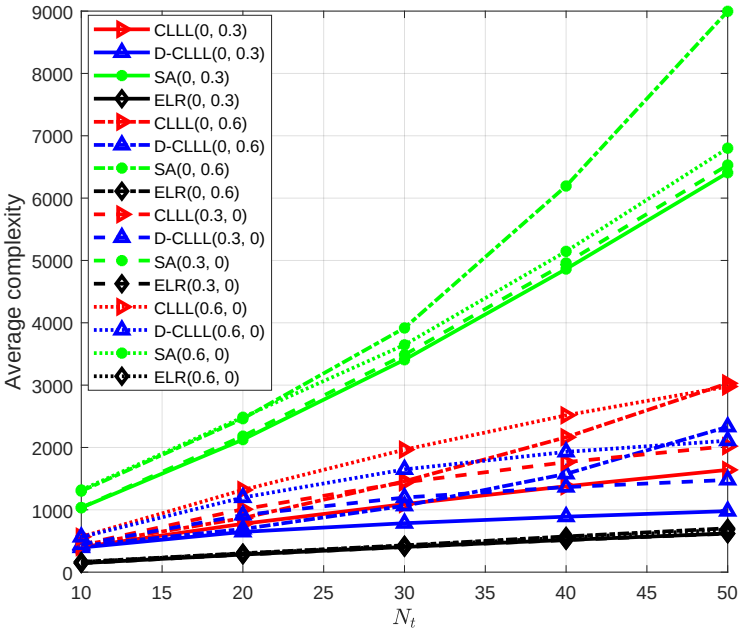

Figure 3.4: Average complexity of LR($\bar{\boldsymbol{H}}$) when SNR = 30dB, 64QAM, with different MIMO sizes and different (ρ_r, ρ_t).

In the next chapter, we will apply LR techniques in MU MIMO systems.

CHAPTER 4

APPLYING LR TECHNIQUES TO MU MIMO SYSTEMS

In this chapter, we first present PELR aided detectors for the STCM systems. We then present an LR aided linear joint transceiver design for downlink transmissions of the MU MIMO system. The content of this chapter is adopted from our publications [98, 99].

4.1 Pairwise ELR aided detectors for the STCM system

The STCM system model has been introduced in Section 2.5.1. The equivalent channel (2.34) has symmetric structure that allow us to reduce complexity. Our goal is to develop LR aided detectors that utilize this structure fully. We propose the PELR aided detectors [98], which has two core components, the PELR algorithms and the generalized pairwise QRD.

Table 4.1: The proposed PELR and PELR-SLB for the STCM systems [98, Table I]

Input: $\boldsymbol{H}$, **Output:** $\tilde{\boldsymbol{H}}, \boldsymbol{T}$	
(S1)	$\tilde{\boldsymbol{H}} = \boldsymbol{H}, \boldsymbol{T} = \boldsymbol{I}_{N_t}, \boldsymbol{C} = \left(\boldsymbol{H}^H \boldsymbol{H}\right)^{-1}, \tilde{\boldsymbol{C}} = \boldsymbol{C}$
(S2)	**Do**
(S3)	$\lambda_{l,k} \leftarrow -\left\lceil \frac{\tilde{C}_{l,k}}{\tilde{C}_{l,l}} \right\rfloor, k = 1, 3, \cdots, N_t - 1, l \neq k$
(S4)	**PELR: If** the largest element of $\tilde{\boldsymbol{C}}$ is irreducible, **break**;
(S5)	**PELR-SLB: If** all $\lambda_{l,k} = 0, \forall l \neq k$, **break**;
(S6)	Find the largest reducible $\tilde{C}_{k,k}$
(S7)	$l = \arg\max_{m=1, m\neq k}^{N_t} \Delta_{m,k}$
(S8)	$\boldsymbol{t}_l \leftarrow \boldsymbol{t}_l - \lambda_{l,k}^* \boldsymbol{t}_k$
(S9)	$\tilde{C}_{m,k} \leftarrow \tilde{C}_{m,k} + \lambda_{l,k} \tilde{C}_{m,l},\ m = 1, \cdots, k-1, k+1, \cdots, N_t$
(S10)	$\tilde{C}_{k,m} \leftarrow \tilde{C}_{m,k}^*,\ m = 1, \cdots, k-1, k+1, \cdots, N_t$
(S11)	$\tilde{C}_{k,k} \leftarrow \tilde{C}_{k,k} - \Delta_{l,k}$
(S12)	$\tilde{\boldsymbol{h}}_l \leftarrow \tilde{\boldsymbol{h}}_l - \lambda_{l,k}^* \tilde{\boldsymbol{h}}_k$
(S13)	$\boldsymbol{t}_{l_p} \leftarrow CP(\boldsymbol{t}_l)$
(S14)	$\tilde{\boldsymbol{c}}_{k_p} \leftarrow CP(\tilde{\boldsymbol{c}}_k)$
(S15)	$\tilde{\boldsymbol{c}}^{(k_p)} \leftarrow CP(\tilde{\boldsymbol{c}}^{(k)})$
(S16)	$\tilde{\boldsymbol{h}}_{l_p} \leftarrow CP(\tilde{\boldsymbol{h}}_l)$
(S17)	**While (true)**

PELR algorithms

The goal of the PELR algorithm is to reduce the maximum equivalent noise variance given the equivalent channel matrix in (2.34) while exploiting the symmetric structure. The PELR algorithms for it are shown in Table 4.1. We explain how they work in the following.

Definition 4. *Let $\boldsymbol{a}$ and $\boldsymbol{b}$ be two vectors with size $2l \times 1$. Vector $\boldsymbol{b}$ is said to be Type-I symmetric to vector $\boldsymbol{a}$ if and only if $\boldsymbol{b} = [-\boldsymbol{a}_{l+1:2l}^H, \boldsymbol{a}_{1:l}^H]^T$. We call $\boldsymbol{a}, \boldsymbol{b}$ a Type-I column pair. Vector $\boldsymbol{b}$ is said to be Type-II symmetric to vector $\boldsymbol{a}$ if and only if $b_{2n-1} = -a_{2n}^*$ and $b_{2n} = a_{2n-1}^*$, $n = 1, .., l$. In this case we call $\boldsymbol{a}, \boldsymbol{b}$ a Type-II column pair. In both cases, we denote that $\boldsymbol{b} = \overrightarrow{CP}(\boldsymbol{a})$ and $\boldsymbol{a} = \overleftarrow{CP}(\boldsymbol{b})$.*

When a column pair $\boldsymbol{a}$ and $\boldsymbol{b}$ are two of the column vectors in a matrix and the column index of vector $\boldsymbol{a}$ (or vector $\boldsymbol{b}$) is k, we denote the column index of the other one as k_p.

Lemma 2. *For the channel matrix $\boldsymbol{H}$ in* (2.34) *(or its MMSE form $\bar{\boldsymbol{H}}$), $\boldsymbol{C} = (\boldsymbol{H}^H\boldsymbol{H})^{-1}$ has $N_t/2$ Type-II column pairs. At the first iteration, if the largest diagonal value $C_{k,k}$ can be reduced by its l-th column and row by $\Delta_{l,k}$, then C_{k_p,k_p} can be reduced by its l_p-th column and row by $\Delta_{l,k}$ as well.*

Proof: See Appendix B.1. ■

Lemma 3. *By having reductions between index pair (l, k) and (l_p, k_p) consecutively during an iteration, the matrix $\tilde{\boldsymbol{C}}$ remains the structure shown in (B.1) after every iteration.*

Proof: See Appendix B.2. ■

The lemmas show two advantages of the PELR algorithms in Table 4.1. First, the pairwise reductions can be carried out iteratively, and the final reduced channel matrix $\tilde{\boldsymbol{H}}$ will maintain the symmetric structure, which enables further complexity reduction in the following detection steps. Second, the updates of $\tilde{\boldsymbol{H}}$, $\boldsymbol{T}$, $\tilde{\boldsymbol{C}}$ resulting from the second reduction during an iteration is computationally free. Note that in Steps 13 to 16 of in Table

4.1, we use $CP(\cdot)$ to represent operations $\overleftarrow{CP}(\cdot)$ and $\overrightarrow{CP}(\cdot)$ for simplicity. We also abuse the notation of $CP(\cdot)$ to include deriving both Type-I and Type-II column pairs.

Generalized pairwise QRD

After the PELR algorithms, the PELR-aided detectors perform linear or SIC detection based on the reduced channel matrix $\tilde{\boldsymbol{H}}$ (see [98] for details). Note that final reduced channel matrix $\tilde{\boldsymbol{H}}$ has symmetric structure. Since the QRD is a main and high-complexity step for LD and SIC, based on the pairwise QR (PQR) in [104], we propose a generalized PQR to exploit the symmetric property of $\tilde{\boldsymbol{H}}$ and reduce its computational complexity. Different from the PQR in [104], the generalized PQR handles the scenarios when the input is a reduced MMSE channel matrix. For PELR-aided MMSE linear or SIC detectors, the reduced channel matrix is expressed as $\tilde{\bar{\boldsymbol{H}}} = [\tilde{\boldsymbol{H}}^T, \sigma_w/\sigma_s\tilde{\boldsymbol{I}}]^T$, where $\tilde{\boldsymbol{H}}$ has $N_t/2$ Type-I column pairs and $\tilde{\boldsymbol{I}}$ has $N_t/2$ Type-II column pairs. Therefore, instead of using Steps 13 and 21 of Algorithm 2 in [104], we use the $CP(\cdot)$ operator to represent the way we compute groups of two columns in $\boldsymbol{Q}$ based on both Type-I column pairs and Type-II column pairs. The generalized PQR algorithm is shown in Table 4.2. It has approximately half of the complexity of QRD, since $(S6)$ and $(S13)$ in Table 4.2 are computationally free.

4.1.1 Complexity analysis

We inspect the complexity of the proposed PELR-aided detectors. We count one complex operation (e.g., multiplication, division, addition, subtraction) as one complex arithmetic operation. For the complexity analysis throughout this chapter, we make use of some complexity results about basic matrix operations from [105]:

- Matrix multiplication of $\boldsymbol{A}_{m\times n}$ and $\boldsymbol{B}_{n\times p}$: $2mnp$.
- Inversion of matrix $\boldsymbol{A}_{m\times m}$ using Gauss elimination: $4m^3/3$.
- SVD of matrix $\boldsymbol{A}_{m\times n}$ ($m \leq n$) when only diagonal matrix $\boldsymbol{\Sigma}$ containing singular

Table 4.2: Generalized PQR for the STCM systems [98, Table II]

Input: $\boldsymbol{H}$, **Output:** $\boldsymbol{Q}, \boldsymbol{R}$	
(S1)	$\boldsymbol{R} \leftarrow \boldsymbol{0}, \boldsymbol{Q} \leftarrow \boldsymbol{H}$
(S2)	**for** $l = 1 : N_t/2$
(S3)	$R_{2l-1,2l-1} \leftarrow \|\boldsymbol{q}_{2l-1}\|$
(S4)	$\boldsymbol{q}_{2l-1} \leftarrow \boldsymbol{q}_{2l-1}/R_{2l-1,2l-1}$
(S5)	$R_{2l,2l} \leftarrow R_{2l-1,2l-1}$
(S6)	$\boldsymbol{q}_{2l} \leftarrow CP(\boldsymbol{q}_{2l-1})$
(S7)	**for** $n = (l+1) : N_t/2$
(S8)	$R_{2l-1,2n-1} \leftarrow \boldsymbol{q}_{2l-1}^H \boldsymbol{q}_{2n-1}$
(S9)	$R_{2l,2n-1} \leftarrow \boldsymbol{q}_{2l}^H \boldsymbol{q}_{2n-1}$
(S10)	$\boldsymbol{q}_{2n-1} \leftarrow \boldsymbol{q}_{2n-1} - \sum_{m=2l-1}^{2l} R_{m,2n-1}\boldsymbol{q}_m$
(S11)	$R_{2l-1,2n} \leftarrow -R_{2l,2n-1}^*$
(S12)	$R_{2l,2n} \leftarrow R_{2l-1,2n-1}^*$
(S13)	$\boldsymbol{q}_{2n} \leftarrow CP(\boldsymbol{q}_{2n-1})$
(S14)	**end**
(S15)	**end**

values and unitary matrix $\boldsymbol{V}$ containing right singular vectors are calculated: $4n^2m + 13m^3$.

First, we count the complexity of the PELR algorithm by the number of iterations and the overall complex arithmetics operations. The PELR algorithm consists of preprocessing that computes $\boldsymbol{H}^H\boldsymbol{H}$ and $\boldsymbol{C}$, and the LR process. Due to the symmetric structure of $\boldsymbol{H}$, computing $\boldsymbol{H}^H\boldsymbol{H}$ requires $2N_rN_t^2$. Similarly, due to the structure of $\boldsymbol{H}^H\boldsymbol{H}$, computing $\boldsymbol{C}$ requires $2/3N_t^3$. Denote the number of iterations of the PELR algorithm and that of the ELR algorithm as iter$_p$ and iter. The total complex arithmetic operations of the PELR and the ELR algorithm is then

$$\theta_{\text{PELR}} = \frac{2}{3}N_t^3 + 2N_rN_t^2 + \text{iter}_p\,(11.5N_t - 1 + 4N_r), \tag{4.1}$$

$$\theta_{\text{ELR}} = \frac{4}{3}N_t^3 + 4N_rN_t^2 + \text{iter}\,(12N_t - 1 + 4N_r). \tag{4.2}$$

Next we give the complexity of the generalized PQR and QR for the MMSE channel matrix.

Note that the generalized PQR saves approximately half of the complexity of the QR.

$$\theta_{PQR(\bar{\boldsymbol{H}})} = (2N_r + N_t)N_t^2 - (2N_r + N_t)N_t/2, \tag{4.3}$$

$$\theta_{QR(\bar{\boldsymbol{H}})} = 2(2N_r + N_t)N_t^2 + (2N_r + N_t)N_t. \tag{4.4}$$

Lastly, the QRD is followed by the detection step and the transformation by $\boldsymbol{T}$. Table 4.3 shows the complexity of the detection and transform step of the PELR-aided LD/SIC.

Table 4.3: PELR aided LD/SIC for the STCM systems [98, Table III]

Steps	Detection (LD/SIC)	Transform ($\boldsymbol{T}$)
PELR-MMSE-LD	$4N_t^2 + 4N_tN_r + 2N_t$	$2N_t^2$
PELR-MMSE-SIC	$3N_t^2 + 4N_tN_r + 2N_t$	$2N_t^2$

4.1.2 Numerical results

Now we examine the complexity of the PELR algorithms, and the complexity and BER of the proposed PELR-aided detectors. The complexity is measured by the number of complex arithmetics. The detectors we compare with include MMSE-SIC, dual CLLL-aided MMSE-SIC ($\delta_c = 3/4$), ELR(-SLB) aided MMSE-SIC, and the proposed PELR(-SLB) aided MMSE-SIC detectors. We define SNR as $N_t\sigma_s^2/\sigma_w^2$. Table. 4.4 compares the complexity of various LR schemes by the average number of iterations when applied to the MMSE channel matrix with 16 QAM, SNR = 25 dB and $N_t = 2N_r$. It shows that PELR (PELR-SLB) approximately halves the average number of iterations of that of ELR (ELR-SLB). As N_t grows, PELR has lowest average complexity while PELR-SLB has the second lowest. Table. 4.4 also shows the average complexity of the detectors. The ELR (-SLB) aided MMSE-SIC requires highest complexity due to computing the $\boldsymbol{H}^H\boldsymbol{H}$ and $\boldsymbol{C}$ without utilizing symmetric structure of the channel matrix. The PELR (-SLB) aided MMSE-SIC reduces the average complexity of the ELR (-SLB) aided MMSE-SIC to its half and maintains similar average complexity compared to the MMSE-SIC and the dual

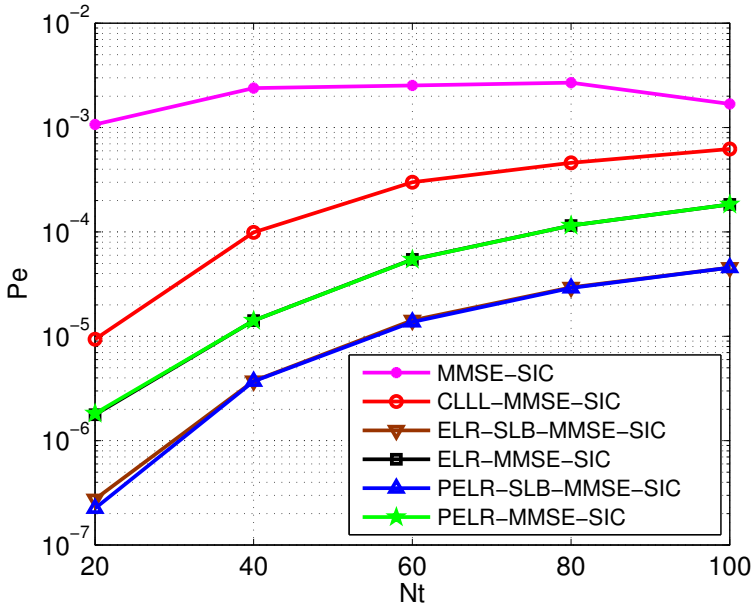

Figure 4.1: BER of various detectors with 16QAM, SNR = 25dB, $N_t = 2N_r$ [98, Figure 1]

CLLL-aided MMSE-SIC.

Figure 4.1 gives the BERs for various SICs with N_t varying from 20 to 100, 16 QAM, SNR = 25dB, and $N_t = 2N_r$. We observe that the PELR (-SLB) aided MMSE-SIC is able to achieve the same BER as the ELR (-SLB) aided MMSE-SIC. Both the PELR (-SLB) aided MMSE-SIC and the ELR (-SLB) aided MMSE-SIC achieve better BER than the dual CLLL-aided MMSE-SIC and MMSE-SIC. Figure 4.2 shows BER vs. SNR of various SICs with 16 QAM, $N_t = 80$, and $N_r = 40$. The PELR aided MMSE-SIC performs the same as the ELR-aided MMSE-SIC. The PELR-SLB aided MMSE-SIC and the ELR-SLB aided MMSE-SIC achieve the lowest BER.

4.2 LR-aided linear joint transceiver design for MU MIMO downlinks

Now we look at the MU MIMO downlink introduced in Section 2.5.2. Our goal is to design a transceiver architecture to minimize sum of MSE, subject to a per-user transmit power constraint. Our design assumes that the number of transmit antennas at BS is greater than or equal to the total number of receive antennas at UEs. It has two steps [99].

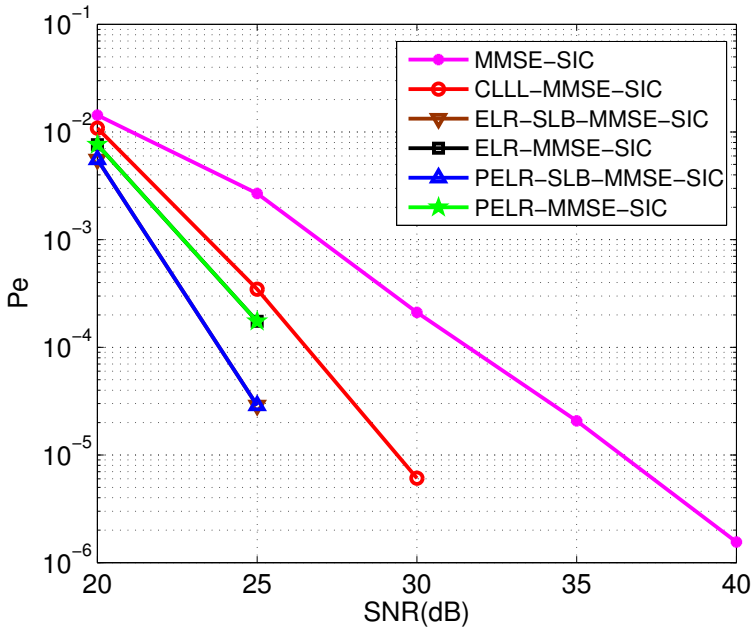

Figure 4.2: BER of various detectors with 16QAM, $N_t = 80$, and $N_r = 40$ [98, Figure 2]

MUI elimination

In the first step, we use either BD or GZI to eliminate MUI (see Section 2.5.2). We effectively decompose the MU-MIMO system to N_u parallel SU-MIMO systems, and the k-th UE receives

$$\boldsymbol{y}_k = \check{\boldsymbol{H}}_k \boldsymbol{A}_k \boldsymbol{s}_k + \boldsymbol{w}_k, k = 1, \cdots, N_u, \tag{4.5}$$

where $\check{\boldsymbol{H}}_k$ equals $\boldsymbol{H}_k \bar{\boldsymbol{V}}_k^{(0)}$ or $\boldsymbol{H}_k \boldsymbol{Q}_k$ depending on whether we use BD or GZI. Matrices $\boldsymbol{A}_k$ will be designed in the second step.

Parallel optimization

After step one, we are dealing with N_u independent SU MIMO optimization problems. Now we are going to optimize sum of the MSEs for each user independently subject to a transmit power constraint. Denoting P_k as the transmit power constraint that we set for the k-th UE, we have $\sum_{k=1}^{K} P_k = P_{total}$. The conventional linear joint transceiver design for

Table 4.4: The complexity of various LR schemes and various detectors, $N_t = 2N_r$.

	N_t	20	40	60	80	100
Iterations	D-CLLL	78	135	168	194	215
	ELR-SLB	31	62	89	113	132
	ELR	20	35	47	56	60
	PELR-SLB	**16**	**32**	**45**	**57**	**67**
	PELR	**10**	**18**	**24**	**28**	**31**
Complex arithmetics	MMSE-SIC	446	1691	3736	6581	10226
	D-CLLL-MMSE-SIC	628	2015	4129	6999	10642
	ELR-SLB-MMSE-SIC	1203	4294	9216	15980	24621
	ELR-MMSE-SIC	1052	3960	8719	15331	23796
	PELR-SLB-MMSE-SIC	**602**	**2143**	**4603**	**7993**	**12299**
	PELR-MMSE-SIC	**533**	**1993**	**4380**	**7693**	**11932**

SU MIMO solves the optimization problem

$$\begin{gathered}\min_{\boldsymbol{A}_k,\boldsymbol{G}_k} E \parallel \boldsymbol{s}_k - \boldsymbol{G}_k(\check{\boldsymbol{H}}_k\boldsymbol{A}_k\boldsymbol{s}_k + \boldsymbol{w}_k) \parallel^2 \\ tr(\sigma_s^2\boldsymbol{A}_k\boldsymbol{A}_k^H) \leq P_k.\end{gathered} \tag{4.6}$$

Once we know $\boldsymbol{A}_k$, the optimum $\boldsymbol{G}_k$ is always the well-known MMSE equalization matrix

$$\boldsymbol{G}_k = (\boldsymbol{A}_k^H\check{\boldsymbol{H}}_k^H\check{\boldsymbol{H}}_k\boldsymbol{A}_k + \sigma_w^2\boldsymbol{R}_s^{-1})^{-1}\boldsymbol{A}_k^H\check{\boldsymbol{H}}_k^H. \tag{4.7}$$

The optimal $\boldsymbol{A}_k$ and $\boldsymbol{G}_k$ are given in [106]. The estimation error $\boldsymbol{s}_k - \hat{\boldsymbol{s}}_k$ has autocorrelation matrix as

$$\boldsymbol{R}_e = (\sigma_w^{-2}\boldsymbol{A}_k^H\check{\boldsymbol{H}}_k^H\check{\boldsymbol{H}}_k\boldsymbol{A}_k + \sigma_s^{-2}\boldsymbol{I}_{r_k})^{-1}. \tag{4.8}$$

The diagonal elements of $\boldsymbol{R}_e$ are the MSEs of $\boldsymbol{s}_k$.

As shown in [65, 43], the MSE can be further reduced using ELR. If we assume $\boldsymbol{A}_k$ is known and write $\dot{\boldsymbol{H}}_k = \check{\boldsymbol{H}}_k\boldsymbol{A}_k$ as an $N_{r_k} \times r_k$ matrix, we have

$$\boldsymbol{y}_k = \dot{\boldsymbol{H}}_k\boldsymbol{s}_k + \boldsymbol{w}_k. \tag{4.9}$$

Using ELR algorithm, we get $\tilde{\boldsymbol{H}}_k = \dot{\boldsymbol{H}}_k\boldsymbol{T}_k$. With the "better" $\tilde{\boldsymbol{H}}_k$, we can rewrite the

model in Eq. (4.9) as

$$\boldsymbol{y}_k = \dot{\boldsymbol{H}}_k \boldsymbol{T}_k \boldsymbol{T}_k^{-1} \boldsymbol{s}_k + \boldsymbol{w}_k = \tilde{\boldsymbol{H}}_k \boldsymbol{z}_k + \boldsymbol{w}_k, \tag{4.10}$$

where we recognize $\boldsymbol{z}_k$ as the lattice-reduced-domain information symbols. Due to the fact that entries of $\boldsymbol{s}_k$ are from $\mathbb{Z}_j$ and $\boldsymbol{T}_k$ is unimodular, entries of $\boldsymbol{z}_k$ remain in $\mathbb{Z}_j$. Given matrices $\boldsymbol{A}_k$ and $\boldsymbol{T}_k$, the optimum $\tilde{\boldsymbol{G}}_k$ to minimize MSE of $\boldsymbol{z}_k$ is computed as

$$\tilde{\boldsymbol{G}}_k = (\tilde{\boldsymbol{H}}_k^H \tilde{\boldsymbol{H}}_k + \sigma_w^2 \boldsymbol{R}_z^{-1})^{-1} \tilde{\boldsymbol{H}}_k^H \tag{4.11}$$

where $\boldsymbol{R}_z = E(\boldsymbol{z}_k \boldsymbol{z}_k^H)$. The estimation error $\boldsymbol{z}_k - \hat{\boldsymbol{z}}_k$ has autocorrelation matrix as (see [65])

$$\tilde{\boldsymbol{R}}_e = \boldsymbol{T}_k^{-1} \boldsymbol{R}_e (\boldsymbol{T}_k^{-1})^H. \tag{4.12}$$

Because the ELR algorithm in [43] reduces the MSEs of $\boldsymbol{z}_k$ and $\boldsymbol{z}_k$ and $\boldsymbol{s}_k$ form an one-to-one mapping relationship, lower sum of the MSEs is achieved.

The optimization problem in lattice-reduced domain for each user is formally formulated as:

$$\begin{aligned} \min_{\boldsymbol{A}_k, \tilde{\boldsymbol{G}}_k, \boldsymbol{T}_k} \quad & E \parallel \boldsymbol{z}_k - \tilde{\boldsymbol{G}}_k (\check{\boldsymbol{H}}_k \boldsymbol{A}_k \boldsymbol{T}_k \boldsymbol{z}_k + \boldsymbol{w}_k) \parallel^2 \\ & tr(\sigma_s^2 \boldsymbol{A}_k \boldsymbol{A}_k^H) \leq P_k, \\ & \boldsymbol{T}_k \in GL_{r_k}(\mathbb{Z}_j) \end{aligned} \tag{4.13}$$

where $GL_n(\mathbb{Z}_j)$ represents the group of $n \times n$ unimodular matrices, and $\boldsymbol{z}_k = \boldsymbol{T}_k^{-1} \boldsymbol{s}_k$.

We then apply the alternating algorithm in [65] to solve the above problem. Since in [65] it is shown that usually one iteration is able to produce a converged result, we set the maximum iteration number to one in our proposed design. Thus for every user, after one iteration of the alternating algorithm, we get matrices $\boldsymbol{A}_k$, $\boldsymbol{T}_k$ and $\tilde{\boldsymbol{G}}_k$. Then, $\boldsymbol{F}_k$ equals $\bar{\boldsymbol{V}}_k^{(0)} \boldsymbol{A}_k$ or $\boldsymbol{Q}_k \boldsymbol{A}_k$ depending on whether we use BD or GZI.

To summarize, with MUI elimination and parallel optimization, we have decomposed the MU-MIMO system into N_u parallel SU-MIMO systems and designed for every user the precoding matrix $\boldsymbol{F}_k$, the decoding matrix $\tilde{\boldsymbol{G}}_k$, and the lattice-reduced-domain transformation matrix $\boldsymbol{T}_k$. The input-output model for the k-th UE is

$$\boldsymbol{y}_k = \boldsymbol{H}_k\boldsymbol{F}_k\boldsymbol{T}_k\boldsymbol{T}_k^{-1}\boldsymbol{s}_k + \boldsymbol{w}_k = \boldsymbol{H}_k\boldsymbol{F}_k\boldsymbol{T}_k\boldsymbol{z}_k + \boldsymbol{w}_k. \tag{4.14}$$

Upon receiving $\boldsymbol{y}_k$, the k-th UE estimates $\boldsymbol{z}_k$ as $\hat{\boldsymbol{z}}_k = \mathcal{Q}(\tilde{\boldsymbol{G}}_k\boldsymbol{y}_k)$, and $\hat{\boldsymbol{z}}_k$ is transformed back to the original symbol domain via $\hat{\boldsymbol{s}}_k = \boldsymbol{T}_k\hat{\boldsymbol{z}}_k$. Once again, we emphasis that because matrix $\boldsymbol{A}_k$ is different in dimension for BD and GZI, BD-based design and GZI-based design will have different performance and complexity.

Finally, the details of our proposed algorithm for the MU-MIMO system is shown in Table 4.5. At (S6) of Table 4.5, $\boldsymbol{A}_k^{(0)}$ is initialized as a scaled identity matrix whose scaling factor is chosen to satisfy the per user transmit power constraint and whose dimensions are chosen to work with matrix $\check{\boldsymbol{H}}_k$ and vector $\boldsymbol{s}_k$. At (S7), ELR algorithm is applied to the extended matrix $\bar{\boldsymbol{H}}_k$ (see [107, 65]).

Table 4.5: Proposed algorithm for LR-aided joint MU-MIMO transceiver optimization [99, Table I]

Input: $\boldsymbol{H}_1, \boldsymbol{H}_2, \cdots, \boldsymbol{H}_{N_u}, \sigma_s^2, \sigma_w^2$ **Output:** $\boldsymbol{F}_1, \boldsymbol{F}_2, \cdots, \boldsymbol{F}_{N_u}, \tilde{\boldsymbol{G}}_1, \tilde{\boldsymbol{G}}_2, \cdots, \tilde{\boldsymbol{G}}_{N_u}, \boldsymbol{T}_1, \boldsymbol{T}_2, \cdots, \boldsymbol{T}_{N_u}$		
(S1)	**If BD is used:** $[\bar{\boldsymbol{V}}_1^{(0)}, \bar{\boldsymbol{V}}_2^{(0)}, \cdots, \bar{\boldsymbol{V}}_{N_u}^{(0)}] = BD[\boldsymbol{H}_1, \boldsymbol{H}_2, \cdots, \boldsymbol{H}_{N_u}]$	$N_u\,(4N_t^2(N_r-m) + 13(N_r-m)^3)$
(S2)	**If GZI is used:** $[\boldsymbol{Q}_1, \boldsymbol{Q}_2, \cdots, \boldsymbol{Q}_{N_u}] = GZI[\boldsymbol{H}_1, \boldsymbol{H}_2, \cdots, \boldsymbol{H}_{N_u}]$	$\frac{11}{3}N_t^3 + \frac{5}{3}N_t^2 + N_u \cdot 2m^2(N_t - \frac{1}{3}m)$
(S3)	For k = 1 to N_u	
(S4)	**If BD is used:** $\check{\boldsymbol{H}}_k = \boldsymbol{H}_k\bar{\boldsymbol{V}}_k^{(0)}$	$2mN_t(N_t - N_r + m)$
(S5)	**If GZI is used:** $\check{\boldsymbol{H}}_k = \boldsymbol{H}_k\boldsymbol{Q}_k$	$2m^2N_t$
(S6)	Initialize: $\boldsymbol{A}_k^{(0)} = [P_k^{1/2}\sigma_s^{-1}r_k^{-1/2}\boldsymbol{I}_{r_k}, \boldsymbol{0}_{r_k\times(size(\check{\boldsymbol{H}}_k,2)-r_k)}]^T$	
(S7)	$\bar{\boldsymbol{H}}_k = \left[\check{\boldsymbol{H}}_k\boldsymbol{A}_k^{(0)}; \frac{\sigma_n}{\sigma_s}\boldsymbol{I}_{r_k}\right]$	$2m^2 \cdot size(\check{\boldsymbol{H}}_k, 2)$
(S8)	$[\tilde{\boldsymbol{H}}_k, \boldsymbol{T}_k]$ = ELR($\bar{\boldsymbol{H}}_k$)	$4m^3 + \frac{4}{3}m^3 + 20m\cdot$(number of basis updates)
(S9)	Obtain $\boldsymbol{A}_k$	$\mathcal{O}(\max(size(\check{\boldsymbol{H}}_k, 2), m)^3)$
(S10)	$\tilde{\boldsymbol{G}}_k = (\boldsymbol{T}_k^H\boldsymbol{A}_k^H\check{\boldsymbol{H}}_k^H\check{\boldsymbol{H}}_k\boldsymbol{A}_k\boldsymbol{T}_k + \sigma_w^2\boldsymbol{R}_z^{-1})^{-1}\boldsymbol{T}_k^H\boldsymbol{A}_k^H\check{\boldsymbol{H}}_k^H$	$\mathcal{O}(\max(size(\check{\boldsymbol{H}}_k, 2), m)^3)$
(S11)	**If BD is used:** $\boldsymbol{F}_k = \bar{\boldsymbol{V}}_k^{(0)}\boldsymbol{A}_k$	$2mN_t(N_t - N_r + m)$
(S12)	**If GZI is used:** $\boldsymbol{F}_k = \boldsymbol{Q}_k\boldsymbol{A}_k$	$2m^2N_t$
(S13)	end	

4.2.1 Complexity analysis

In this section, we analyze the complexity of our proposed design by evaluating the number of complex arithmetic operations. In the complexity analysis, we assume the number of receive antennas to be the same for N_u users, i.e., $N_{r_k} = m$ for all k, and the number of streams each user receives to be the same as the number of receive antenna, i.e., $r_k = N_{r_k} = m$ for all k. The complexity of the MUI elimination step is determined by the complexity of BD or GZI. From [64], the number of complex arithmetic operations required is

$$N_u \left(4N_t^2(N_r - m) + 13(N_r - m)^3\right) \tag{4.15}$$

for BD, and

$$\frac{11}{3}N_t^3 + \frac{5}{3}N_t^2 + N_u \cdot 2m^2(N_t - \frac{1}{3}m) \tag{4.16}$$

for GZI. The complexity of other steps of our algorithm is shown on the right part of Table 4.5. For the ELR algorithm [43], $4m^3$ and $\frac{4}{3}m^3$ arithmetic operations are required at initialization to compute the gram matrix of $\bar{\boldsymbol{H}}_k$ and the inverse of gram matrix. Then, around $20m$ complex arithmetic operations are required per basis update. From Table II of [43], for an $m \times m$ matrix $\boldsymbol{A}$ with IID Rayleigh variable entries, the average number of basis updates is approximately m. Though the entries of matrix $\bar{\boldsymbol{H}}_k$ is not IID Rayleigh, we anticipate the average number of basis update to be close to the first order of m. The complexity of our design will be further analyzed through simulations in the next section.

4.2.2 Numerical results

In this section, we compare the error performance and complexity of our proposed design (BD-LR-J, GZI-LR-J) with several existing schemes: BD with linear MMSE receiver at each UE (BD) [59], BD combined with conventional joint transceiver design that minimizes sum of MSEs (BD-J) [66], successive minimum mean-squared error (SMMSE) pre-

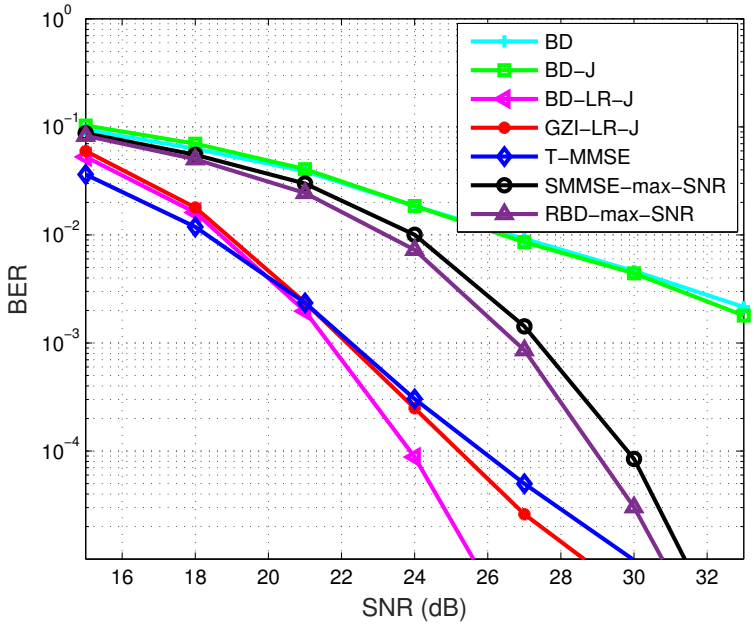

Figure 4.3: BER performance, where $N_t = 24$, $N_{r_k} = r_k = 4$, 6 users, 4QAM.

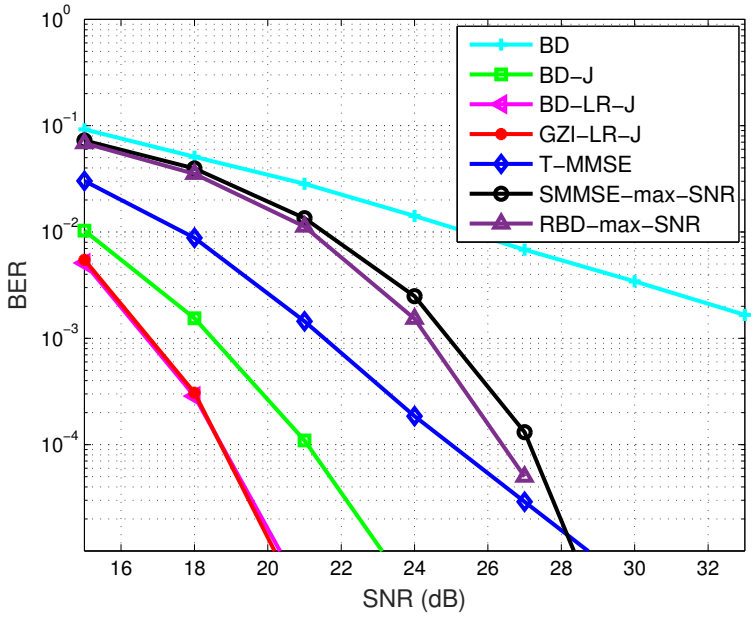

Figure 4.4: BER performance, where $N_t = 28$, $N_{r_k} = r_k = 4$, 6 users, 4QAM.

coding combined with maximum SNR design (SMMSE-max-SNR) [62], regularized block diagonalization (RBD) combined with maximum SNR design (RBD-max-SNR) [63], and minimum total MMSE design (T-MMSE) [56]. Channel coefficients of each user's channel $\boldsymbol{H}_k$ are modeled as IID complex Gaussian variables with zero mean and unit variance,

Table 4.6: (a) Average computational complexity (10^6) for computing precoding and decoding matrices with $N_t = 32$ and 6 users. (b) Average computational complexity (10^6) for computing precoding and decoding matrices with $N_{r_k} = 4$ and 6 users.

	2	3	4	5
BD-LR-J	1.46	1.19	1.36	1.94
GZI-LR-J	0.13	0.14	0.16	0.20
BD-J	1.45	1.18	1.34	1.91
T-MMSE	3.97	5.41	6.05	7.08
SMMSE-max-SNR	1.06	1.97	3.12	4.53
RBD-max-SNR	0.80	1.15	1.67	2.43

(a)

	24	26	28	30	32
BD-LR-J	0.93	1.01	1.10	1.21	1.36
GZI-LR-J	0.09	0.11	0.12	0.14	0.16
BD-J	0.92	0.99	1.08	1.19	1.34
T-MMSE	2.66	3.34	4.12	5.02	6.05
SMMSE-max-SNR	1.61	1.93	2.29	2.69	3.12
RBD-max-SNR	1.16	1.27	1.39	1.52	1.67

(b)

and SNR $= 10\log_{10}\left(\frac{P_{total}}{\sigma_n^2}\right)$. For BD, BD-J and our proposed BD/GZI-LR-J, we assume that transmit power is equally allocated to all users. For SMMSE-max-SNR, RBD-max-SNR and T-MMSE, power allocation schemes among users are already included in those designs. Figure 4.3 shows the error performance of the algorithms above for $N_t = 24$, $N_{r_k} = r_k = 4$, 6 users, $4QAM$. The maximum number of iteration is set to be 150 for T-MMSE. BD-LR-J achieves the best BER performance than the other schemes, showing more than 3dB gain than the others when BER = 10^{-5}. In Figure 4.4, when the number of transmit antennas increases, all schemes except BD enjoy performance improvement, and BD-LR-J/GZI-LR-J enjoys approximately 3 dB gain over BD-J when BER = 10^{-5}.

Now we plot the average total number of complex arithmetic operations required to calculate the precoding matrices $\boldsymbol{F}_k$ and decoding matrices $\boldsymbol{G}_k$ (for BD/GZI-LR-J, also the LR domain transformation matrices $\boldsymbol{T}_k$) for each design except for BD. The maximum number of iteration is set to 5 for T-MMSE and SNR is set to 25dB. First, we fixed the number of transmit antennas to be 32 and varies the number receive antennas (m) per user. In Table 4.6(a), the iterative scheme T-MMSE has the highest complexity. The complexity of BD-LR-J decreases and then increases with number of antennas per UE, because its complexity is an interplay of $N_t - N_r + m$ and m. The complexity of GZI-LR-J increases with the number of antennas per UE, and remains lowest most of the time among all the com-

pared schemes. Next, we fixed the number of receive antennas per UE to be 4 and varies the number transmit antennas. In Table 4.6(b), T-MMSE still has the highest complexity, and the complexity of GZI-LR-J remains the lowest among all the considered schemes.

4.3 Chapter summary

In this chapter, first, we proposed PELR-aided detectors for STCM systems at large MIMO dimensions. By utilizing the symmetric property of the equivalent channel matrix, the proposed detectors reduced approximately half of the complexity of the ELR-aided detectors. With similar complexity, the PELR-aided detectors achieve better BER compared to other state-of-the-art detectors. Then, we present a linear joint transceiver design for MU MIMO downlink system using LR algorithms. In pursuit of a low complexity design, we first completely eliminate MUI using existing methods (e.g., BD or GZI), and then for each user, we formulate a transceiver optimization problem in lattice-reduced domain with the goal of minimizing sum of the MSEs of information symbols, and solve it sub-optimally using LR algorithms. The advantages of our proposed design in terms of performance and complexity are demonstrated through numerical simulations.

In the next chapter, we delve into the details of LR algorithm and design learning-based LR algorithms.

CHAPTER 5
LEARNING-BASED LR ALGORITHMS

In this chapter, utilizing RL techniques, we design LR algorithms that learn to efficiently reduce channel matrices according to pre-defined objectives, through trial-and-error interactions with the channel matrices.

5.1 Reinforcement learning (RL)

Certain decision problems can be formulated using a Markov decision process (MDP) framework, where an agent acts in an environment represented by states and gets feedback from the environment through a reward signal. When the state transition model and reward function are known, MDPs can be solved by dynamic programming techniques such as policy iterations or value iterations. In reality, the transition model and reward function are most likely unknown. Thus, RL algorithms are used to learn a sequence of actions to optimize certain accumulated rewards, based on trial-and-error interactions with the environment. Its policy is represented by a table or a function approximator (e.g., neural networks) and updated as learning goes on.

5.2 RL-based LR algorithms

There are many similarities between an RL agent and an LR algorithm. LR carries out a sequence of elementary column operations to reduce a matrix. The column operations is solely based on the channel matrix, which can be viewed as the environment. Based on these similarities, an RL framework is proposed to solve the LR problem, shown in Figure 5.1. Using this framework, we then propose various RL-based LR algorithms, which differ in their objective, action space and reward functions. We explore three objectives:

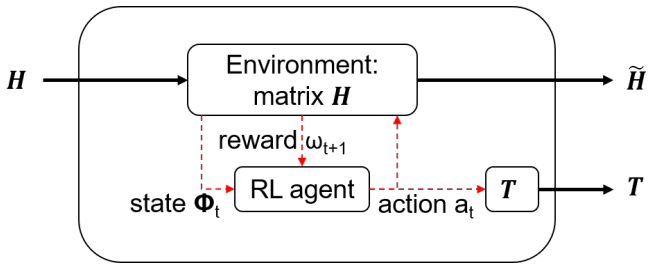

Figure 5.1: RL-based LR algorithms.

- Minimize the od in (2.24);
- Minimize the Seysen metric $SA(\boldsymbol{H})$ in (2.30);
- Minimize the largest diagonal element of the noise covariance matrix $\boldsymbol{C} = (\boldsymbol{H}^H \boldsymbol{H})^{-1}$.

Now we explain the definitions of state, action, and reward in detail.

5.2.1 The states

A state vector $\boldsymbol{\phi}$ captures the characteristics of the environment in an RL problem, which, in our case, is the channel matrix $\boldsymbol{H}$. To reduce the length of the state vector, we set it to be the real and imaginary parts of the upper triangular entries of Gram matrix $\boldsymbol{G} = \boldsymbol{H}^H \boldsymbol{H}$. Thus, a state vector $\boldsymbol{\phi}$ has a length of N_t^2. To handle the continuous state space, one usually uses either function approximation (e.g., tile coding, neural network) or state space discretization. We adopt state space discretization (based on distributions of the state values) as it enables simpler implementation. After that, we discretize the k-th element of a state vector into L_k levels, $k = 1, \cdots, N_t^2$, giving finer discretization to more frequent values. The total number of states is $\prod_{k=1}^{N_t^2} L_k$.

5.2.2 The actions

In general, an RL agent has a set of actions that it picks from at each state. We define an action as picking out an index pair (m, n), $1 \leq m, n \leq N_t$ and $m \neq n$, and update the m-th

column with the n-th column as

$$\tilde{\boldsymbol{h}}_m \leftarrow \tilde{\boldsymbol{h}}_m + \lambda_{m,n}\tilde{\boldsymbol{h}}_n, \tag{5.1}$$

$$\tilde{\boldsymbol{t}}_m \leftarrow \tilde{\boldsymbol{t}}_m + \lambda_{m,n}\tilde{\boldsymbol{t}}_n. \tag{5.2}$$

$\lambda_{m,n}$ is computed according to the following three sets of actions:

- $\mathcal{A}_{sy}$ (base on Seysen metric):

$$\lambda_{m,n} = -\left\lceil 0.5\left(\frac{\tilde{\boldsymbol{\alpha}}_n^T\tilde{\boldsymbol{\alpha}}_m^*}{\|\tilde{\boldsymbol{\alpha}}_m\|^2} - \frac{\tilde{\boldsymbol{h}}_n^H\tilde{\boldsymbol{h}}_m}{\|\tilde{\boldsymbol{h}}_n\|^2}\right)\right\rfloor; \tag{5.3}$$

- $\mathcal{A}_{elr}$ (base on noise covariance matrix):

$$\lambda_{m,n} = \left\lceil \frac{C_{m,n}^*}{C_{m,m}} \right\rfloor; \tag{5.4}$$

- $\mathcal{A}_{sr}$ (base on size reduction):

$$\lambda_{m,n} = -\left\lceil \frac{\tilde{\boldsymbol{h}}_n^H\tilde{\boldsymbol{h}}_m}{\|\tilde{\boldsymbol{h}}_n\|^2} \right\rfloor. \tag{5.5}$$

Note that $\lambda_{m,n}$ might be zero. In that case, that action happens to have no effect on the channel matrix. The cardinality of the action set is $N_t(N_t - 1)$.

5.2.3 The rewards

We have defined an agent that interacts with the environment by taking actions at discrete time step t. Now we introduce the definition of reward ω, a feedback signal from the environment in response to the agent's action a at state $\boldsymbol{\phi}$. To achieve different objectives, we design reward differently. Here we provide three reward functions.

- $\mathcal{RW}_{od}$:This reward reflects the amount of reduction of od and is defined as

$$\omega_{t+1} = \frac{od(\boldsymbol{H}_t) - od(\boldsymbol{H}_{t+1})}{od(\boldsymbol{H}_{t+1}) + \epsilon}, \tag{5.6}$$

  where ϵ is a small constant (e.g., 10^{-8}) to avoid a zero denominator.

- $\mathcal{RW}_{sy}$:This reward depends on the reduction of Seysen metric and is defined as

$$\omega_{t+1} = SA(\boldsymbol{H}_t) - SA(\boldsymbol{H}_{t+1}). \tag{5.7}$$

- $\mathcal{RW}_{elr}$:This reward depends on the noise covariance matrix and is defined as

$$\omega_{t+1} = (C_{m,m})_t - (C_{m,m})_{t+1}\,. \tag{5.8}$$

5.2.4 Improving learning speed

To increase the learning speed of the RL agent, we propose "action set pruning" and "learning with supervision".

Action set pruning

We have previously seen that an action a may have no effect on channel matrix at time step t when $(\lambda_{m,n})_t = 0$. Therefore, it is of no use to take action a again at $t+1$. On the other hand, if $(\lambda_{m,n})_t \neq 0$, then $(\lambda_{m,n})_{t+1} = 0$. In either case, we do not want to take action a again since we know it will not have effect at $\boldsymbol{\phi}_{t+1}$. Thus, we propose using a set $\mathcal{S}_u$ to keep temporary "useless" actions and to prune the action set properly at each time step. We always choose actions from action set minus those in $\mathcal{S}_u$. The algorithm to manage this set is given in Table 5.1. A learning episode (i.e., one sequence of reductions) terminates when the size of $\mathcal{S}_u$ equals size of the action set.

Learning with supervision

We allow RL agent to learn from existing LR algorithms (see e.g., [108]). Specifically, during training, the RL agent is given the information on how the existing LR algorithms would act, so that the RL agent can learn those actions first.

Table 5.1: Manage the set of temporarily "useless" actions

Output: $\mathcal{S}_u$, **Input:** $\mathcal{S}_u$, N_t	
(S1)	**if** $\lvert\mathcal{S}_u\rvert == N_t(N_t-1)$
(S2)	terminate current learning episode
(S3)	**else**
(S4)	choose a_t from actions not in $\mathcal{S}_u$
(S5)	**end**
(S6)	**if** $(\lambda_{m,n})_t == 0$
(S7)	add a_t into $\mathcal{S}_u$
(S8)	**else**
(S9)	$\mathcal{S}_u = \{a_t\}$
(S10)	**end**

5.2.5 Value-based RL

We adopt value-based RL algorithms, which have been successfully applied to solve problems of moderate size, such as improving performance of TCP (see e.g., [109, 110]). In value-based RL, an agent learns the value of a state-action pair $(\boldsymbol{\phi}, a)$, denoted as $\mathbb{Q}(\boldsymbol{\phi}, a)$, which represents the value of being in state $\boldsymbol{\phi}$ and performs an action a, and acts optimally ever after. Denote the learned value function as $\hat{\mathbb{Q}}(\boldsymbol{\phi}, a)$. At the start of training, the learned value function over all state-action pairs is initialized (to zeros, random values, etc). It is then updated at each time step based on the interaction between the RL agent and the environment. We adopt a temporal difference learning algorithm SARSA [111] to update the estimated value function, i.e.,

$$\hat{\mathbb{Q}}(\boldsymbol{\phi}_t, a_t) \xleftarrow{\alpha_t} \omega_{t+1} + \gamma_d \hat{\mathbb{Q}}(\boldsymbol{\phi}_{t+1}, a_{t+1}), \tag{5.9}$$

where $x \xleftarrow{\alpha_t} y$ means $x = (1-\alpha_t)x + \alpha_t y$, α_t is the learning rate as a function of time step t, and $\gamma_d \in (0, 1]$ is the discount factor that discounts future rewards. Assuming the learned value function is close enough to the true $\mathbb{Q}(\boldsymbol{\phi}, a)$, the best action at state $\boldsymbol{\phi}$ is given by

$$a = \arg\max_{a'} \hat{\mathbb{Q}}(\boldsymbol{\phi}, a'). \tag{5.10}$$

To balance exploration and exploitation (E2), we adopt the epsilon-greedy strategy, which means that among the actions not in the set $\mathcal{S}_u$, we explore a random action with probability ϵ_x, and otherwise stick to the best action currently known. The RL-based LR algorithm is given in Table 5.2. Finally, based on the combinations of the action and reward, we propose four RL-based LR algorithms:

- RL-SY, which uses action set $\mathcal{A}_{sy}$ and reward function $\mathcal{RW}_{sy}$;
- RL-YOD, which uses action set $\mathcal{A}_{sy}$ and reward function $\mathcal{RW}_{od}$;
- RL-ELR, which uses action set $\mathcal{A}_{elr}$ and reward function $\mathcal{RW}_{elr}$;
- RL-SR, which uses action set $\mathcal{A}_{sr}$ and reward function $\mathcal{RW}_{od}$.

5.3 Complexity analysis

The complexity of the RL-based LR algorithms mainly comes from two parts. The first part is regular DSP logic, including matrices updates and rewards computing. The second part is RL, including state quantization, action selection, and value function update. First we consider the DSP part. For state representation and simpler computation of $\lambda_{m,n}$ in Eqs. (5.5), (5.3), and (5.4), Gram matrix $\boldsymbol{G} = \boldsymbol{H}^H\boldsymbol{H}$, inverse Gram matrix $\boldsymbol{C} = (\boldsymbol{H}^H\boldsymbol{H})^{-1}$, and matrix $\boldsymbol{T}$ are maintained and updated during reduction. Updating them takes about $24N_t$ real arithmetic operations due to the symmetric structure of $\boldsymbol{G}$ and $\boldsymbol{C}$. Computing $\lambda_{m,n}$ and rewards in Eqs. (5.6), (5.7), and (5.8) cost $\mathcal{O}(1)$ real arithmetic operation. Next we

Table 5.2: The learning process of RL-based LR algorithm over n channel realizations

Procedure name: RL	
Output: value function $\mathbb{Q}(\cdot)$, **Input:** $N_r, N_t, \boldsymbol{H}^{(1)}, \boldsymbol{H}^{(2)}, \cdots, \boldsymbol{H}^{(nchn)}$	
(S1)	initialize ϵ_x, γ_d, α_t
(S2)	initialize action set and state set
(S3)	initialize value function $\mathbb{Q}(\cdot)$
(S4)	**for** $k = 1 : nchn$
(S5)	$[\tilde{\boldsymbol{H}}^{(k)}, \boldsymbol{T}^{(k)}] =$ RL-H$(\boldsymbol{H}^{(k)}, \epsilon_x, \gamma_d, od_{th})$
(S6)	**end**
Procedure name: RL-H	
Output: $\tilde{\boldsymbol{H}}, \boldsymbol{T}$, **Input:** $\boldsymbol{H}$, ϵ_x, γ_d, od_{th}, **Global:** $\mathbb{Q}(\cdot)$	
(S1)	$\boldsymbol{H}_0 = \boldsymbol{H}, \boldsymbol{T}_0 = \boldsymbol{I}$. $od = od(\boldsymbol{H}_0)$.
(S2)	$t = 0$
(S3)	**if** $od > od_{th}$
(S4)	s_t = get_state$(\boldsymbol{H}_t)$, $\mathcal{S}_u = \{\}$. $a_t =$ epsilon-greedy$(\boldsymbol{\phi}_t, \mathbb{Q}, \mathcal{S}_u)$.
(S5)	**while** (1)
(S6)	$[m, n] =$ get_columns(a_t), compute $\lambda_{m,n}$
(S7)	**if** $\lambda_{m,n} \neq 0$
(S8)	get $\boldsymbol{H}_{t+1}, \boldsymbol{T}_{t+1}$ as Eqs. (5.1), (5.2)
(S9)	$\mathcal{S}_u = \{a_t\}$
(S10)	**else**
(S11)	add a_t into $\mathcal{S}_u$
(S12)	**end**
(S13)	**if** $\lvert\mathcal{S}_u\rvert == N_t(N_t - 1)$
(S14)	break
(S15)	**else**
(S16)	$\boldsymbol{\phi}_{t+1} =$ get_state$(\boldsymbol{H}_{t+1})$
(S17)	$\omega_{t+1} =$ rw$(\boldsymbol{H}_{t+1}, \boldsymbol{H}_t)$
(S18)	$a_{t+1} =$ epsilon-greedy$(\boldsymbol{\phi}_{t+1}, \mathbb{Q}, \mathcal{S}_u)$
(S19)	$\mathbb{Q}(\boldsymbol{\phi}_t, a_t) \xleftarrow{\alpha_t} \omega_{t+1} + \gamma_d \mathbb{Q}(\boldsymbol{\phi}_{t+1}, a_{t+1})$
(S20)	$t = t + 1$
(S21)	**end**
(S22)	**end**
(S23)	**end**
(S24)	$\tilde{\boldsymbol{H}} = \boldsymbol{H}_t, \boldsymbol{T} = \boldsymbol{T}_t$

consider complexity of RL. Quantizing the RL state takes $\mathcal{O}(N_t^2)$. Action selection takes $\mathcal{O}(N_t^2)$. Value function update costs $\mathcal{O}(1)$. When learning process is sufficiently long, one can set learning rate α_t to zero, which means that rewards are no longer computed and value function no longer updated. In that case, RL complexity is further reduced.

5.4 Numerical results

We compare the BER and complexity of our proposed RL-based LR algorithms with the existing LR algorithms for MIMO detection. The existing LR algorithms include CLLL

($\delta_c = 0.75$) [33], a greedy implementation of the SA [97], and ELR [43]. For the default setup of RL-based LR algorithms, $od_{th} = 0.1$, discount factor $\gamma_d = 1$, learning rate $\alpha_t = 0.1$, and exploration factor $\epsilon_x = 0.1$. The elements of the state vector are discretized into L levels, i.e., $L_k = L, k = 1, \cdots, N_t^2$. For $N_r = N_t = 2, 3, 4$, $L = 100, 6, 2$ respectively. All LR algorithms work in conjunction with the MMSE-SIC (MSIC) detector. SD is used to provide BER benchmark. To compare the complexity of various LR algorithms, we adopt the real arithmetic operations. The following types of channel models are adopted: IID complex Gaussian channel, and spatially correlated complex Gaussian channel.

5.4.1 IID complex Gaussian channel

Figure 5.2 shows BER performance of SD, RL-SY, RL-YOD, RL-SR, RL-ELR, CLLL, SA, and ELR, at varying SNR, for 64 QAM, 4×4 MIMO. We see that SD achieves the lowest BER, while RL-SY and RL-YOD learn to perform similarly with CLLL and SA. RL-ELR outperforms ELR because it learns to carry out more basis update than ELR. On the other hand, RL-SR performs the worst among its comparisons under 4×4 MIMO. This shows that its action set has limitations in reducing channel matrix with MIMO size larger than two. Table 5.3 shows BER for various detectors with MIMO size varying from 2 to 4, at SNR 25dB. We see that CLLL performs slightly better than SA, RL-SY, and RL-YOD, which hold the same BER performance. RL-ELR performs better than ELR. RL-SR loses its performance at $N_r = N_t = 4$.

Table 5.4 shows number of real arithmetics for various LR algorithms with MIMO size varying from 2 to 4, at SNR 25dB. For learning-based LRs, we plot complexity from the DSP part. It is encouraging to see that learning-based LRs have lower DSP complexity than SA and CLLL, even at MIMO sizes of three and four, where limited discretization on value function degrades effect of learning. The savings in DSP complexity of RL-SY and RL-YOD, compared to SA, mainly come from not computing or updating Δ and λ for every pair of columns of the channel matrix during reductions. RL-ELR has similar or

Table 5.3: BER vs varying MIMO size, IID complex Gaussian channel, 64QAM, SNR = 25dB

	SD	SA	CLLL	ELR
$N_r = N_t = 2$	0.0013	0.0017	0.0017	0.0017
$N_r = N_t = 3$	$2.4083 * 10^{-4}$	$4.8120 * 10^{-4}$	$4.0229 * 10^{-4}$	$6.7673 * 10^{-4}$
$N_r = N_t = 4$	$3.5375 * 10^{-5}$	$1.5147 * 10^{-4}$	$1.2629 * 10^{-4}$	$3.4215 * 10^{-4}$
	RL-SY	RL-YOD	RL-SR	RL-ELR
$N_r = N_t = 2$	0.0017	0.0017	0.0017	0.0017
$N_r = N_t = 3$	$4.8830 * 10^{-4}$	$4.9367 * 10^{-4}$	$5.3557 * 10^{-4}$	$5.3598 * 10^{-4}$
$N_r = N_t = 4$	$1.5791 * 10^{-4}$	$1.4136 * 10^{-4}$	$8.1615 * 10^{-4}$	$2.2723 * 10^{-4}$

Table 5.4: Average number of real arithmetics operations vs varying MIMO size, IID complex Gaussian channel, 64QAM, SNR = 25dB

	CLLL	SA	ELR	RL-SY	RL-YOD	RL-SR	RL-ELR
$N_r = N_t = 2$	117.096	362.351	53.459	71.002	71.807	40.448	58.282
$N_r = N_t = 3$	488.298	1342.79	191.531	438.047	437.418	182.977	324.207
$N_r = N_t = 4$	1210.03	3097.10	414.305	1118.17	1239.13	475.698	871.395

higher complexity compared to ELR. But RL-ELR has better BER than ELR.

5.4.2 Spatially correlated complex Gaussian channel

In practice, MIMO channels are likely to be correlated, which affects the performance and complexity of LR-aided detectors [99]. We incorporate Kronecker correlation model in [102, 103] to describe the correlations between the faded envelopes of the MIMO sub-channels (see (3.1)). In the simulation, we set $\rho_t = \rho_r = 0.8$, $N_t = N_r = 2$. Figure 5.3 shows BER performance of various detectors for 64 QAM, from which we see that correlation at transmit and receive antennas degrades system BER performance. We also see that learning-based LR-aided detectors are able to learn to perform similarly compared to existing LR detectors. When comparing the DSP complexity in terms of real arithmetics of various LRs in Figure 5.4, we see that complexity of learning-based LR algorithms and existing LR algorithms suffers similarly with channel correlation. Thus, same as when channel is IID, RL-SR, RL-ELR, RL-SY and RL-YOD have lower DSP complexity than CLLL and SA, and RL-SR has the lowest DSP complexity among all.

5.4.3 What do RL-based LR algorithms learn?

By design, we expect an RL-based LR algorithm to learn to pick out the optimal two columns for reduction every time the RL-based LR algorithm "sees" a (partially reduced) channel matrix, in order to maximize sum of rewards before an episode terminates. The RL-based LR algorithm does so by learning the value of experiencing a channel matrix (state) and picking out two certain columns (action). In this section, we show the learning process of an RL-SY agent in 2×2 IID Rayleigh fading MIMO channels. For such MIMO channels, it is not hard to compute the optimal sequence of reduction for maximum reduction of Seysen metric. Also, due to action pruning with queue, the RL-SY agent only need to learn to perform an optimal first step. Therefore, we show how RL-SY learns to perform a right first step as it learns. Also, since we use tabular RL and discretize the value function into a value table, the level of discretization affects how well RL agent distinguishes between states and thus how well it learns.

In Figure 5.5, we plot the ratio of suboptimal decisions RL-SY performs as training time goes on, when various levels of discretization L are used. Here one unit of training time means 100 realizations of IID channel matrix. When $L = 10$, we see that the ratio of suboptimal decisions drops quickly as training starts (from training time 0 to 5), and oscillate between 0.28 and 0.29. This is partly because of the constant exploration factor ($\epsilon_x = 0.1$), which encourages the agent to explore actions that may be suboptimal. But the high suboptimal decision ratio is also due to the small L_k that limits the ability of the agent to distinguish channel matrices. By increasing the level of discretization L on value function from $L = 10$ to $L = 20$, we observe a reduce in suboptimal decision ratio. But further increase from $L = 20$ to $L = 40$ does not help. The reason may be the difficulty in learning a larger size value table. We also plot the effect of exploration rate ϵ_x on the ratio of suboptimal decisions in Figure 5.6. As training goes on, agents with smaller ϵ_x make less suboptimal decisions. Nevertheless, the relatively large suboptimal decision ratios in both Figures 5.5 and 5.6 implies the limitation of tabular RL.

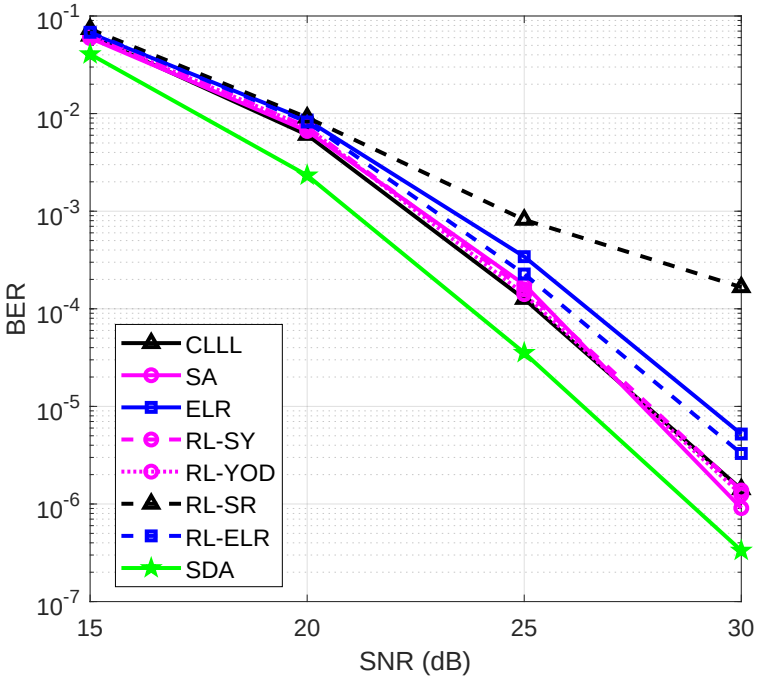

Figure 5.2: BER vs SNR, IID complex Gaussian channel, 64QAM, 4×4 MIMO

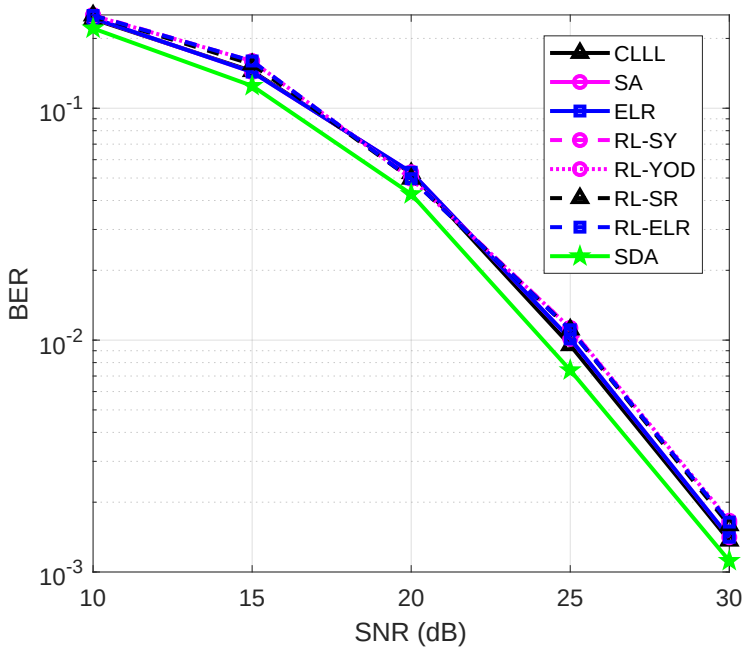

Figure 5.3: BER vs SNRdB, spatially correlated complex Gaussian channel, 64QAM, 2×2 MIMO, $\rho_t = \rho_r = 0.8$

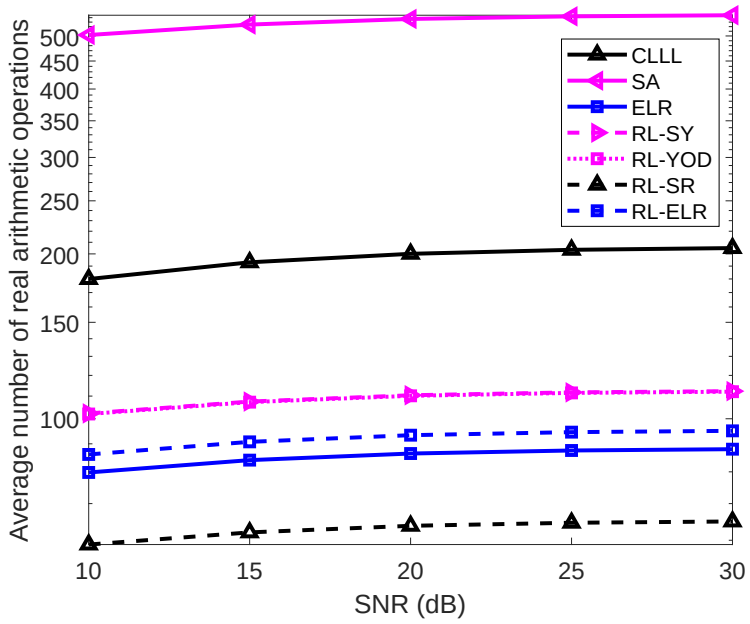

Figure 5.4: Average number of real arithmetics, for DSP, 2×2 spatially correlated complex Gaussian channel, 64QAM, $\rho_t = \rho_r = 0.8$

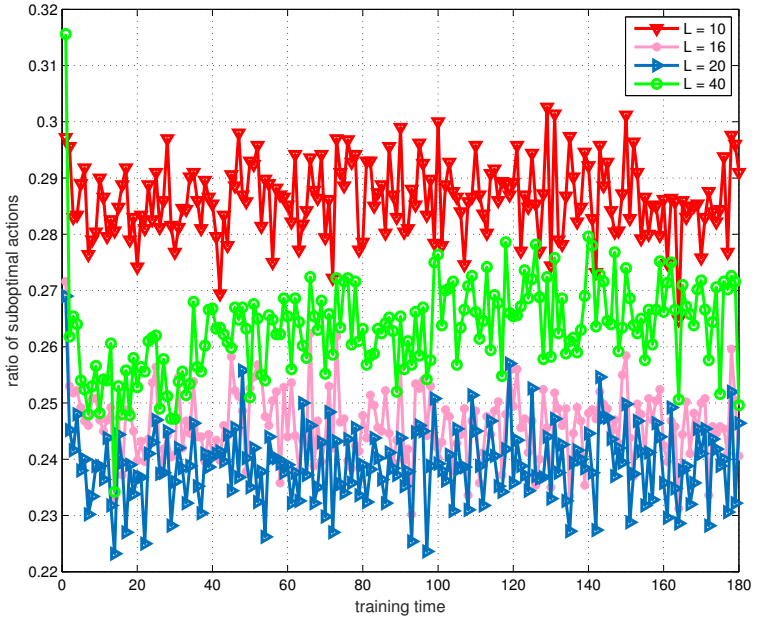

Figure 5.5: Effect of discretization level on learning of RL-SY. Training time is in the unit of every one hundred channel matrices, 2×2 MIMO.

5.5 Chapter summary

In this chapter, we proposed four RL-based LR algorithms, differing in their action set and reward combination. We demonstrated the possibility of having diverse "reduce criteria"

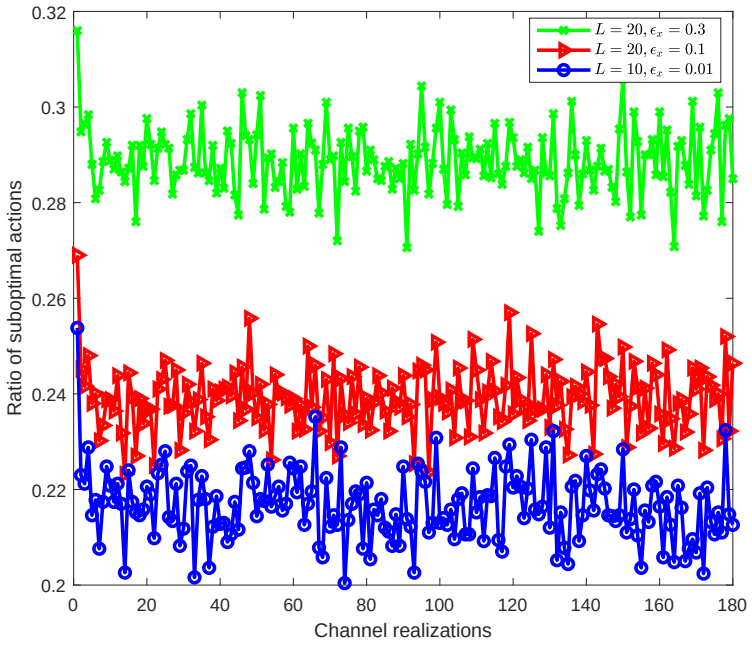

Figure 5.6: Effect of exploration factor on learning of RL-SY. Training time is in the unit of every one hundred channel matrices, 2×2 MIMO.

and then achieving reduction by an RL framework. We compared the BER and DSP complexity of RL-based LR-aided detectors with existing LR-aided detectors for up to 4×4 MIMO. Simulation results show that RL-based LR-aided detectors achieve similar BER as that of the existing LR-aided detectors. As for complexity, even when limited by small discretization level L (for 3×3 and 4×4 MIMO), the RL-based LR-aided detectors are able to achieve lower DSP complexity compared to existing LR-aided detectors, which showed the tradeoff between storage and computational complexity.

In the next chapter, we investigate the impact of size and propagation environment on channel quality and the performance of LDs in massive MIMO systems.

CHAPTER 6

OD OF MASSIVE MIMO CHANNELS: DISTRIBUTION AND RELATIONSHIP WITH PERFORMANCE

In this chapter, we examine the impact of massive MIMO size and propagation environment on the performance LDs. The content of this chapter is adopted from our publication [112].

6.1 Massive MIMO channel model

Consider a general spatial-multiplexing massive MIMO system with N_r receive and N_t transmit antennas ($N_r \gg N_t$). Such system model includes the single-user and some of the multi-user massive MIMO scenarios (see e.g., [113, 114]). The massive MIMO channel is assumed to be narrowband and denoted by an $N_r \times N_t$ matrix $\boldsymbol{H}$, where $H_{m,n}$ is the IID channel coefficient between the m-th receive and the n-th transmit antenna, $m = 1, \cdots, N_r$, and $n = 1, \cdots, N_t$. Moreover, $H_{m,n}$ is modeled by the complex Weibull distribution [115, 116], i.e.,

$$H_{m,n} = (X + jY)^{\frac{2}{c}}, \tag{6.1}$$

where X and Y are independent real Gaussian RVs with zero mean and one half variance, and the positive real number c is the Weibull parameter. We choose the Weibull distribution because of its excellence in modeling various propagation channels, including indoor and outdoor sub-6 GHz channels, as well as indoor mmWave channels [117, 118, 119]. The input-output relationship of the massive MIMO system is

$$\boldsymbol{y} = \boldsymbol{H}\boldsymbol{s} + \boldsymbol{w}, \tag{6.2}$$

where $\boldsymbol{s}$ is an $N_t \times 1$ signal vector, $\boldsymbol{y}$ is the $N_r \times 1$ receive vector, and $\boldsymbol{w}$ is an $N_r \times 1$ zero mean complex Gaussian noise with $E(\boldsymbol{w}\boldsymbol{w}^H) = {\sigma_w}^2 \boldsymbol{I}_{N_r}$. Next, we examine od and

its statistics as functions of N_r, N_t, and Weibull parameter c.

6.2 Statistics of od and performance of LDs

First, we derive the od of massive MIMO as N_r goes to infinity. Let $\boldsymbol{h}_k$ and $\boldsymbol{h}_p$ denote the k-th and p-th ($k \neq p$) columns of the channel matrix $\boldsymbol{H}$. We have

$$\lim_{N_r\to\infty} \frac{1}{N_r}\|\boldsymbol{h}_k\|^2 = E(|H_{m,n}|^2) = \Gamma(1+2/c), \tag{6.3}$$

$$\lim_{N_r\to\infty} \frac{1}{N_r}\boldsymbol{h}_k^H\boldsymbol{h}_p = |E(H_{m,n})|^2, \tag{6.4}$$

$$\lim_{N_r\to\infty} \frac{1}{N_r}\boldsymbol{H}^H\boldsymbol{H} = v_2\boldsymbol{I}_{N_t} + v_1\mathbf{1}\mathbf{1}^H, \tag{6.5}$$

where $\Gamma(z) = \int_0^\infty x^{z-1}e^{-x}dx$ is the Gamma function, $\mathbf{1}$ is an $N_t \times 1$ column vector of ones, $v_1 = |E(H_{m,n})|^2$, and $v_2 = E(|H_{m,n}|^2) - v_1$. Thus, given N_t,

$$\lim_{N_r\to\infty} od(\boldsymbol{H}) = 1 - \frac{v_2^{N_t}(1+v_1N_t/v_2)}{\Gamma(1+2/c)^{N_t}}. \tag{6.6}$$

When $2/c$ is a positive integer, $E(H_{m,n}) = 0$, and thus $v_1 = 0$, and $\lim_{N_r\to\infty} od(\boldsymbol{H}) = 0$. When $2/c$ is not an integer, $\lim_{N_r\to\infty} od(\boldsymbol{H})$ depends on the value of c and N_t. We sample three values of Weibull parameter c, $c = 2, 3.6, 1$, to model three different propagation channels. We examine the mean $E(\cdot)$ and variance $V(\cdot)$ of od as functions of N_r and N_t for these various propagation channels. As a result, we offer insights on the choice of massive MIMO size for LDs to achieve desirable performance.

6.2.1 Rayleigh fading ($c = 2$)

When $c = 2$, the massive MIMO channel has Rayleigh fading envelopes. From Eq. (6.6), $\lim_{N_r\to\infty} od(\boldsymbol{H}) = 0$. The mean and variance of od are given in [45]. Given N_t, $\lim_{N_r\to\infty} E(od) = 0$ and $\lim_{N_r\to\infty} V(od) = 0$. This confirms with [10, 11] that the massive MIMO channel with Rayleigh fading envelops offers asymptotically favorable prop-

agation. But when $N_t = N_r$, $\lim_{N_r \to \infty} E(od) = 1$ and $\lim_{N_r \to \infty} V(od) = 0$. Taking the derivative of $V(od)$ with respect to N_r, we notice that $V(od)$ decreases monotonically as N_r increases for small N_t (e.g., $N_t = 2$), while increases first and then decreases as N_r increases for large N_t. We did not show the plots of $E(od)$ and $V(od)$ for $c = 2$ because they are almost identical to those when $c = 1$.

6.2.2 LoS mmWave ($c = 3.6$)

Based on measurements in [119], we use $c = 3.6$ to denote an massive MIMO channel with mmWave LoS connections between each pairs of the transmit and receive antennas. From Eq. (6.6),

$$\lim_{N_r \to \infty} od(\boldsymbol{H}) = \begin{cases} 0.0845, & N_t = 2, \\ 0.7260, & N_t = 8, \\ 0.9998, & N_t = 32. \end{cases} \tag{6.7}$$

It means that this massive MIMO channel is non-orthogonal even when N_r goes to infinity. As shown in Figure 6.1, $E(od)$ of LoS mmWave massive MIMO decreases with increasing N_r and eventually converges to a non-zero value computed by Eq. (6.7). In Figure 6.2, we see that $E(od)$ increases as N_t increases. Given $N_r = 512$, we need to bound N_t by 18 so that $E(od) \leq 0.99$. In Figure 6.3, we plot $V(od)$ of the LoS mmWave massive MIMO. For $N_t = 2$, $V(od)$ decreases monotonically as N_r increases. But for large N_t, $V(od)$ increases first and then decreases as N_r increases.

6.2.3 Severely fading ($c = 1$)

When $c = 1$, Weibull distribution becomes the negative exponential distribution, which can be used to model a composite small-scale/shadowing fading, or a severely fading channel [119]. From Eq. (6.6), $\lim_{N_r \to \infty} od(\boldsymbol{H}) = 0$. Thus, severely fading massive MIMO becomes orthogonal as N_r goes to infinity. Shown in Figure 6.1, compared to the LoS mmWave channel, $E(od)$ of the severely fading channel is much smaller at the same mas-

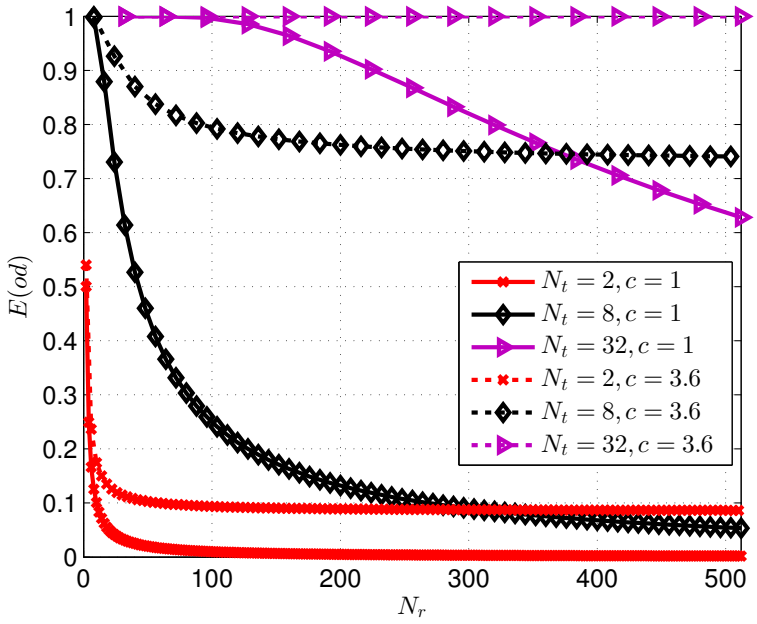

Figure 6.1: $E(od)$ vs. the number of receive antennas N_r, Weibull fading [112, Figure 1(a)]

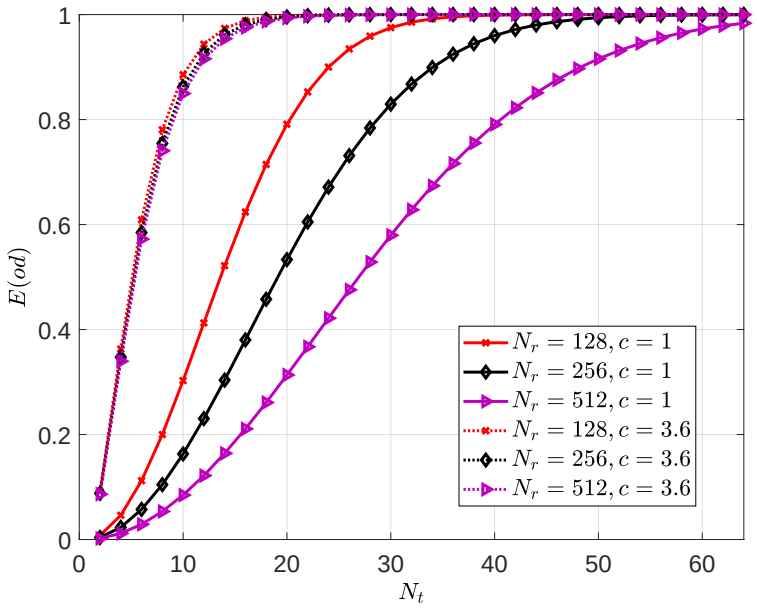

Figure 6.2: $E(od)$ vs. the number of transmit antennas N_t, Weibull fading [112, Figure 1(b)]

sive MIMO size. From Figure 6.2, we observe that when $N_r = 128, 256$, and 512, N_t should not exceed $34, 50$, and 70 in order to have $E(od) < 0.99$.

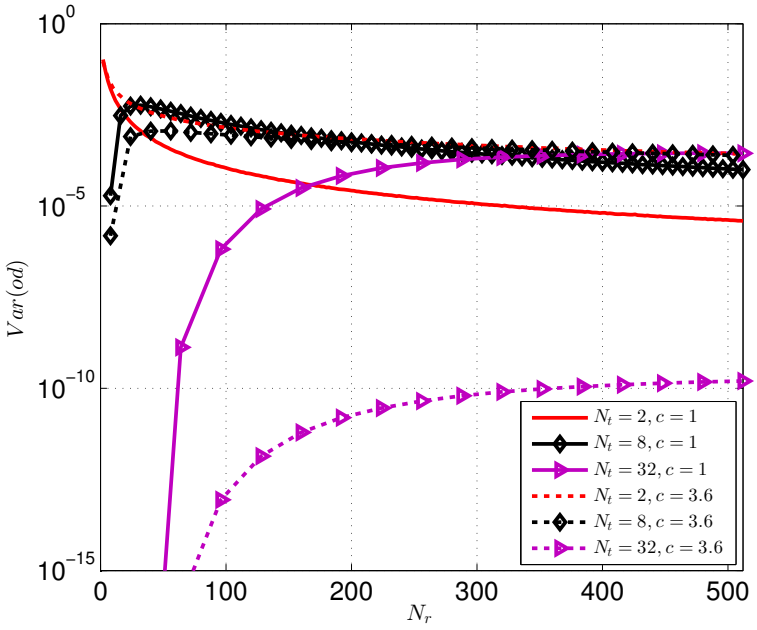

Figure 6.3: V(od) vs. the number of antennas N_r, Weibull fading [112, Figure 1(c)]

6.3 Distribution of od and diversity of LDs

In this section, we investigate the probability density function (pdf) of od for the massive MIMO channel and link it to the performance of LDs.

6.3.1 Distribution of od

First, we consider a partially Rayleigh fading case: channels of Weibull fading ($c \neq 2$) or random types of fading exist between N_r receive antennas and only one of the transmit antennas, and channels of Rayleigh fading exist between N_r receive antennas and the rest of the transmit antennas.

Proposition 4. *$\boldsymbol{H}$ is an $N_r \times N_t$ matrix with IID entries. The entries in its k-th column vector $\boldsymbol{h}_k$ are Weibull distributed with parameter c ($c \neq 2$), and the rest of its entries are*

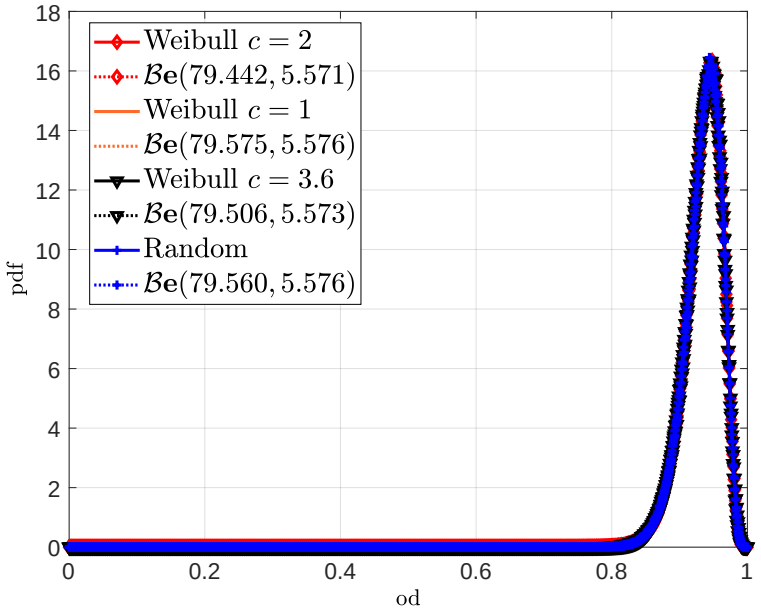

Figure 6.4: Distribution of od for IID fadings, $N_r = 20$ and $N_t = 10$ [112, Figure 2(a)]

$\mathcal{N}_c(0, 1)$. *Then the pdf of* $od(\boldsymbol{H})$ *is a scaled Meijer G-function,*

$$f(x) = \prod_{n=1}^{N_t-1} \frac{\Gamma(N_r)}{\Gamma(N_r - n)} \cdot G_{N_t-1,0}^{N_t-1,0}\left((1-x)\middle|\begin{matrix} N_r - 1, & \cdots, & N_r - 1 \\ N_r - 2, & \cdots, & N_r - N_t \end{matrix}\right), \tag{6.8}$$

where the Meijer G-function is defined in [120, p.374]. Furthermore, regardless of the distribution of $\boldsymbol{h}_k$*, the pdf of* $od(\boldsymbol{H})$ *is the one shown in Eq.* (6.8).

Proof: See Appendix C.1. ■

Figure 6.4 shows the distributions of $od(\boldsymbol{H})$ when a single column vector in the channel matrix $\boldsymbol{H}$ experiences Weibull or any other random fading, which is the same as the distribution of $od(\boldsymbol{H})$ when $\boldsymbol{H}$ has IID Rayleigh fading envelopes.

For more general cases, we investigate the approximate distribution of od. Beta distribution approximates the distribution of od well when the MIMO channel experiences Rayleigh fading [45], but does not fit well when the MIMO channel experiences more general fading. Especially, Beta distribution fails to fit the tail of the complementary cumulative distribution function ($ccdf$) of od. To better fit the distribution of od in general cases,

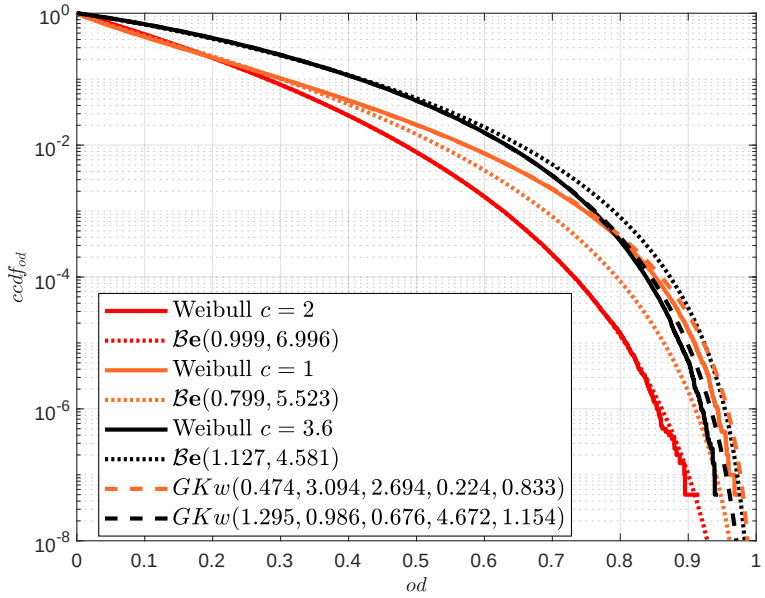

Figure 6.5: $ccdf$ of od, fit with Beta distribution, $N_r = 8$ and $N_t = 2$ [112, Figure 2(b)]

in this paper, we consider the generalized Kumaraswamy distribution (GKw) [121], which is a continuous distribution of five parameters (i.e., $\vartheta_1, \cdots, \vartheta_5$) on the interval $[0, 1]$. The pdf of GKw distribution is

$$GKw(x; \vartheta_1, \vartheta_2, \vartheta_3, \vartheta_4, \vartheta_5) = \frac{\vartheta_5 \vartheta_1 \vartheta_2 x^{\vartheta_1 - 1}}{B(\vartheta_3, \vartheta_4 + 1)} (1 - x^{\vartheta_1})^{\vartheta_2 - 1} \cdot \left(1 - (1 - x^{\vartheta_1})^{\vartheta_2}\right)^{\vartheta_3 \vartheta_5 - 1} \cdot \left(1 - \left(1 - (1 - x^{\vartheta_1})^{\vartheta_2}\right)^{\vartheta_5}\right)^{\vartheta_4}, \tag{6.9}$$

where $B(u, v) = \int_0^1 x^{u-1}(1 - x)^{v-1} dx$. When $\vartheta_1 = \vartheta_2 = \vartheta_5 = 1$, GKw reduces to the Beta distribution. Figure 6.5 shows that GKw fits $od(\boldsymbol{H})$ much better compared to Beta.

Result 1: The od of a general MIMO channel matrix with IID Weibull distribution can be modeled by GKw distribution as in Eq. (6.9).

In Table 6.1, we evaluate the goodness-of-fit (GOF) of GKw and Beta using three statistical methods (see also [122]): log likelihood (LogL), Bayesian information criteria (BIC), and residual sum of squares (RSS). When $c \neq 2$, GKw provides better GOF than Beta in all three metrics.

Table 6.1: Evaluating the GOF of GKw and Beta models via statistical methods on 5 datasets each containing 5×10^6 samples of od, where $(N_r, N_t) = (8, 2)$ [112, Table I]

Samples of od	Statistical methods	GKw	Beta
$c = 2$	LogL	5442600	$\mathbf{5442607}$
	BIC	1.088512×10^7	$\mathbf{1.088518 \times 10^7}$
	RSS	$\mathbf{1.6348 \times 10^{-4}}$	1.7965×10^{-4}
$c = 1$	LogL	$\mathbf{5434390}$	5403768
	BIC	$\mathbf{1.086870 \times 10^7}$	1.080750×10^7
	RSS	$\mathbf{1.69608 \times 10^{-3}}$	7.21654×10^{-1}
$c = 3.6$	LogL	$\mathbf{3314657}$	3306305
	BIC	$\mathbf{6.629236 \times 10^6}$	6.612579×10^6
	RSS	$\mathbf{1.27482 \times 10^{-3}}$	2.43866×10^{-1}
$c = 2.5$	LogL	$\mathbf{5369373}$	5369302
	BIC	$\mathbf{1.073866 \times 10^7}$	1.073857×10^7
	RSS	$\mathbf{2.4223 \times 10^{-4}}$	1.42534×10^{-3}
$c = 1.5$	LogL	$\mathbf{5404661}$	5404112
	BIC	$\mathbf{1.080924 \times 10^7}$	1.080819×10^7
	RSS	$\mathbf{4.4714 \times 10^{-4}}$	1.12555×10^{-2}

6.3.2 Diversity with probability

Given the GKw distribution of od, we know that the od of an massive MIMO system in model (6.1) will not be bounded by a number smaller than one. Thus, by Lemma 1, LD does not collect the same diversity as MLD when both N_r and N_t are finite. However, in practice, we only evaluate a detector during a finite time interval. Based on a chosen communication standard, a finite observation interval may translate to a number of channel realizations. For example, with packet length in LTE standard, a time interval of 2.2 years corresponds to at most 10^{12} channel realizations. To quantify the diversity of LDs within a finite interval, we introduce *diversity with probability*.

Definition 5 (diversity with probability). *For a random channel $\boldsymbol{H}$, if $P(od(\boldsymbol{H}) \geq \epsilon_1) < \epsilon_2$, where $\epsilon_1, \epsilon_2 \in (0, 1)$, then LDs collect the same diversity as MLD does during n channel realizations with probability $p_d = (1 - \epsilon_2)^n$.*

In fact, p_d defines the probability of n channel realizations all having od smaller than ϵ_1. For example, if $\epsilon_2 = 10^{-14}$, $n = 10^{12}$, then $p_d = 0.99$. Now we find out the constraint

Table 6.2: Thresholds of N_r to collect full diversity for 2.2 years with $p_d = 0.99$ (estimated with linear interpolation) [112, Table II]

	$c=2$		$c=1$		$c=3.6$	
N_t	N_r	ϵ_1	N_r	ϵ_1	N_r	ϵ_1
2	**8**	0.99	**14**	0.99	**11**	0.99
4	**13**	0.99	**18**	0.99	**19**	0.99
8	**25**	0.99	**29**	0.99	**46**	0.99
16	**58**	0.99	**61**	0.99	**353**	0.999
32	**166**	0.99	**184**	0.99	**702**	$1-5\times10^{-10}$
64	**544**	0.99	**720**	0.99	**21873**	$1-10^{-14}$

on N_r given N_t and ϵ_1 to achieve $\epsilon_2 = 10^{-14}$. Given the pdf of od, the $ccdf$ of od is

$$P(od(\boldsymbol{H}) \geq \epsilon_1) = 1 - I_{\left(1-\left(1-\epsilon_1^{\vartheta_1}\right)^{\vartheta_2}\right)}^{\vartheta_5}(\vartheta_3, \vartheta_4 + 1), \tag{6.10}$$

where $I_x(u,v) = B(u,v)^{-1}\int_0^x w^{u-1}(1-w)^{v-1}dw$ is the incomplete Beta function ratio. In general, given the Weibull parameter c, Eq. (6.10) is a function of N_r and N_t. In Table 6.2, we estimate N_r so that for given ϵ_1 and N_t, $P(od(\boldsymbol{H}) \geq \epsilon_1) = 10^{-14}$ is satisfied. Given N_t, ϵ_1, and c, by using an N_r that exceeds the threshold shown in Table 6.2, LDs collect the full diversity as MLD does for 2.2 years with probability 0.99. Figure 6.6 numerically shows the same diversity achieved by ZF LD and MLD over 10^6 channel realizations.

6.4 Chapter summary

In this chapter, we study the performance of LDs in massive MIMO systems by investigating the od of massive MIMO channels. The Weibull distribution is adopted for modeling the envelope fading and various propagation channels are simulated by varying the Weibull parameter c. First, we study and compare the mean and variance of od as functions of N_r and N_t for various channels, and offer insights on the choice of massive MIMO size for LDs to perform desirably. Then, by modeling od using the GKw distribution, we estimate the thresholds of N_r (given the propagation channel and N_t) needed for LDs to collect the same diversity as the MLD does with high probability in practice.

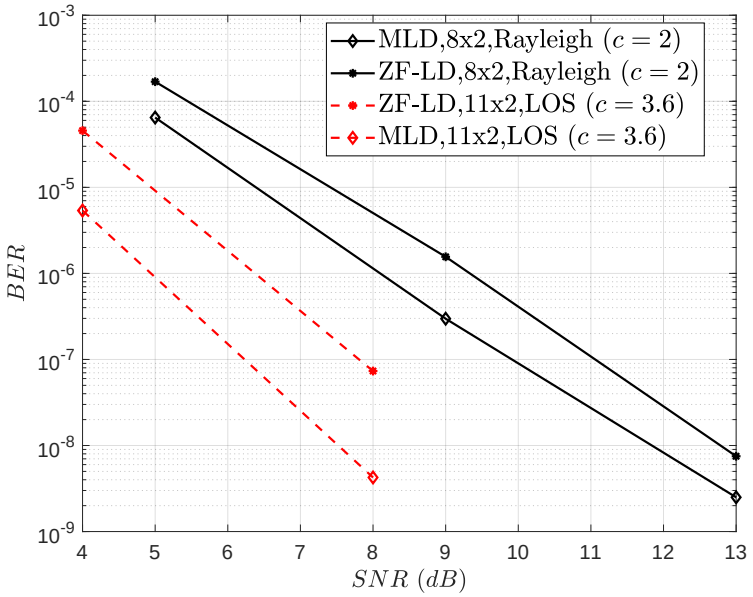

Figure 6.6: BER versus SNR of ZF LD and MLD, 4QAM [112, Figure 2(c)]

In the next chapter, we design channel assisted strategies at linear receivers to reduce latency and complexity of the ARQ process.

CHAPTER 7
CA STRATEGIES FOR HIGH-RELIABILITY LOW-LATENCY COMMUNICATIONS

The next generation wireless communication systems are designed to support diverse services ranging from enhanced mobile broadband to high-reliability low-latency communications. For the latter, ARQ is an important technique to meet the reliability constraint but often at the cost of latency. In this chapter, targeting MIMO systems with linear receivers, we propose CA strategies to reduce latency for basic ARQ and Type-I HARQ processes.

7.1 System model

Figure 7.1 illustrates an ARQ system at PHY and MAC layers. The processing unit of the MAC is in packets with length L_p bits, which contains N_p payload bits and N_c cyclic redundancy check (CRC) bits. Like in [86], we consider bursty communications, where an idle time period exists between two subsequent packet transmissions. We use the stop-and-wait (SAW) ARQ protocol for simplicity. To avoid excessive delay, we limit the maximum number of times a packet can be transmitted to M. A packet is accepted if no error is detected or M transmissions is reached. At the PHY, the system contains N_t transmit and N_r receive antennas. In the following, we introduce the transmitter, channel, and receiver model in detail.

7.1.1 Transmitter model

The left side of Figure 7.1 depicts the transmitter model used in the ARQ system. At the transmitter, single-codeword transmission is used [123, 9]. The packet is sent down to the PHY, channel coded (for HARQ) and modulated into $\frac{L_p}{R_c \log_2 |\mathcal{S}|}$ symbols, where R_c is the code rate and $|\mathcal{S}|$ is the size of the alphabet set $\mathcal{S}$. We assume that the modulation scheme

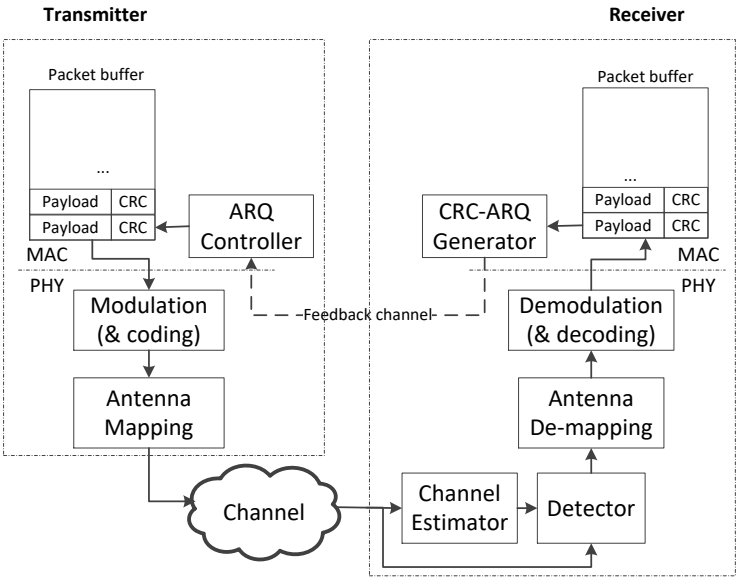

Figure 7.1: Layer architecture of a CRC-ARQ system

is chosen beforehand and fixed. The modulated symbols of the packet are multiplexed into N_t transmit antennas, sent through the channel, and received by the N_r antennas at the receiver. After sending a packet, if the Mth transmission for that packet has not been reached, the transmitter waits for an ARQ response from the receiver. If it receives an acknowledgment (ACK), the transmitter starts transmitting a new packet. If it receives a negative acknowledgment (NACK), the transmitter transmits the same packet again. On the other hand, if the Mth transmission for that packet has been reached, the transmitter starts transmitting a new packet.

7.1.2 Channel model

Consider a narrowband fading MIMO channel model described by an $N_r \times N_t$ random channel matrix $\boldsymbol{H}$, where $H_{m,n}$ denotes the channel coefficient between the n-th transmit and m-th receive antenna. The equivalent discrete-time baseband input-output relationship is expressed as

$$\boldsymbol{y} = \boldsymbol{H}\boldsymbol{s} + \boldsymbol{w}, \tag{7.1}$$

where $\boldsymbol{y}$ is the $N_r \times 1$ receive vector, $\boldsymbol{s}$ is an $N_t \times 1$ symbol vector with $E(\boldsymbol{s}\boldsymbol{s}^H) = \sigma_s^2 \boldsymbol{I}_{N_t}$, $\boldsymbol{w}$ is an $N_r \times 1$ additive complex Gaussian noise vector with $E(\boldsymbol{w}\boldsymbol{w}^H) = \sigma_w^2 \boldsymbol{I}_{N_r}$, and σ_s^2 and σ_w^2 are the signal variance and noise variance, respectively. For convenience, we define

$$\gamma_0 = \frac{\sigma_s^2}{\sigma_w^2 \log_2 |\mathcal{S}|}. \tag{7.2}$$

We also make a few assumptions:

A1) The channel remains invariant during a packet, but varies independently among packets including retransmitted ones;

A2) an ACK or a NACK is sent to the transmitter through a separate error-free feedback channel, which can be realized by using strong forward error correction (FEC) code;

A3) Channel is known at the receiver but not transmitter. Symbol and noise variances σ_s^2 and σ_w^2 are also known at the receiver.

Assumption A2) allows us to focus on the utilization of channel quality and simplifies our analysis. Assumption A3) saves channel resources and enables us to handle fast-fading situation, where sending back channel information in time to the transmitter is challenging.

7.1.3 Receiver model

The right side of Figure 7.1 illustrates the structure of the receiver. When receiving a packet, the receiver performs channel estimation based on the preamble. After attaining the estimated channel, the receiver detects the modulated symbols based on system model (7.1). Due to the constraint of complexity and power, the linear ZF receiver defined in Eq. (2.4) is deployed. The detected symbols are then demodulated (and channel decoded for HARQ). At the MAC layer of the receiver, CRC parity check is performed. If a packet error is detected and the number of transmissions is smaller than the limit M, the ARQ generator at the receiver sends a NACK to the ARQ controller at the transmitter through the feedback

channel. If a packet error is not detected and M is not reached, the ARQ generator sends an ACK instead. Note that although the probability of undetected error is small, it is not neglected. Hereafter, we refer to the system described above as the CRC-ARQ system.

7.2 Performance metrics

In this section, we define the performance metrics including reliability, latency, and receiver complexity for CRC-ARQ systems. The metrics will depend on system parameters such as signal variance σ_s^2, noise variance σ_w^2, packet length L_p, number of antennas N_t, N_r, and the detection scheme used. However, when expressing the metrics, we treat these parameters as constants and do not explicitly state the dependence. This simplification in notation is also used when analyzing intermediate variables.

Now, we recall the definition of average packet error rate (PER). Let $P(\text{err}|\boldsymbol{H})$ be the probability of packet error given the channel realization $\boldsymbol{H}$. Then the average PER $P(\text{err})$ is defined as

$$P(\text{err}) = E_{\boldsymbol{H}}\left(P(\text{err}|\boldsymbol{H})\right). \tag{7.3}$$

7.2.1 Reliability

Reliability $\mathcal{R}$ of the CRC-ARQ system is measured by the probability that the receiver accepts a packet with errors, which happens when CRC fails to detect error or packet is received with errors for M transmissions. Now let us define two events:

- Ψ_d: the event that received packet contains detectable errors;
- Ψ_u: the event that received packet contains undetectable errors.

From the definition, $P(\text{err}) = P(\Psi_d) + P(\Psi_u)$. Then, based on assumption A1), the reliability of the CRC-ARQ system is

$$\begin{aligned}\mathcal{R} &= P(\Psi_d)^{M-1}\left(P(\Psi_d) + P(\Psi_u)\right) + P(\Psi_d)^{M-2}P(\Psi_u) + \cdots + P(\Psi_d)P(\Psi_u) + P(\Psi_u) \\ &= \frac{P(\Psi_u)\left(1 - P(\Psi_d)^M\right)}{1 - P(\Psi_d)} + P(\Psi_d)^M, \end{aligned} \tag{7.4}$$

where $P(\Psi_d) = P(\text{err}) - P(\Psi_u)$. The smaller $\mathcal{R}$ is, the more reliable the CRC-ARQ system is. Note that the reliability of the CRC-ARQ system is a function of $P(\text{err})$, the average probability of undetected error $P(\Psi_u)$, and the maximum number of transmissions per packet M.

7.2.2 Average latency

Define latency τ as the number of channel uses to receive a packet. Let us define two constants during each round: D (in channel uses) represents the ARQ feedback delay, and $\varrho\left(\frac{L_p}{R_c \log_2 |\mathcal{S}|}\right)$ represents the delay for detecting, demodulating, and decoding a packet of length L_p [86]. The definition of $\varrho(\cdot)$ relies on the employed coding scheme, and thus is not specified. As we can see, τ depends on the number of transmissions K that a packet needs, and K is an RV. Then,

$$\tau(K) = \begin{cases} K\frac{L_p}{R_c \log_2 |\mathcal{S}|} + K\varrho\left(\frac{L_p}{R_c \log_2 |\mathcal{S}|}\right) + KD, & K < M, \\ M\frac{L_p}{R_c \log_2 |\mathcal{S}|} + M\varrho\left(\frac{L_p}{R_c \log_2 |\mathcal{S}|}\right) + (M-1)D, & K = M. \end{cases} \tag{7.5}$$

Thus, the average latency $E_K(\tau(K))$ for the CRC-ARQ system is

$$\begin{aligned} E_K(\tau(K)) = &\frac{1 - MP(\Psi_d)^{M-1} + (M-1)P(\Psi_d)^M}{1 - P(\Psi_d)} \cdot \left(\frac{L_p}{R_c \log_2 |\mathcal{S}|} + \varrho\left(\frac{L_p}{R_c \log_2 |\mathcal{S}|}\right) + D\right) \\ &+ \left(M\left(\frac{L_p}{R_c \log_2 |\mathcal{S}|} + \varrho\left(\frac{L_p}{R_c \log_2 |\mathcal{S}|}\right) + D\right) - D\right) P(\Psi_d)^{M-1}, \end{aligned} \tag{7.6}$$

where $P(\Psi_d) = P(\text{err}) - P(\Psi_u)$. It can be seen that average latency of CRC-ARQ system monotonically increases with M and $P(\text{err})$.

7.2.3 Receiver complexity

We define the receiver complexity Θ as the number of arithmetic computations required to receive one information bit. Denoting the complexity to complete a task as θ_{task}, the receiver complexity Θ of receiving one information bit after K transmissions is

$$\Theta(K) = \frac{K}{L_p - N_c} \left(\theta_{\text{detect}} + \theta_{\text{demod}} + \theta_{\text{decode}} + \theta_{\text{deCRC}}\right), \tag{7.7}$$

and $E_K(\Theta(K)) = \frac{E(K)}{L_p - N_c} \left(\theta_{\text{detect}} + \theta_{\text{demod}} + \theta_{\text{decode}} + \theta_{\text{deCRC}}\right)$.

7.3 The CA strategy for basic ARQ in SISO systems

To reduce latency of CRC-ARQ process, we utilize the relationship between the channel quality and the average PER $P(\text{err})$. Since packets that experience "bad" channels are more likely to be erroneous and require retransmissions, we may request a retransmission immediately after channel estimation if we find that the channel quality falls below a threshold. In this way, the steps of detection, demodulation, and decoding are skipped, and transmission latency and receiver complexity are reduced. In the following, we explain how to choose a metric for channel quality and design its threshold for the basic ARQ process when $N_r = N_t = 1$ (i.e., the SISO system), and when ML decoding and coherent demodulation are applied at the receiver. Note that ML decoding and ZF LD perform the same in the SISO case. When the CA strategy is added to the CRC-ARQ system, we refer to the system as the CA-CRC-ARQ system.

7.3.1 CA-CRC-ARQ

In the SISO system, we choose the receive SNR $\gamma = |h|^2\gamma_0$ as the channel quality, where h is the channel realization. Let us compute the average PER for SISO systems:

$$P(\text{err}) = E_h\left(P(\text{err}|h)\right) = E_\gamma\left(f\left(\gamma\right)\right), \tag{7.8}$$

where $f(\gamma)$ is the PER under AWGN channel with receive SNR γ when ML decoding and coherent demodulation are deployed. The exact expression of $f(\gamma)$ for QAM can be found at [124, Eq. (23)].

Thus, we place a CA module in between channel estimation and the detector, as shown in Figure 7.2. If γ is smaller than a threshold γ_{th}, a NACK is sent to transmitter immediately. Otherwise, the packet continues to be processed by the receiver. Therefore, for CA-CRC-ARQ, the probability of packet error given receive SNR γ is

$$P_{ca}(\text{err}|\gamma) = \begin{cases} f(\gamma), & \gamma > \gamma_{th}, \\ 1, & \gamma < \gamma_{th}. \end{cases} \tag{7.9}$$

Thus,

$$P_{ca}(\text{err}) = E_\gamma\left(P_{ca}(\text{err}|\gamma)\right) = \int_0^{\gamma_{th}} p(\gamma)d\gamma + \int_{\gamma_{th}}^{\infty} f(\gamma)p(\gamma)d\gamma, \tag{7.10}$$

where $p(\gamma)$ is the *pdf* of γ. It can be seen that

$$P_{ca}(\text{err}) > P(\text{err}), \tag{7.11}$$

when γ_{th} is finite.

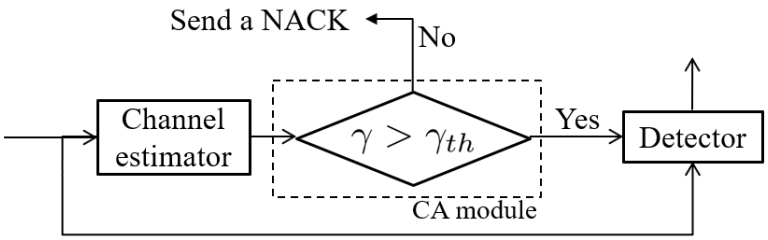

Figure 7.2: CA-CRC-ARQ for SISO systems

7.3.2 Performance metrics of CA-CRC-ARQ

Reliability

Let us compute the reliability of CA-CRC-ARQ systems, denoted as $\mathcal{R}_{ca}$. Let $P_{ca}(\Psi_d|\gamma)$ represents the probability of detected packet error of CA-CRC-ARQ given receive SNR γ. Then,

$$P_{ca}(\Psi_d|\gamma) = \begin{cases} P(\Psi_d|\gamma), & \gamma > \gamma_{th}, \\ 1, & \gamma < \gamma_{th}, \end{cases} \tag{7.12}$$

and

$$P_{ca}(\Psi_d) = E_\gamma(P_{ca}(\Psi_d|\gamma)). \tag{7.13}$$

Also, the probability of undetected packet error of CA-CRC-ARQ given γ is

$$P_{ca}(\Psi_u|\gamma) = \begin{cases} P(\Psi_u|\gamma), & \gamma > \gamma_{th}, \\ 0, & \gamma < \gamma_{th}. \end{cases} \tag{7.14}$$

Therefore,

$$P_{ca}(\Psi_u) = \int_{\gamma_{th}}^{\infty} P(\Psi_u|\gamma)p(\gamma)d\gamma < P(\Psi_u), \tag{7.15}$$

where $p(\gamma)$ is the pdf of γ. The reliability of CA-CRC-ARQ is

$$\begin{aligned}\mathcal{R}_{ca} &= P_{ca}(\Psi_d)^{M-1}P(\text{err}) + P_{ca}(\Psi_d)^{M-2}P_{ca}(\Psi_u) + \cdots + P_{ca}(\Psi_d)P_{ca}(\Psi_u) + P_{ca}(\Psi_u) \\ &= \frac{P_{ca}(\Psi_u)\left(1 - P_{ca}(\Psi_d)^M\right)}{1 - P_{ca}(\Psi_d)} + P_{ca}(\Psi_d)^M - \left(P_{ca}(\text{err}) - P(\text{err})\right)P_{ca}(\Psi_d)^{M-1}.\end{aligned} \tag{7.16}$$

From (7.16), increasing γ_{th} leads to larger $P_{ca}(\text{err})$ (and $P_{ca}(\Psi_d)$) but lower $P_{ca}(\Psi_u)$, which has competing effects on reliability.

Average latency

If a packet is received after K total transmissions, where $\tilde{K}$ retransmission requests are sent by the CA module, the latency $\tau_{ca}(K, \tilde{K})$ of the packet transmission is

$$\tau_{ca}(K,\tilde{K}) = \begin{cases} K \cdot T_{\text{CA}} + \tilde{K}\left(\frac{L_p}{\log_2|\mathcal{S}|} + D\right) + (K - \tilde{K})\left(\frac{L_p}{\log_2|\mathcal{S}|} + \varrho(\frac{L_p}{\log_2|\mathcal{S}|}) + D\right), & K < M, \\ M \cdot T_{\text{CA}} + \tilde{K}\left(\frac{L_p}{\log_2|\mathcal{S}|} + D\right) + (M - \tilde{K})\left(\frac{L_p}{\log_2|\mathcal{S}|} + \varrho(\frac{L_p}{\log_2|\mathcal{S}|}) + D\right) - D, & K = M, \end{cases} \tag{7.17}$$

where T_{CA} is the time in channel uses to make a CA decision. The probability that a packet takes K total transmissions and $\tilde{K}$ CA re-transmissions is

$$P_{ca}(K,\tilde{K}) = \begin{cases} \mathrm{C}_{K-1}^{\tilde{K}} P(\gamma < \gamma_{th})^{\tilde{K}} \left(P(\gamma > \gamma_{th})P(\Psi_d|\gamma > \gamma_{th})\right)^{K-1-\tilde{K}} \\ \qquad \cdot P(\gamma > \gamma_{th})(1 - P(\Psi_d|\gamma > \gamma_{th})), K < M, \\ \mathrm{C}_{M-1}^{\tilde{K}} P(\gamma < \gamma_{th})^{\tilde{K}} \left(P(\gamma > \gamma_{th})P(\Psi_d|\gamma > \gamma_{th})\right)^{M-1-\tilde{K}}, K = M, \end{cases} \tag{7.18}$$

where C_n^k denotes the number of k-combinations (without repetition) from a set of n distinct elements, $K = 1, 2, \cdots, M$ and $\tilde{K} = 0, 1, \cdots, K-1$. Therefore, the average latency of the CA-CRC-ARQ system is

$$E_{K,\tilde{K}}(\tau_{ca}(K,\tilde{K})) = \sum_{K=1}^{M}\sum_{\tilde{K}=0}^{K-1} P_{ca}(K,\tilde{K})\tau_{ca}(K,\tilde{K}). \tag{7.19}$$

Note that increasing γ_{th} increases the number of retransmissions requested by CA module, which can reduce latency and receiver complexity to a certain point.

Receiver complexity

If a packet is received after K total transmissions, where $\tilde{K}$ retransmission requests are sent by the CA module, the computational complexity $\Theta_{ca}(K, \tilde{K})$ of receiving one information bit is

$$\Theta_{ca}(K, \tilde{K}) = \frac{K\theta_{\text{CA}} + (K - \tilde{K})\left(\theta_{\text{detect}} + \theta_{\text{demod}} + \theta_{\text{deCRC}}\right)}{L_p - N_c}, \tag{7.20}$$

and

$$E(\Theta_{ca}(K, \tilde{K})) = \sum_{K=1}^{M} \sum_{\tilde{K}=0}^{K-1} P_{ca}(K, \tilde{K}) \Theta_{ca}(K, \tilde{K}). \tag{7.21}$$

7.3.3 The design of γ_{th}

Now we further analyze the effect of γ_{th} on the reliability and latency of CA-CRC-ARQ, with the primary goal of improving latency without degrading reliability.

Proposition 5. *For the CA-CRC-ARQ system, there theoretically exists $\gamma_b > 0$ so that when $0 < \gamma_{th} \leq \gamma_b$, CA-CRC-ARQ system has better reliability than that of the CRC-ARQ system.*

Proof: See Appendix D.1. ■

Now let us analyze the average latency of CA-CRC-ARQ. To simplify our analysis, we consider the value range of γ_{th} so that $P_{ca}(\text{err}) \approx P(\text{err})$, i.e., the values of γ_{th} that are close to zero. From the definition of delay for CRC-ARQ and CA-CRC-ARQ in Eqs. (7.5) and (7.17), and given that $T_{\text{CA}} \approx 0$, we have

$$\tau_{ca}(K, \tilde{K}) < \tau(K), \ \forall \tilde{K}. \tag{7.22}$$

On the other hand, we have

$$\sum_{\tilde{K}=0}^{K-1} P_{ca}(K,\tilde{K}) = P_{ca}(\Psi_d)^{K-1}(1-P_{ca}(\Psi_d)) \approx P(\Psi_d)^{K-1}(1-P(\Psi_d)), \tag{7.23}$$

where we have used the fact that if $P_{ca}(\text{err}) \approx P(\text{err})$ then $P_{ca}(\Psi_d) \approx P(\Psi_d)$. Then it can be shown that

$$E(\tau_{ca}) < E(\tau). \tag{7.24}$$

For the receiver complexity of CA-CRC-ARQ system, given $\theta_{\text{CA}} \approx 0$, we have $\Theta_{ca}(K,\tilde{K}) < \Theta(K),\ \forall \tilde{K}$. Because of Eq. (7.23), it can be shown that

$$E(\Theta_{ca}) < E(\Theta). \tag{7.25}$$

To summarize, we want γ_{th} to be in the range of $(0, \gamma_b]$, and also sufficiently small that $P_{ca}(\text{err}) \approx P(\text{err})$. Due to the difficulty of expressing γ_b in a closed-form, we use a sub-optimal approach to select γ_{th}: we simply consider the second constraint. In other words, we limit the difference $P_{ca}(\text{err}) - P(\text{err})$ to a small number ϵ_0, and determine γ_{th} by exploring its one-to-one relationship with $P_{ca}(\text{err}) - P(\text{err})$. The problem is formed as:

$$\max\ \gamma_{th} \tag{7.26}$$

$$s.t.\ P_{ca}(\text{err}) - P(\text{err}) \leq \epsilon_0. \tag{7.27}$$

In our experiments, ϵ_0 is determined by taking samples in near-zero value range and selecting ones that provide improved reliability and latency.

From Eqs. (7.8) and (7.10), the difference between the average PER of CA-CRC-ARQ and CRC-ARQ is

$$P_{ca}(\text{err}) - P(\text{err}) = \int_0^{\gamma_{th}} (1-f(\gamma))p(\gamma)d\gamma \leq \overline{p(\gamma)} \int_0^{\gamma_{th}} (1-f(\gamma))d\gamma, \tag{7.28}$$

Table 7.1: Design steps for the CA-CRC-ARQ protocols.

S1)	Compute the average PER for the CRC-ARQ system, and identify the channel quality that directly affects the average PER
S2)	Add the CA module, which requests early ARQ feedback whenever the determined channel quality is lower than a threshold
S3)	Compute the average PER for the CA-CRC-ARQ system as a function of the threshold
S4)	Set the difference between the average PER of the CA-CRC-ARQ system and that of the CRC-ARQ system to a small number ϵ, and find the corresponding threshold

where $\overline{p(\gamma)}$ is the maximum of $p(\gamma)$ on its support region. Thus, $\overline{p(\gamma)}$ depends on channel distribution. For Rayleigh fading channel with unity gain, γ is an exponential distributed RV with mean γ_0, so $\overline{p(\gamma)} = \gamma_0^{-1}$. Knowing $\overline{p(\gamma)}$ and $f(\gamma)$ (see [124, Eq. (23)]), we may set Eq. (7.28) to ϵ_0 and numerically find γ_{th}. Table 7.2 gives γ_{th} for different average receive SNR, 16-QAM, and Rayleigh channel.

7.3.4 Discussion

For continuous communications using selective repeat ARQ process or parallel SAW ARQ processes (e.g., [9]), the idle time between subsequent (re)transmissions can be used for sending other packets. But the advantage of our proposed scheme in terms receiver complexity and reliability can still be shown. We summarize the steps to design the CA-CRC-ARQ in Table 7.1. Next, we design CA-CRC-ARQ for various systems.

7.4 CA strategies for basic ARQ in MIMO systems

In this section, we propose CA strategies for basic ARQ process in MIMO systems.

7.4.1 The CA strategy for STC MIMO

Let us first consider an STC MIMO system with N_r receive and two transmit antennas. Alamouti code is used at the transmitter. By constructing an equivalent channel matrix and

carrying out ZF LD (see [94]), the input-output model in (2.32) becomes

$$q_k = \|\boldsymbol{H}\|_F s_k + w_k,\ k = 1, 2 \tag{7.29}$$

where $\|\cdot\|_F$ denotes Frobenius norm of a matrix, which coincides with the SISO system model. The receive SNR for this case is $\gamma = \|\boldsymbol{H}\|_F^2 \gamma_0$.

Therefore, for STC-MIMO systems, we can select the receive SNR γ as the channel quality. Given threshold γ_{th}, if $\gamma < \gamma_{th}$, the receiver requests a retransmission of the packet immediately. Otherwise, the packet proceeds to the detection module. The threshold γ_{th} can be designed similarly as in the case of the SISO system. If we assume the MIMO channel has IID complex Gaussian entries with zero mean and unit variance, then $2\|\boldsymbol{H}\|_F^2$ is Chi-square distributed with $4N_r$ DoF. Thus, the maximum of $p(\gamma)$ on its support region can be found as

$$\overline{p(\gamma)} = \frac{2\gamma_0^{-1}}{2^{2N_r}\Gamma(2N_r)}(4N_r - 2)^{(2N_r-1)}e^{-2N_r+1}, \tag{7.30}$$

Substituting Eq. (7.30) into Eq. (7.28) and setting the latter to ϵ_0, we can numerically find γ_{th} again. For example, γ_{th} is shown in Table 7.2 for $N_r = 4$, $L_p = 1080$, 16-QAM.

7.4.2 The CA strategy for SM MIMO

Now let us consider the SM MIMO system with N_r receive and N_t transmit antennas, described in model (7.1). The entries in the channel matrix are IID complex Gaussian distributed with zero mean and unit variance. When ZF LD is used, the equivalent input-output model is given in (2.9). Therefore, with ZF LD, the packet can be viewed as N_t sub-packets where each one goes through a separate sub-channel with post processing SNR,

$$\gamma_k = \frac{\gamma_0}{\left((\boldsymbol{H}^H\boldsymbol{H})^{-1}\right)_{k,k}},\ k = 1, \cdots, N_t. \tag{7.31}$$

The sub-channel SNRs are identically distributed Chi-square variables with $2(N_r - N_t + 1)$ DoF. The packet will be correctly received if each sub-packet is correctly received.

Denote $P(\text{err}_k|\gamma_k)$ as the probability of error on the k-th sub-packet under post processing SNR γ_k. Then, the probability of packet error for system model (7.1) with ZF LD is

$$P(\text{err}|\boldsymbol{H}) = 1 - \prod_{k=1}^{N_t} \left(1 - P(\text{err}_k|\gamma_k)\right). \tag{7.32}$$

Note that Eq. (7.32) assumes that sub-packet error events are independent of each other given a fixed channel matrix $\boldsymbol{H}$. Even though correlation exists between the equivalent noise in the sub-channels, the correlation between sub-packet error events are greatly mitigated by the different variance that the equivalent sub-channel noise takes, and we find Eq. (7.32) to be a close approximation to the PER conditioned on $\boldsymbol{H}$. Thus, the average PER is

$$P(\text{err}) = 1 - \int \prod_{k=1}^{N_t} \left(1 - P(\text{err}_k|\gamma_k)\right) p(\gamma_1, \cdots, \gamma_{N_t}) d\gamma_1 \cdots d\gamma_{N_t}, \tag{7.33}$$

where $p(\gamma_1, \cdots, \gamma_{N_t})$ is the joint density function of $\gamma_1, \cdots, \gamma_{N_t}$.

Since the worst sub-channel dominates packet error probability, we select the minimum sub-channel SNR to indicate the overall MIMO channel quality. The CA module is placed in between channel estimator and detector, and request a retransmission when

$$\min_k \gamma_k \leq \gamma_{th}. \tag{7.34}$$

For CA-CRC-ARQ,

$$P_{ca}(\text{err}|\boldsymbol{H}) = \begin{cases} 1, & \min_k \gamma_k \leq \gamma_{th}, \\ P(\text{err}|\boldsymbol{H}), & \text{otherwise}. \end{cases} \tag{7.35}$$

Thus,

$$P_{ca}(\text{err}) = 1 - \int_{\epsilon_{th}}^{\infty} \prod_{k=1}^{N_t} \left(1 - P(\text{err}_k|\gamma_k)\right) p(\gamma_1, \cdots, \gamma_{N_t}) d\gamma_1 d \cdots d\gamma_{N_t}. \tag{7.36}$$

Therefore,

$$P_{ca}(\text{err}) - P(\text{err}) = \int\limits_{\exists \gamma_k < \gamma_{th}} \prod_{k=1}^{N_t} \left(1 - P(\text{err}_k|\gamma_k)\right) p(\gamma_1, \cdots, \gamma_{N_t}) d\gamma_1 \cdots d\gamma_{N_t}. \quad (7.37)$$

Then, following S4) in Table 7.1 for the CA-CRC-ARQ, γ_{th} can be found numerically by setting Eq. (7.37) to ϵ_0. We provide γ_{th} for SM-MIMO system with respect to pre-processing receive SNR in Table 7.2. The reliability, latency, and receiver complexity can be analyzed similarly as in section 7.3.

7.5 CA strategies for Type-I HARQ

Type-I HARQ is the simplest version of HARQ schemes, where packets are CRC and FEC coded before modulation and transmission. At the receiver, channel decoding is performed before CRC decoding. If CRC detects a packet error, a retransmission request is sent and the same codeword will be transmitted again. For simplicity, we assume that receiver does not buffer previously received packets. Now we consider CA strategies for Type-I HARQ in SISO systems and MIMO systems.

7.5.1 The CA strategy for Type-I HARQ in SISO systems

To get the average PER in the case of coded packet transmission, we first compute the average PER of coded packet transmission under the AWGN channel. Given the receive SNR γ, for QAM, the PER can be approximated by (see [124])

$$f(\gamma) = \begin{cases} 1, & 0 < \gamma < \gamma_{pn}, \\ g_1 e^{-g_2 \gamma}, & \gamma > \gamma_{pn}, \end{cases} \quad (7.38)$$

where g_1, g_2, γ_{pn} are from the least-squares fitting of the empirical PER curve. Note that g_1, g_2, γ_{pn} depend on the packet length L_p and the modulation scheme. For 16-QAM and

$L_p = 1080$, $g_1 = 4.6900$, $g_2 = 0.5064$, $\gamma_{pn} = 6.0010$.

Thus, we still choose γ as channel quality, and request a retransmission immediately when γ falls below a threshold γ_{th}. Let us assume $\gamma_{th} > \gamma_{pn}$. Using Eq. (7.38), the difference between average PER of CA-CRC-ARQ and CRC-ARQ is

$$\begin{aligned} P_{ca}(\text{err}) - P(\text{err}) &= \int_{\gamma_{pn}}^{\gamma_{th}} \left(1 - g_1 e^{-g_2\gamma}\right) p(\gamma) d\gamma \\ &\leq \overline{p(\gamma)} \left(\gamma_{th} - \gamma_{pn} + \frac{g_1}{g_2}\left(e^{-g_2\gamma_{th}} - e^{-g_2\gamma_{pn}}\right)\right), \end{aligned} \tag{7.39}$$

where $\overline{p(\gamma)}$ is the maximum of $p(\gamma)$ on its support region. With Rayleigh fading channel, $\overline{p(\gamma)} = \gamma_0^{-1}$. Therefore, by setting Eq. (7.39) to a small number ϵ_0, we can solve γ_{th} numerically. Table 7.3 gives γ_{th} for different average receive SNR, for Rayleigh channel and 16-QAM.

7.5.2 The CA strategy for Type-I HARQ in SM-MIMO

Now, we analyze the average PER of coded packet transmission in the SM-MIMO. After channel coding, the coded packet is modulated and divided into N_t parts, each going through a separate sub-channel. The post-processing SNR γ_k for the kth sub-channel is given in Eq. (7.31). Given a fixed $\boldsymbol{H}$, the symbol errors in each sub-channel can be approximated as independent events. Thus, the average symbol error rate (SER) given channel matrix $\boldsymbol{H}$ is

$$\text{SER}(\boldsymbol{H}) = \frac{1}{N_t} \sum_{k=1}^{N_t} P(\hat{s}_k \neq s_k | \gamma_k) \leq P(\hat{s}_k \neq s_k | \gamma_m), \tag{7.40}$$

where γ_m is the minimum sub-channel SNR. Then, we may approximate the upper bound of the average PER given channel matrix $\boldsymbol{H}$ (i.e., $P(\text{err}|\boldsymbol{H})$) using $f(\gamma_m)$, where $f(\gamma)$ is the coded PER under the AWGN channel with SNR γ. In other words, $P(\text{err}|\boldsymbol{H}) \leq \overline{P(\text{err}|\boldsymbol{H})} \approx f(\gamma_m)$. Thus, we select the minimum sub-channel SNR as the channel quality

Table 7.2: Empirical ϵ_{th} for basic ARQ, Rayleigh channel, $L_p = 1080$, 16-QAM, $\epsilon_0 = 10^{-3}$.

SISO	$10\log_{10}(\gamma_0)$	0	4	8	12	16	20	24	28
	$\lvert h\rvert^2\gamma_0$	7.503	7.825	8.196	8.630	9.151	9.797	10.631	11.777
ST-MIMO	$10\log_{10}(\gamma_0)$	0	1	2	3	4	5	6	7
	$\lVert\boldsymbol{H}\rVert_F^2\gamma_0$	8.223	8.326	8.433	8.545	8.662	8.785	8.913	9.048
SM-MIMO	$10\log_{10}(N_t\gamma_0)$	8	12	16	20	24	28	32	36
	$\min_k \frac{\gamma_0}{((\boldsymbol{H}^H\boldsymbol{H})^{-1})_{k,k}}$	4.750	4.754	5.474	6.000	6.279	6.309	7.528	8.459

again. The CA module requests a retransmission when

$$\min_k \gamma_k \leq \gamma_{th}. \tag{7.41}$$

Now we calculate the average PER for CRC-ARQ and CA-CRC-ARQ. Based on previous reasoning,

$$P(\text{err}) \leq \int f(\gamma_m) p_m(\gamma_m) d\gamma_m := \overline{P(\text{err})}, \tag{7.42}$$

$$P_{ca}(\text{err}) \leq \int_0^{\gamma_{th}} p_m(\gamma_m) d\gamma_m + \int_{\gamma_{th}}^{\infty} f(\gamma_m) p_m(\gamma_m) d\gamma_m := \overline{P_{ca}(\text{err})}, \tag{7.43}$$

where $p_m(\gamma)$ is the distribution of the minimum sub-channel SNR of the MIMO channel, and

$$\overline{P_{ca}(\text{err})} - \overline{P(\text{err})} = \int_0^{\gamma_{th}} (1 - f(\gamma_m)) p_m(\gamma_m) d\gamma_m. \tag{7.44}$$

Following S4) in Table 7.1 for the CA-CRC-ARQ, we set Eq. (7.44) to a small number ϵ_0 and find γ_{th} numerically. For the IID Rayleigh fading MIMO channel, we list γ_{th} with respect to pre-processing receive SNR in Table 7.3.

7.6 Numerical results

In this section, we evaluate the reliability, latency, and receiver complexity of CA-CRC-ARQ and CRC-ARQ schemes with simulations. We assume a narrowband Rayleigh fading

Table 7.3: Empirical ϵ_{th} for Type-I HARQ, Rayleigh channel, $L_p = 1080$, 16-QAM. For SISO, $\epsilon_0 = 10^{-5}$. For SM MIMO, $\epsilon_0 = 10^{-10}$.

SISO	$10\log_{10}(\gamma_0)$	12	15	18	21	24	27	30
	$\lvert h\rvert^2\gamma_0$	3.9824103	3.9828300	3.9836669	3.9853351	3.9886565	3.9952564	4.0083184
SM MIMO	$10\log_{10}(N_t\gamma_0)$	16	20	24	28	32	36	40
	$\min_k \frac{\gamma_0}{((\boldsymbol{H}^H\boldsymbol{H})^{-1})_{k,k}}$	3.9819888	3.9819887	3.9819899	3.9819954	3.9820045	3.9820172	3.9820000

Table 7.4: Number of arithmetic operations taken by different modules to receive a packet of length L_p

CA decision	Detection	Demod	FEC decoding	CRC decoding
$2N_t^2N_r + \frac{4N_t^3}{3} + N_t$	$4N_t^2N_r + \frac{4N_t^3}{3} + \frac{2N_rL_p}{R_c\log_2\lvert\mathcal{S}\rvert}$	$\frac{L_p}{R_c\log_2\lvert\mathcal{S}\rvert}$	2^6L_p	L_pN_c

channel with a bandwidth of 1MHz. The packet length L_p is 1080, the CRC length N_c is 8, and the maximum number of transmissions M is set to 5. 16-QAM is used. We assume that CA decision takes 0.01ms and ARQ feedback delay is 5ms [80]. For simplicity, we treat $\varrho(\cdot)$ as a linear function. We further assume that decoding time per symbol is 0.01ms in SISO, 0.015ms in ST-MIMO, and 0.025ms in SM-MIMO systems. For Type-I HARQ, rate-$3/4$ convolutional code is used, where each stage is 1-bit and constraint length is 7 [94, p.522]. The complexity in terms of arithmetic operations of each module in MIMO systems is listed in Table 7.4. One addition, subtraction, multiplication and division are counted as one arithmetic operation.

7.6.1 CA strategies for basic ARQ

In this section, we evaluate the CA strategy for basic ARQ process.

The CA strategy in SISO systems

First, we evaluate the performance of CRC-ARQ and CA-CRC-ARQ in uncoded SISO systems. In Figure 7.3, we see that the reliability of CA-CRC-ARQ is significantly higher than that of CRC-ARQ at high SNR. Figure 7.4 shows that CA-CRC-ARQ has much lower latency than the other ARQ scheme. To compare the receiver complexity of the ARQ

schemes, we first plot the average number of retransmission requests made by CA and CRC in CA-CRC-ARQ and the number of retransmission requests in CRC-ARQ in Figure 7.5. We observe that a large portion of retransmission requests is made by CA in CA-CRC-ARQ. Recall that for CRC-ARQ to request a retransmission, the receiver needs to carry out detection, demodulation, and CRC decoding. For CA-CRC-ARQ, if the retransmission request is made by CA, the complexity cost is only due to making the CA decision. This indicates that CA-CRC-ARQ reduces the complexity of ARQ compared to CRC-ARQ, which is confirmed by Figure 7.6, showing CA-CRC-ARQ taking the lowest average number of arithmetics to receive one information bit at the receiver.

In sum, when the pdf of the channel is bounded on its support region (e.g. Rayleigh distributed), we can find γ_{th} such that CA-CRC-ARQ greatly reduces latency and complexity at low SNR and improves system reliability at high SNR. Similar to using a longer CRC, employing CA strategy improves reliability. But quite different from having a longer CRC, CA strategy greatly reduces latency and receiver complexity.

The CA strategy in STC MIMO systems

Now we examine performance of CA strategy in an Alamouti STC-MIMO system with $N_t = 2$ and $N_r = 4$. In Figure 7.3, we observe that CA-CRC-ARQ slightly increases the reliability of CRC-ARQ at high SNR. But as shown in Figure 7.4, CA-CRC-ARQ reduces the latency of CRC-ARQ by a significant percentage at low to moderate SNRs, which is desirable. Since a large portion of retransmission requests is made by CA in CA-CRC-ARQ, its receiver complexity is the lowest among comparisons in Figure 7.6.

CA strategies in SM MIMO systems

Now we investigate the performance of CA-CRC-ARQ in the SM-MIMO system with $N_r = N_t = 4$. Other than CRC-ARQ and CA-CRC-ARQ (denoted as CA-CRC-SNR), we include results of the CC-ARQ [88], denoted as CA-CRC-OD in the figures. CA-CRC-OD

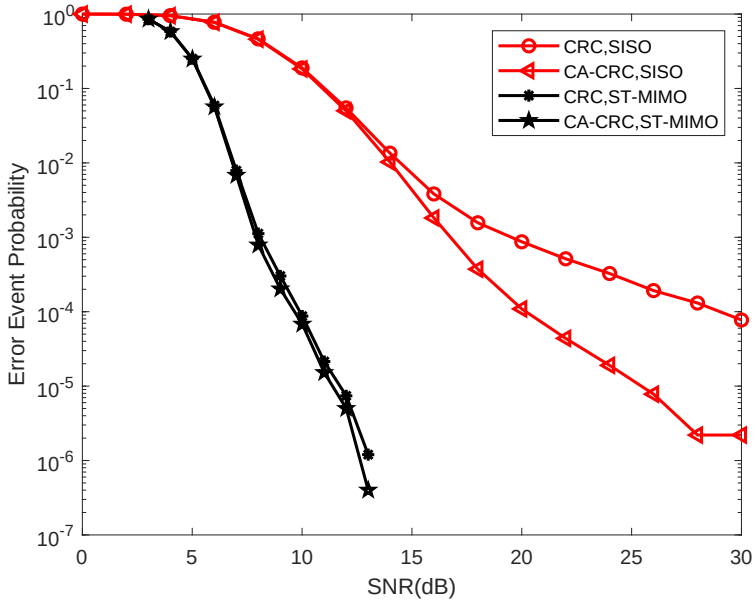

Figure 7.3: Reliability of different ARQ schemes in SISO and 4×2 ST-MIMO systems, $L_p = 1080$

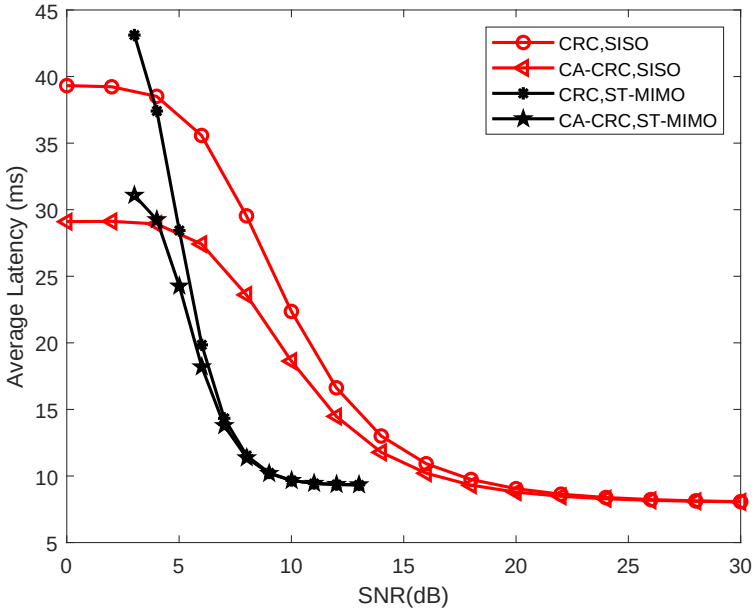

Figure 7.4: Latency of different ARQ schemes in SISO and 4×2 ST-MIMO systems, $L_p = 1080$

controls the od of the channel matrix $\boldsymbol{H}$, and requests a retransmission immediately when $od(\boldsymbol{H}) \geq 0.9962$. Since LDs collect the same diversity as the MLD when od of the channel matrix is bounded by a number smaller than one [45], CA-CRC-OD achieves full spatial

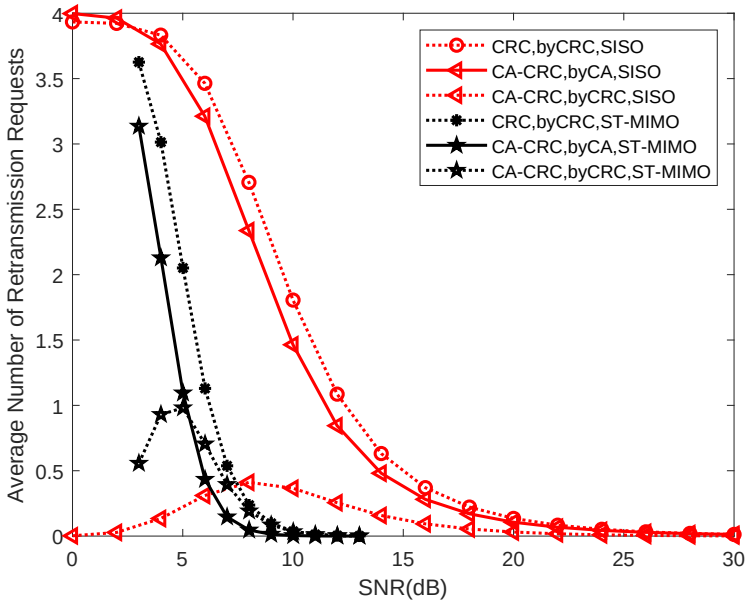

Figure 7.5: Number of retransmission requests made by different ARQ schemes in SISO and 4×2 ST-MIMO systems, $L_p = 1080$

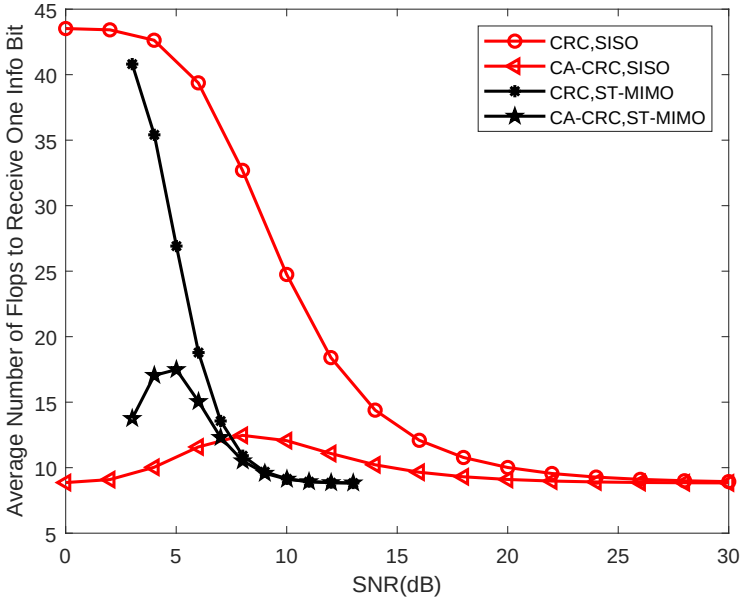

Figure 7.6: Average number of flops required by different ARQ schemes to receive one information bit in SISO and 4×2 ST-MIMO systems, $L_p = 1080$

diversity.

In Figure 7.7, we see that the reliability of CA-CRC-SNR is higher than that of CRC-ARQ and CA-CRC-OD at most of high SNR levels. In Figure 7.8, we see that CA-CRC-

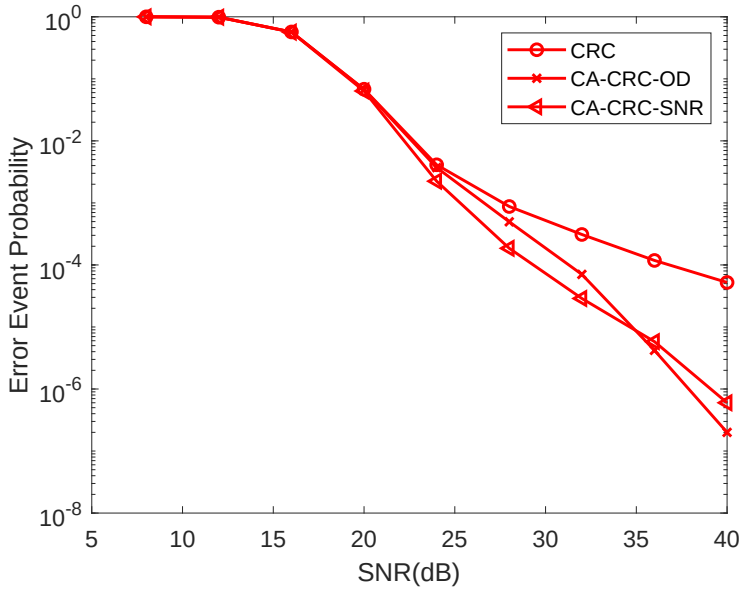

Figure 7.7: Reliability of different ARQ schemes in 4×4 MIMO system, $L_p = 1080$

SNR has the lowest latency compared to the other two in low to moderate SNRs. CA-CRC-OD also has lower latency compared to CRC-ARQ, but the advantage is less significant. Figure 7.10 shows that at low SNR, CA-CRC-SNR serves a large percentage of the ARQ request by CA module and saves the complexity. However, for CA-CRC-OD, since its retransmission criterion is not directly related to the packet error probability, it serves a small number of the retransmission requests by CC module. Therefore, compared to CA-CRC-SNR, the complexity reduction by CA-CRC-OD is smaller. The complexity advantage of CA-CRC-SNR at low SNR can be seen in Figure 7.11.

7.6.2 CA strategies for Type-I HARQ

Now we examine the performance of CA strategy for Type-I HARQ process in SISO and MIMO systems.

The CA strategy in SISO systems

Figure 7.12 shows the reliability of the ARQ schemes. We see that the reliability of CA-CRC-ARQ is higher than CRC-ARQ at high SNR. Figure 7.13 shows the latency of the

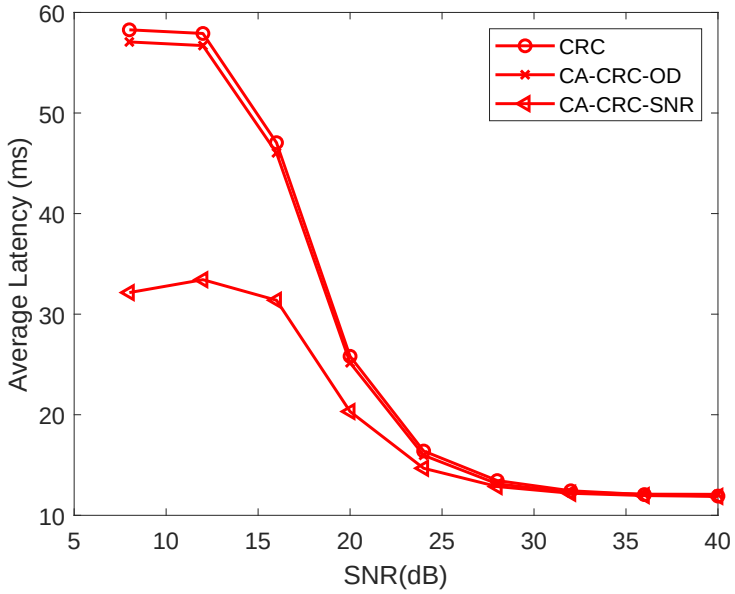

Figure 7.8: Latency of different ARQ schemes in 4×4 MIMO system, $L_p = 1080$

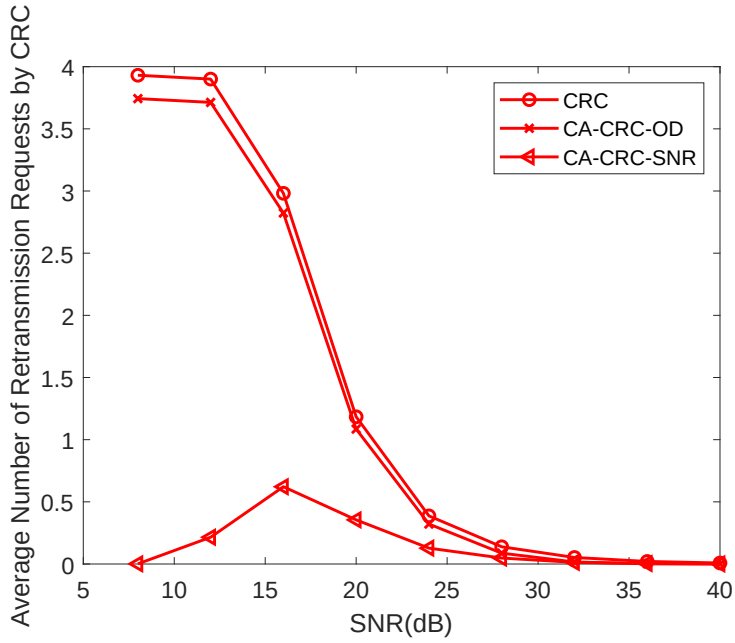

Figure 7.9: Number of retransmissions requested by CRC-ARQ schemes in 4×4 MIMO system, $L_p = 1080$

ARQ schemes. The latency of CA-CRC-ARQ is much lower than CRC-ARQ at low SNR. We then plot the average number of arithmetics needed to successfully receive one information bit at the receiver for the ARQ schemes in Figure 7.14. CA-CRC-ARQ significantly

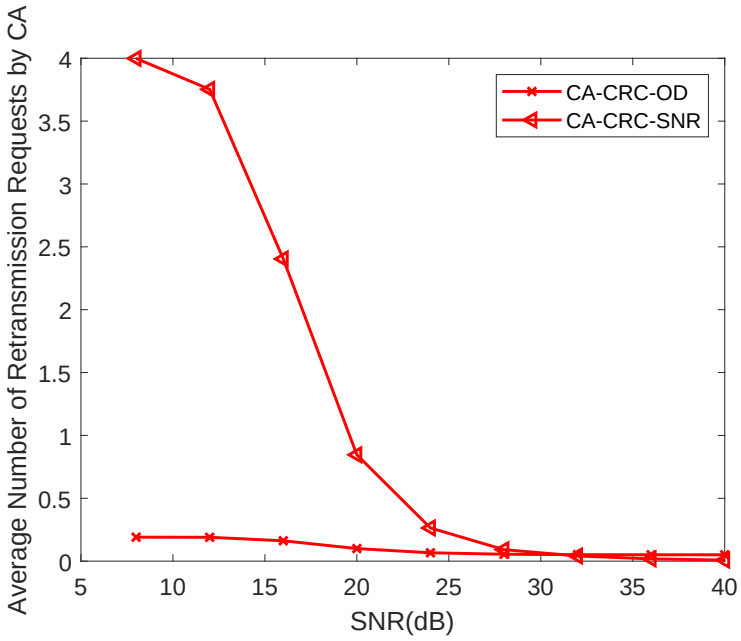

Figure 7.10: Number of retransmissions requested by CA module in 4×4 MIMO system, $L_p = 1080$

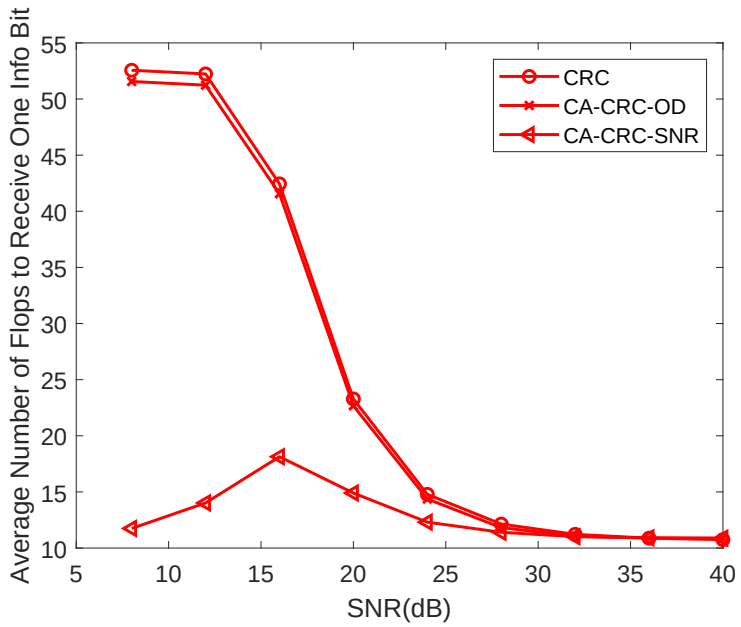

Figure 7.11: Average number of flops required by different ARQ schemes to receive one information bit in 4×4 MIMO system, $L_p = 1080$

reduces the complexity of ARQ compared to CRC-ARQ. Recall that for CRC-ARQ to request a retransmission, the receiver needs to carry out detection, demodulation, channel

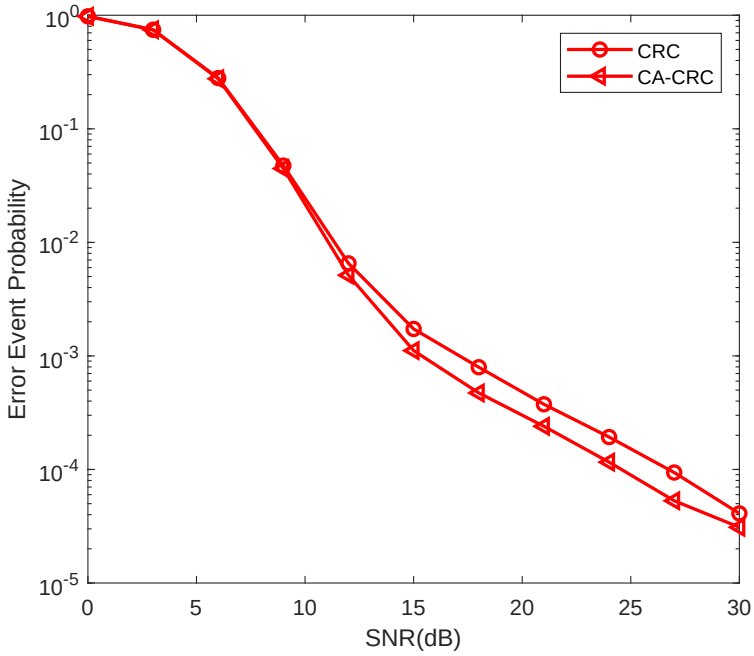

Figure 7.12: Reliability of different ARQ schemes in coded SISO system, $L_p = 1080$

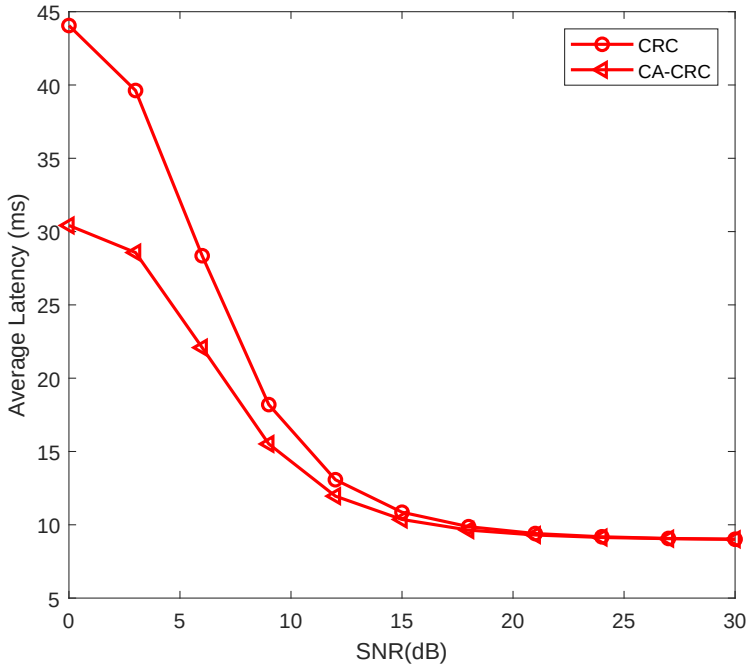

Figure 7.13: Latency of different ARQ schemes in coded SISO system, $L_p = 1080$

decoding, and CRC parity check. For CA-CRC-ARQ, if the retransmission request is made by CA, the complexity cost is only due to CA decision making.

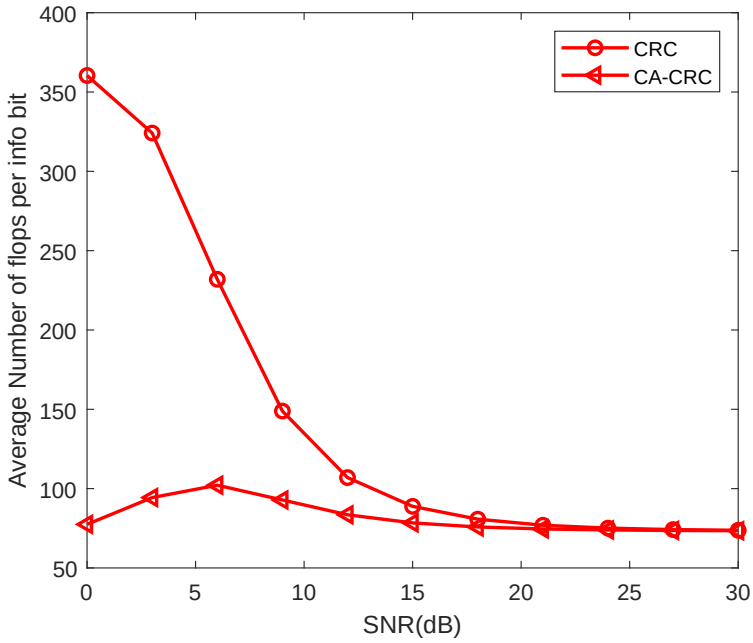

Figure 7.14: Average number of flops required by different ARQ schemes to receive one information bit in coded SISO system, $L_p = 1080$

The CA strategy in SM MIMO systems

Now we investigate the performance of CA strategy in the SM-MIMO system with $N_r = N_t = 4$. Three ARQ schemes are evaluated and ZF LD is used. In Figure 7.15, we see that the reliability of CA-CRC-SNR is higher compared to CRC-ARQ, but lower than CA-CRC-OD at high SNR. This indicates that the selection of channel quality and the design of threshold can be further improved, in the case of coded SM-MIMO systems. At low SNR, CA-CRC-SNR serves a large portion of the retransmission requests by CA module and saves the complexity cost. For CA-CRC-OD, since its retransmission criterion is not directly related to the probability of packet error, it serves a fixed small number of the retransmission requests by CA module. Therefore, compared to CA-CRC-SNR, the complexity reduction of CA-CRC-OD is small. The latency and complexity advantage of CA-CRC-SNR at low SNR can be seen in Figures 7.16 and 7.17.

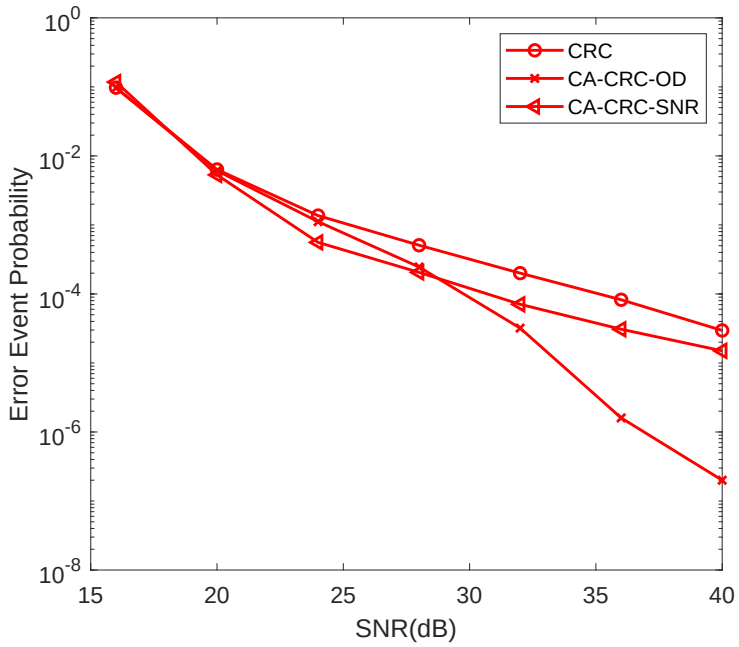

Figure 7.15: Reliability of different ARQ schemes in 4×4 coded MIMO system, $L_p = 1080$

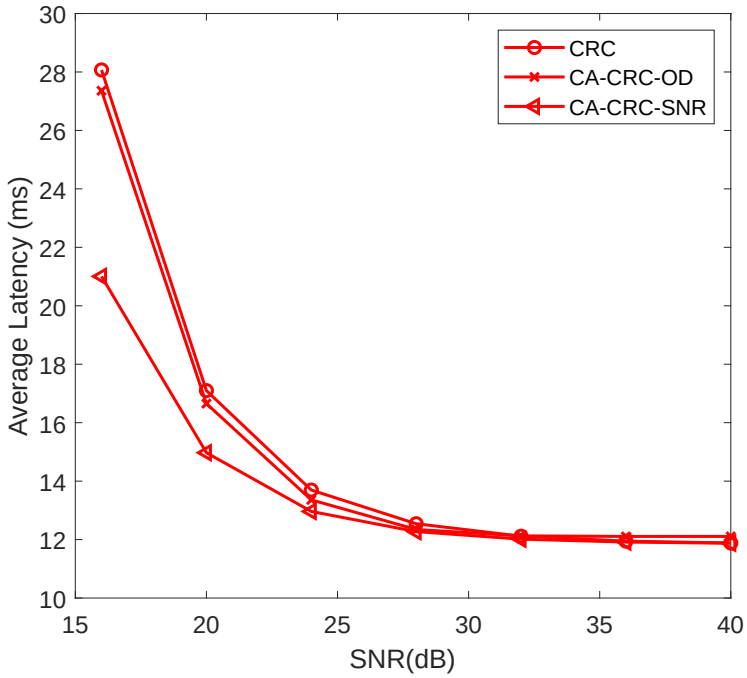

Figure 7.16: Latency of different ARQ schemes in 4×4 coded MIMO system, $L_p = 1080$

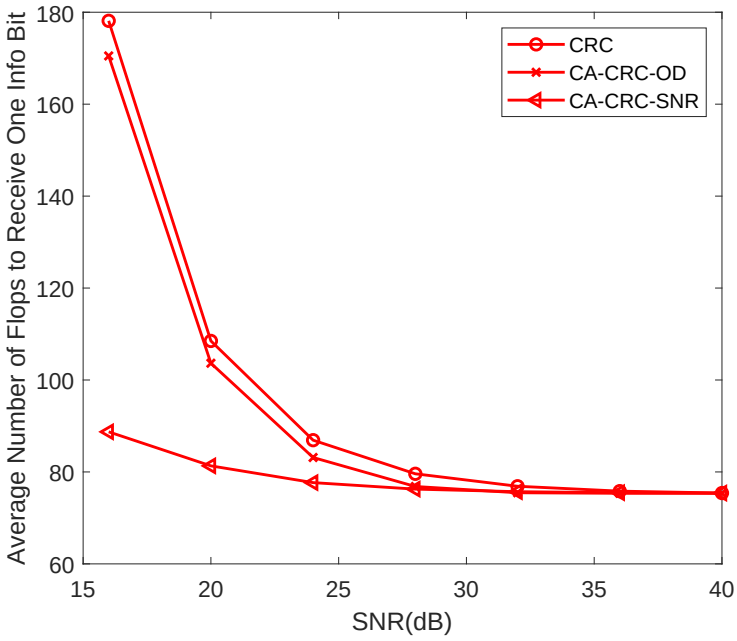

Figure 7.17: Average number of flops required by different ARQ schemes to receive one information bit in 4×4 coded MIMO system, $L_p = 1080$

7.7 Chapter summary

In this chapter, we proposed CA strategies for basic ARQ and Type-I HARQ process for linear receivers in SISO and MIMO systems. The CA strategies work as follows: in SISO systems, the receiver requests a retransmission immediately if the receive SNR is below certain threshold. In SM-MIMO systems, the linear receivers select the minimal sub-channel post processing SNR as the channel quality and immediately request a retransmission when it falls below certain threshold. As shown by simulations, the proposed CA strategies reduce average latency and receiver complexity at low to moderate SNR levels, and improve reliability at high SNR regime, for both basic ARQ and Type-I HARQ process.

CHAPTER 8
CONCLUSION

8.1 Contributions

In this dissertation, channel-quality-driven high-performance receivers are developed for various MIMO systems, and channel assisted ARQ techniques are proposed for high-reliability low-latency communications. The contributions include:

- We quantified the maximum information rate of MIMO transmission with LR-aided linear equalizers employed. We studied the complexity of LR algorithms when the MIMO channel is spatially correlated, and demonstrated the effect of SNR and correlation coefficient on the average complexity of LR algorithms.

- We proposed PELR aided detectors for STCM systems at large MIMO dimensions. By fully utilizing the symmetric property of the equivalent channel matrix, the proposed detectors reduced approximately half of the complexity of the ELR aided detectors. With similar complexity, the PELR aided detectors achieve better BER compared to other state-of-the-art detectors.

- We presented a linear joint transceiver design for MU MIMO downlink system using LR algorithms. We compared the error performance and complexity of our proposed design with several existing schemes and show that our design performs very well with low complexity especially when each user is equipped with a large number of antennas (e.g., more than three) and receives spatially multiplexed data streams.

- We proposed four RL-based LR algorithms, differing in their objectives, action set and reward functions. We demonstrated the possibility of having "customized" criterion of reduction and achieving it using RL. Simulation results show that RL-based

LR-aided detectors achieve similar BER and lower DSP complexity compared to existing LR-aided detectors for up to 4×4 MIMO.

- We studied the performance of LDs in massive MIMO systems of finite number of antennas under various propagation conditions. We provided the thresholds of N_r (given propagation channel and N_t) needed for LDs to collect the same diversity as the MLD does with high probability in practice.

- We proposed CA strategies for basic ARQ and Type-I HARQ process for linear receivers in MIMO systems. Shown by simulations, the proposed CA-ARQ strategies reduce latency and receiver complexity at low to moderate SNR levels, and improve reliability at high SNR regime, for both ARQ processes.

8.2 Future research

To expand on the results from the proposed research, future research topics include:

- Develop LR algorithms for MU MIMO uplink where UEs may have different number of antennas and adopt different modulation schemes; Investigate the options of power allocation and the impact of imperfect CSI in LR aided transceiver architecture design for the MU MIMO downlink;

- Investigate deep RL based LR algorithms (e.g., deep Q-learning, actor-critic methods), to improve the performance of RL-based LR-aided detectors and enable high-performance detection for large MIMO;

- Investigate the distribution of od and the performance of LDs in more complex multi-user massive MIMO models; Investigate the impact of channel correlation on the distribution of od and performance of LDs.

- Design and analyze CA strategies for frequency-selective MIMO systems; Combine multiple channel qualities to decide whether to send early feedback; Modify CA

strategies to consider when limited buffering of packets at the receiver is available.

8.3 Publications

A list of publications related to this dissertation is shown below.

Journal publications:

[J1] **Y. Kong**, X. Ma, and J. Lu, "Orthogonality deficiency of massive MIMO channels: Distribution and relationship with performance," *IEEE Signal Process. Lett.*, accepted.

[J2] **Y. Kong** and X. Ma, "Channel-assisted ARQ strategies for high-reliability low-latency communications," to be submitted to *IEEE Trans. Commun.*.

[J3] Q. Zhou, Y-W. Chen, S. Shen, **Y. Kong**, M. Xu, J. Zhang, and G-K. Chang, "Proactive real-time interference avoidance in 5G millimeter-wave over fiber mobile fronthaul using SARSA reinforcement learning," *Optics Letters*, vol. 44, no. 17, to appear.

Conference publications:

[C1] **Y. Kong**, H. Zang, and X. Ma, "Improving TCP congestion control with machine intelligence," in *Proc. ACM SIGCOMM Workshop on Network Meets AI & ML (NetAI'18)*. Budapest, Hungary, Aug. 2018.

[C2] **Y. Kong**, X. Ma, and Y. Wang, "Applying lattice reduction technique to space-time coded multiplexing systems," in *Proc. Int. Workshop on Computing, Networking and Communications (CNC'18)*, Maui, HI, Mar. 2018, pp. 275-279.

[C3] R. Zhang, **Y. Kong**, X. Ma, and D. Wang, "Adaptive video transmission designs over underwater acoustic channels," in *Proc. Int. Workshop on Computing, Networking and Communications (CNC'18)*, Maui, HI, Mar. 2018, pp. 295-299.

[C4] **Y. Kong**, H. Zang, and X. Ma, "Human network usage patterns revealed by telecom data," in Proc. IEEE Int. Conf. on Big Data (Big Data'16), Washington, DC, Dec. 2016, pp. 1621-1626.

[C5] **Y. Kong**, H. Zang, and X. Ma, "Quick model fitting using a classifying engine," in Proc. IEEE Int. Conf. on Big Data (Big Data'16), Washington, DC, Dec. 2016, pp. 2728-2733.

[C6] X. Ma and **Y. Kong**, "Capacity analysis of lattice reduction aided equalizers for MIMO systems," in Proc. Military Commu. Conf. (MILCOM'15), Tampa, FL, Oct. 2015, pp. 866-871.

[C7] **Y. Kong**, Q. Zhou, and X. Ma, "Lattice reduction aided transceiver design for MU MIMO downlink transmissions," in Proc. Military Commu. Conf. (MILCOM'14), Baltimore, MD, Oct. 2014, pp. 556-562.

[C8] **Y. Kong** and X. Ma, "Lattice reduction techniques in MIMO systems with correlated channels," in Proc. Military Commu. Conf. (MILCOM'14), Baltimore, MD, Oct. 2014, pp. 575-580.

Patent applications:

[P1] H. Zang and **Y. Kong**. "Congestion control in network communications," U.S. Patent Application No. 62/810,134, Filed on Feb. 25, 2019.

[P2] H. Zang and **Y. Kong**. "TCP congestion control based on packet loss prediction," U.S. Patent Application No. 62/654,023, Filed on Apr. 6, 2018. Provisional.

[P3] H. Zang and **Y. Kong**. "Apparatus and method for dataset model fitting using a classifying engine," U.S. Patent Application No. 15/277,970, Filed on Sep. 27, 2016.

Appendices

APPENDIX A

PROOF FOR CHAPTER 3

A.1 Proof of Proposition 1

Using Hadamard's inequality, it can be shown that $C_{zf}^{LR}(\boldsymbol{H}) \leq C_{ml}^{LR}(\boldsymbol{H})$.

A.2 Proof of Proposition 2

At high SNR, given (3.14) and with Jensen's inequality, we have that

$$\begin{aligned} 0 \geq \log_2 E_{\boldsymbol{H}} \left(\frac{1 - od((\boldsymbol{H}^\dagger)^H)}{1 - od((\tilde{\boldsymbol{H}}^\dagger)^H)} \right) &\geq E_{\boldsymbol{H}} \left(\log_2 \left(\frac{1 - od((\boldsymbol{H}^\dagger)^H)}{1 - od((\tilde{\boldsymbol{H}}^\dagger)^H)} \right) \right) \\ &= E_{\boldsymbol{H}} \left(C_{zf}(\boldsymbol{H}) \right) - E_{\boldsymbol{H}} \left(C_{zf}^{LR}(\boldsymbol{H}) \right). \end{aligned} \tag{A.1}$$

From the definition of dual ELR algorithm and [43, Proposition 1], we have $od((\boldsymbol{H}^\dagger)^H) \geq od((\tilde{\boldsymbol{H}}^\dagger)^H)$ for every channel matrix $\boldsymbol{H}$. Thus $E_{\boldsymbol{H}} \left(\log_2 \left(\frac{1-od((\tilde{\boldsymbol{H}}^\dagger)^H)}{1-od((\boldsymbol{H}^\dagger)^H)} \right) \right) \geq 0$.

A.3 Proof of Proposition 3

From (3.3), the outage diversity of LR-aided MLE is the same as that of MLE. When $od(\tilde{\boldsymbol{H}}) \leq \epsilon_1 < 1$, by [45, Lemma 2], there exists ϵ_2 so that $od((\tilde{\boldsymbol{H}}^\dagger)^H) \leq \epsilon_2 < 1$. From (3.3) and (3.11), we have

$$C_{ml}(\boldsymbol{H}) - C_{zf}^{LR}(\boldsymbol{H}) = C_{ml}^{LR}(\boldsymbol{H}) - C_{zf}^{LR}(\boldsymbol{H}) \leq -\log_2(1 - \epsilon_2) := C_0, \tag{A.2}$$

where C_0 is a finite number. Thus, $P(C_{zf}^{LR}(\boldsymbol{H}) < C_{th}) \leq P(C_{ml}(\boldsymbol{H}) < C_{th} + C_0)$. At the same time, since $C_{zf}^{LR}(\boldsymbol{H}) \leq C_{ml}(\boldsymbol{H})$, we have $P(C_{ml}^{LR}(\boldsymbol{H}) < C_{th}) \leq P(C_{zf}^{LR}(\boldsymbol{H}) < C_{th})$. Therefore, the outage diversity of LR-aided ZFE is the same as that of MLE.

APPENDIX B

PROOF FOR CHAPTER 4

B.1 Proof of Lemma 2

Given the structure of $\boldsymbol{H}$ in (2.34), we have

$$\boldsymbol{H}^H\boldsymbol{H} = \begin{bmatrix} \boldsymbol{M}_{1,1} & \boldsymbol{M}_{1,2} & ... & \boldsymbol{M}_{1,\frac{N_t}{2}} \\ \boldsymbol{M}_{2,1} & \boldsymbol{M}_{2,2} & ... & \boldsymbol{M}_{2,\frac{N_t}{2}} \\ ... & ... & ... & ... \\ \boldsymbol{M}_{\frac{N_t}{2},1} & \boldsymbol{M}_{\frac{N_t}{2},1} & ... & \boldsymbol{M}_{\frac{N_t}{2},\frac{N_t}{2}} \end{bmatrix}, \tag{B.1}$$

where

$$\boldsymbol{M}_{l,k} = \begin{bmatrix} \boldsymbol{b}_{2l-1}^H\boldsymbol{b}_{2k-1} + \boldsymbol{b}_{2l}^{*H}\boldsymbol{b}_{2k}^* & \boldsymbol{b}_{2l-1}^H\boldsymbol{b}_{2k} - \boldsymbol{b}_{2l}^{*H}\boldsymbol{b}_{2k-1}^* \\ \boldsymbol{b}_{2l}^H\boldsymbol{b}_{2k-1} - \boldsymbol{b}_{2l-1}^{*H}\boldsymbol{b}_{2k}^* & \boldsymbol{b}_{2l}^H\boldsymbol{b}_{2k} + \boldsymbol{b}_{2l-1}^{*H}\boldsymbol{b}_{2k-1}^* \end{bmatrix}.$$

It is shown in (B.1) that $\boldsymbol{H}^H\boldsymbol{H}$ has $N_t/2$ Type-II column pairs. Thus, the diagonal of $\boldsymbol{H}^H\boldsymbol{H}$ has $N_t/2$ pairs of real values. The matrix $\boldsymbol{C}$ has the same structure as $\boldsymbol{H}^H\boldsymbol{H}$, and also has $N_t/2$ Type-II column pairs and $N_t/2$ pairs of real entries on its diagonal. For the channel matrix in MMSE form, we have $\bar{\boldsymbol{H}} = [\boldsymbol{H}^T, \sigma_w/\sigma_s\boldsymbol{I}_{N_t}]^T$ and $\bar{\boldsymbol{H}}^H\bar{\boldsymbol{H}} = \boldsymbol{H}^H\boldsymbol{H} + \sigma_w^2/\sigma_s^2\boldsymbol{I}_{N_t}$. Therefore, $\boldsymbol{C} = (\bar{\boldsymbol{H}}^H\bar{\boldsymbol{H}})^{-1}$ still has the same structure for the channel matrix in MMSE form.

Suppose that at the first iteration, the largest diagonal value $C_{k,k}$ can be reduced by its l-th column and row by $\Delta_{l,k}$. From [43], we have $\lambda_{l,k} = -\left\lceil \frac{C_{l,k}}{C_{l,l}} \right\rfloor$ and $\Delta_{l,k} = -|\lambda_{l,k}|^2 C_{l,l} -$

$\lambda_{l,k}^* C_{l,k} - \lambda_{l,k} C_{k,l}$. If $k < k_p$ and $l < l_p$, or $k > k_p$ and $l > l_p$, then

$$\lambda_{l_p,k_p} = -\left\lceil \frac{C_{l_p,k_p}}{C_{l_p,l_p}} \right\rfloor = -\left\lceil \frac{C_{l,k}^*}{C_{l,l}} \right\rfloor = \lambda_{l,k}^*, \tag{B.2}$$

$$\begin{aligned} \Delta_{l_p,k_p} &= -|\lambda_{l_p,k_p}|^2 C_{l_p,l_p} - \lambda_{l_p,k_p}^* C_{l_p,k_p} - \lambda_{l_p,k_p} C_{k_p,l_p} \\ &= -|\lambda_{l,k}|^2 C_{l,l} - \lambda_{l,k} C_{l,k}^* - \lambda_{l,k}^* C_{k,l}^* = \Delta_{l,k}, \end{aligned} \tag{B.3}$$

where the last step is because that $C_{l,k} = C_{k,l}^*$. Otherwise, we can similarly show that $\lambda_{l_p,k_p} = -\lambda_{l,k}^*$ and $\Delta_{l_p,k_p} = \Delta_{l,k}$. Therefore, C_{k_p,k_p} can be reduced by its l_p-th column and row by $\Delta_{l,k}$.

B.2 Proof of Lemma 3

At the start of an iteration, let

$$\tilde{\boldsymbol{h}}_l = \begin{bmatrix} \boldsymbol{b}_l \\ -\boldsymbol{b}_{l+1}^* \end{bmatrix}, \tilde{\boldsymbol{h}}_{l_p} = \begin{bmatrix} \boldsymbol{b}_{l+1} \\ \boldsymbol{b}_l^* \end{bmatrix}, \tilde{\boldsymbol{h}}_k = \begin{bmatrix} \boldsymbol{b}_k \\ -\boldsymbol{b}_{k+1}^* \end{bmatrix}, \tilde{\boldsymbol{h}}_{k_p} = \begin{bmatrix} \boldsymbol{b}_{k+1} \\ \boldsymbol{b}_k^* \end{bmatrix},$$

where we assume that $l < l_p$ and $k < k_p$ (WLOG). From [43], after reductions between index pair (l, k) and (l_p, k_p), we have $\tilde{\boldsymbol{h}}_l \leftarrow \tilde{\boldsymbol{h}}_l - \lambda_{l,k}^* \tilde{\boldsymbol{h}}_k$ and $\tilde{\boldsymbol{h}}_{l_p} \leftarrow \tilde{\boldsymbol{h}}_{l_p} - \lambda_{l_p,k_p}^* \tilde{\boldsymbol{h}}_{k_p}$. In other words, at the end of that iteration,

$$\tilde{\boldsymbol{h}}_l = \begin{bmatrix} \boldsymbol{b}_l - \lambda^* \boldsymbol{b}_k \\ -\boldsymbol{b}_{l+1}^* + \lambda^* \boldsymbol{b}_{k+1}^* \end{bmatrix}, \tilde{\boldsymbol{h}}_{l_p} = \begin{bmatrix} \boldsymbol{b}_{l+1} - \lambda \boldsymbol{b}_{k+1} \\ \boldsymbol{b}_l^* - \lambda \boldsymbol{b}_k^* \end{bmatrix},$$

where $\lambda_{l,k} = \lambda$, and $\lambda_{l_p,k_p} = \lambda^*$. This shows that after the two consecutive reductions, columns $\tilde{\boldsymbol{h}}_l$ and $\tilde{\boldsymbol{h}}_{l_p}$ remains a Type-I column pair. Therefore the structure of $\tilde{\boldsymbol{H}}$ is maintained, and thus so is that of $\tilde{\boldsymbol{C}}$.

APPENDIX C

PROOF FOR CHAPTER 6

C.1 Proof of Proposition 4

Without loss of generality, assume $k = 1$. Let $\boldsymbol{Q}$ and $\boldsymbol{R}$ be the unitary matrix and upper triangular matrix from the QRD of $\boldsymbol{H}$. Regardless of the fading distribution of $\boldsymbol{h}_1$, we first show that: 1) The entries of $\boldsymbol{R}$ are independent of each other; 2) $R_{n,n}$, $n = 2, \cdots, N_t$, are such that $2R_{n,n}^2$ are Chi-square distributed with $2(N_r - n + 1)$ degrees of freedom (DoF); and 3) The off-diagonal entries, $R_{m,n}$ for $m < n$, are $\mathcal{N}_c(0, 1)$. To prepare for the proof, we denote a vector $\boldsymbol{h}$ having i.i.d. entries from $\mathcal{N}_c(0, 1)$ as $\boldsymbol{h} \sim \mathcal{N}_c^I(0, 1)$ and establish the following lemma.

Lemma 4. *Let a random vector $\boldsymbol{x}$ of size $N \times 1$ be $\mathcal{N}_c^I(0, 1)$, and let $\boldsymbol{A}$ be a random unitary matrix on $\mathcal{U}_N$ and independent of $\boldsymbol{x}$, where $\mathcal{U}_N$ is the set of order-N unitary matrices. Then, $\boldsymbol{y} = \boldsymbol{A}\boldsymbol{x}$ is $\mathcal{N}_c^I(0, 1)$, and $\boldsymbol{y}$ is independent of $\boldsymbol{A}$.*

Proof: See Appendix C.2. ■

The proof of Lemma 4 is similar to the proof of Lemma 3.1 in [125], except that the former addresses the complex case. Now we consider QRD with Householder transform (HT) [126]. From the first column $\boldsymbol{h}_1$ of $\boldsymbol{H}$, we derive an HT matrix $\boldsymbol{A}_1$ so that $\boldsymbol{A}_1\boldsymbol{h}_1 = r_{11}\boldsymbol{e}_1$, where $\boldsymbol{A}_1$ only depends on $\boldsymbol{h}_1/\|\boldsymbol{h}_1\|$, $\boldsymbol{e}_1 = [1, 0, \cdots, 0]^T$, and $r_{11}^2 = \|\boldsymbol{h}_1\|^2$. Then,

$$\boldsymbol{A}_1\boldsymbol{H} = [\boldsymbol{A}_1\boldsymbol{h}_1, \cdots, \boldsymbol{A}_1\boldsymbol{h}_{N_t}] = \begin{bmatrix} r_{11} & r_{12} & \cdots & r_{1N_t} \\ 0 & \boldsymbol{h}_2^{(2)} & \cdots & \boldsymbol{h}_{N_t}^{(2)} \end{bmatrix}. \tag{C.1}$$

Since $\boldsymbol{h}_1$ has i.i.d. entries, $\boldsymbol{A}_1$ and r_{11} are independent. According to Lemma 4, the column

vectors

$$\begin{bmatrix} r_{1n} \\ \boldsymbol{h}_n^{(2)} \end{bmatrix} = \boldsymbol{A}_1 \boldsymbol{h}_n, n = 2, \cdots, N_t, \tag{C.2}$$

are independent of r_{11} and each other, and are $\mathcal{N}_c^I(0,1)$. Thus, $[r_{12}, \cdots, r_{1N_t}]$ and $\boldsymbol{H}_2 = [\boldsymbol{h}_2^{(2)}, \cdots, \boldsymbol{h}_{N_t}^{(2)}]$ are independent of each other, and are $\mathcal{N}_c^I(0,1)$. Continuing the reduction with $\boldsymbol{H}_2$ leads to an array of unitary matrices $\boldsymbol{A}_1, \cdots, \boldsymbol{A}_{N_t-1}$ so that $\boldsymbol{A}_{N_t-1} \cdots \boldsymbol{A}_1 \boldsymbol{H} = \boldsymbol{R}$, where $\boldsymbol{R}$ is an upper triangular matrix. By previous reasoning, the entries of $\boldsymbol{R}$ are independent of each other and satisfy condition iii). Also, during the n-th reduction ($n \geq 2$), since $\boldsymbol{h}_n^{(n)} \sim \mathcal{N}_c^I(0,1)$, $2r_{nn}^2$ is Chi-square distributed with $2(N_r - n + 1)$ DoF. Thus, condition ii) is met.

Given conditions 1) to 3), we know $2\sum_{m=1}^{n-1} |R_{m,n}|^2$ is Chi-square distributed with $2(n-1)$ DoF. We also know that a Chi-square distributed RV with $2k$ DoF is a Gamma RV with parameters $(k, 2)$. Therefore, by [127, p. 188], $R_{n,n}^2/(R_{n,n}^2 + \sum_{m=1}^{n-1} |R_{m,n}|^2) \sim \mathcal{B}\boldsymbol{e}(N_r - n + 1, n - 1)$, where $\mathcal{B}\boldsymbol{e}(a,b)$ means Beta distribution with parameters (a,b). Since $1 - od = \prod_{n=2}^{N_t} \left(R_{n,n}^2/(R_{n,n}^2 + \sum_{m=1}^{n-1} |R_{m,n}|^2)\right)$, $1 - od$ is a product of $N_t - 1$ independent Beta RV $b_1, \cdots, b_{N_t-1}$, where $b_k \sim \mathcal{B}\boldsymbol{e}(N_r - k, k)$. By [128, Theorem 7] and a change of variable, the pdf of od is then given in Eq. (6.8).

C.2 Proof of Lemma 4

The set of order-N unitary matrices $\mathcal{U}_N$ forms a compact topological group. By [129], there uniquely exists a normalized and left-translation-invariant measure μ given the set $\mathcal{U}_N$. In other words, $\mu(\mathcal{U}_N) = 1$ and $\mu(\boldsymbol{A}\mathcal{U}_N^*) = \mu(\mathcal{U}_N^*)$, where $\mathcal{U}_N^*$ is any measurable subset of $\mathcal{U}_N$ and $\boldsymbol{A}$ is any element of $\mathcal{U}_N$. We assume in the following that all distributions are measurable with the measure μ, and all integrals are computed with the measure μ.

Define $f_1(\boldsymbol{x})$ as the distribution of $\boldsymbol{x}$, $f_2(\boldsymbol{A})$ the distribution of $\boldsymbol{A}$, and $f_3(\boldsymbol{y}, \boldsymbol{A})$ the

joint distribution of $(\boldsymbol{y}, \boldsymbol{A})$. Considering two measurable sets $\mathscr{Y}$ and $\mathscr{A}$, we have

$$\int_{\mathscr{A}} \int_{\mathscr{Y}} f_3(\boldsymbol{y}, \boldsymbol{A})\, d\boldsymbol{y}\, d\boldsymbol{A} = \text{Prob}\left((\boldsymbol{y}, \boldsymbol{A}) \in \mathscr{Y} \times \mathscr{A}\right), \tag{C.3}$$

where $\text{Prob}(\cdot)$ denotes the probability of random events. For a fixed $\boldsymbol{A}$, we have

$$\begin{aligned} \text{Prob}(\boldsymbol{y} \in \mathscr{Y}|\boldsymbol{A}) &= \text{Prob}(\boldsymbol{x} \in \boldsymbol{A}^H \mathscr{Y}|\boldsymbol{A}) \\ &\overset{(E1)}{=} \text{Prob}(\boldsymbol{x} \in \mathscr{Y}) = \int_{\mathscr{Y}} f_1(\boldsymbol{x})\, d\boldsymbol{x}, \end{aligned} \tag{C.4}$$

where the equality $(E1)$ is due to the orthogonal invariance of complex Gaussian [91, Appendix A], and the fact that $\boldsymbol{x}$ and $\boldsymbol{A}$ are independent. Thus, $\boldsymbol{y}$ has the same distribution as that of $\boldsymbol{x}$.

Substituting Eq. (C.4) into Eq. (C.3), we have

$$\begin{aligned} \int_{\mathscr{A}} \int_{\mathscr{Y}} f_3(\boldsymbol{y}, \boldsymbol{A})\, d\boldsymbol{y}\, d\boldsymbol{A} &= \int_{\mathscr{A}} f_2(\boldsymbol{A}) \text{Prob}(\boldsymbol{y} \in \mathscr{Y}|\boldsymbol{A})\, d\boldsymbol{A} \\ &= \int_{\mathscr{A}} \int_{\mathscr{Y}} f_2(\boldsymbol{A}) f_1(\boldsymbol{y})\, d\boldsymbol{y}\, d\boldsymbol{A}. \end{aligned} \tag{C.5}$$

Therefore, $f_3(\boldsymbol{y}, \boldsymbol{A}) = f_2(\boldsymbol{A}) f_1(\boldsymbol{y})$ almost everywhere. Thus, $\boldsymbol{y}$ and $\boldsymbol{A}$ are independent.

APPENDIX D

PROOF FOR CHAPTER 7

D.1 Proof of Proposition 5

Let us denote $P(\Psi_d)$ as d, $P(\Psi_u)$ as u. Let us represent $P_{ca}(\Psi_d)$ as $d + \Delta_1(\gamma_{th})$, and $P_{ca}(\Psi_u)$ as $u - \Delta_2(\gamma_{th})$, By the definition of $P_{ca}(\Psi_d)$ and $P_{ca}(\Psi_u)$ in Eqs. (7.13) and (7.15), we have

$$\Delta_1(\gamma_{th}) = \int_0^{\gamma_{th}} (1 - P(\Psi_d|\gamma))p(\gamma)d\gamma, \tag{D.1}$$

$$\Delta_2(\gamma_{th}) = \int_0^{\gamma_{th}} P(\Psi_u|\gamma)p(\gamma)d\gamma. \tag{D.2}$$

We also know that $\Delta_1(\gamma_{th}) \geq \Delta_2(\gamma_{th})$, with equality when $\gamma_{th} = 0$. Thus,

$$\begin{aligned}\mathcal{R} - \mathcal{R}_{ca} = \frac{u(1-d^M)}{1-d} + d^M - \frac{(u - \Delta_2(\gamma_{th}))(1 - (d + \Delta_1(\gamma_{th}))^M)}{1 - (d + \Delta_1(\gamma_{th}))} \\ - (d + \Delta_2(\gamma_{th}))(d + \Delta_1(\gamma_{th}))^{M-1}.\end{aligned} \tag{D.3}$$

When $\gamma_{th} = 0$, $\mathcal{R} - \mathcal{R}_{ca} = 0$. On the other hand,

$$\Delta_1'(\gamma_{th}) = (1 - P(\Psi_d|\gamma_{th}))p(\gamma_{th}), \tag{D.4}$$

$$\Delta_2'(\gamma_{th}) = P(\Psi_u|\gamma_{th})p(\gamma_{th}). \tag{D.5}$$

Thus,

$$\begin{aligned}(\mathcal{R}-\mathcal{R}_{ca})' =&\Delta_2'(\gamma_{th})\left(1+\cdots+(d+\Delta_1(\gamma_{th}))^{M-2}\right)\\ &-(u-\Delta_2(\gamma_{th}))\Delta_1'(\gamma_{th})\left(1+\cdots+(M-2)(d+\Delta_1(\gamma_{th}))^{M-3}\right)\\ &-(u+d)\Delta_1'(\gamma_{th})(M-1)(d+\Delta_1(\gamma_{th}))^{M-2}. \end{aligned} \tag{D.6}$$

When $\gamma_{th}=0$, we have

$$\begin{aligned}(\mathcal{R}-\mathcal{R}_{ca})'_{\gamma_{th}=0} =&p(0)\cdot\left(P(\Psi_u|0)\left(1+\cdots+d^{M-2}\right)\right.\\ &-u(1-P(\Psi_d|0))\left(1+\cdots+(M-2)d^{M-3}\right)\\ &\left.-(u+d)(1-P(\Psi_d|0))(M-1)d^{M-2}\right). \end{aligned} \tag{D.7}$$

Consider a moderate average receive SNR so that $u \ll d$ and $u \ll P(\Psi_u|0)$, we have

$$\begin{aligned}(\mathcal{R}-\mathcal{R}_{ca})'_{\gamma_{th}=0} =& p(0)\cdot\left(P(\Psi_u|0)\left(1+\cdots+d^{M-2}\right)\right.\\ &\left.-(1-P(\Psi_d|0))(M-1)d^{M-1}\right). \end{aligned} \tag{D.8}$$

When L is large,

$$P(\Psi_u|0)+P(\Psi_d|0)=1-P(\text{err}|0)=1, \tag{D.9}$$

thus

$$(\mathcal{R}-\mathcal{R}_{ca})'_{\gamma_{th}=0}=p(0)\cdot P(\Psi_u|0)\sum_{k=1}^{M-1}d^{k-1}(1-d^{M-k})>0. \tag{D.10}$$

Therefore, there exists γ_b so that when $0<\gamma_{th}\leq\gamma_b$, $\mathcal{R}-\mathcal{R}_{ca}>0$.

REFERENCES

[1] J. H. Winters, "On the capacity of radio communication systems with diversity in a Rayleigh fading environment," *IEEE J. Sel. Areas Commun.*, vol. 5, no. 5, pp. 871–878, 1987.

[2] G. J. Foschini and M. J. Gans, "On limits of wireless communications in a fading environment when using multiple antennas," *Wireless personal communications*, vol. 6, no. 3, pp. 311–335, 1998.

[3] E. Telatar, "Capacity of multi-antenna Gaussian channels," *European Transactions on telecommunications*, vol. 10, no. 6, pp. 585–595, 1999.

[4] G. J. Foschini, "Layered space-time architecture for wireless communication in a fading environment when using multi-element antennas," *Bell System Technical Journal*, vol. 1, no. 2, pp. 41–59, 1996.

[5] L. Zheng and D. N. Tse, "Diversity and multiplexing: A fundamental tradeoff in multiple-antenna channels," *IEEE Trans. Inf. Theory*, vol. 49, no. 5, pp. 1073–1096, 2003.

[6] G. B. Giannakis, Z. Liu, X. Ma, and S. Zhou, *Space-time coding for broadband wireless communications*. John Wiley & Sons, 2007.

[7] P. W. Wolniansky, G. J. Foschini, G. Golden, and R. A. Valenzuela, "V-BLAST: An architecture for realizing very high data rates over the rich-scattering wireless channel," in *Proc. IEEE URSI International Symposium on Signals, Systems, and Electronics*, 1998, pp. 295–300.

[8] S. M. Alamouti, "A simple transmit diversity technique for wireless communications," *IEEE J. Sel. Areas Commun.*, vol. 16, no. 8, pp. 1451–1458, 1998.

[9] E. Dahlman, S. Parkvall, and J. Skold, *4G: LTE/LTE-advanced for mobile broadband*, 2nd ed. Academic Press, 2013.

[10] F. Rusek, D. Persson, B. K. Lau, E. G. Larsson, T. L. Marzetta, O. Edfors, and F. Tufvesson, "Scaling up MIMO: Opportunities and challenges with very large arrays," *IEEE Signal Process. Mag.*, vol. 30, no. 1, pp. 40–60, 2013.

[11] E. G. Larsson, O. Edfors, F. Tufvesson, and T. L. Marzetta, "Massive MIMO for next generation wireless systems," *IEEE communications magazine*, vol. 52, no. 2, pp. 186–195, 2014.

[12] A Chockalingam and B. S. Rajan, *Large MIMO systems*. Cambridge University Press, 2014.

[13] K. Nishimori, R. Kudo, N. Honma, Y. Takatori, and M. Mizoguchi, "16x16 multiuser MIMO testbed employing simple adaptive modulation scheme," in *Proc. IEEE VTC*, 2009, pp. 1–5.

[14] T. L. Marzetta, E. G. Larsson, H. Yang, and H. Q. Ngo, *Fundamentals of massive MIMO*. Cambridge University Press, 2016.

[15] S. Malkowsky, J. Vieira, L. Liu, P. Harris, K. Nieman, N. Kundargi, I. C. Wong, F. Tufvesson, V. Öwall, and O. Edfors, "The world's first real-time testbed for massive MIMO: Design, implementation, and validation," *IEEE Access*, vol. 5, pp. 9073–9088, 2017.

[16] E. Viterbo and J. Boutros, "A universal lattice code decoder for fading channels," *IEEE Trans. Inf. Theory*, vol. 45, no. 5, pp. 1639–1642, Jul. 1999.

[17] E. Agrell, T. Eriksson, A. Vardy, and K. Zeger, "Closest point search in lattices," *IEEE Trans. Inf. Theory*, vol. 48, no. 8, pp. 2201–2214, Aug. 2002.

[18] J. Jaldén and B. Ottersten, "On the complexity of sphere decoding in digital communications," *IEEE Trans. Signal Process.*, vol. 53, no. 4, pp. 1474–1484, Apr. 2005.

[19] K.-W. Wong, C.-Y. Tsui, R.-K. Cheng, and W.-H. Mow, "A VLSI architecture of a K-best lattice decoding algorithm for MIMO channels," in *Proc. IEEE ISCAS*, Phoenix-Scottsdale, AZ, Aug. 2002, pp. 273–276.

[20] K. Vishnu Vardhan, S. K. Mohammed, A. Chockalingam, and B. Sundar Rajan, "A low-complexity detector for large MIMO systems and multicarrier CDMA systems," *IEEE J. Sel. Areas Commun.*, vol. 26, no. 3, pp. 473–485, Apr. 2008.

[21] B. Sundar Rajan, S. K. Mohammed, A. Chockalingam, and N. Srinidhi, "Low-complexity near-ML decoding of large non-orthogonal STBCs using reactive tabu search," in *Proc. IEEE ISIT*, Seoul, Korea, Jun. 2009, pp. 1993–1997.

[22] N. Srinidhi, T. Datta, A. Chockalingam, and B. S. Rajan, "Layered tabu search algorithm for large-MIMO detection and a lower bound on ML performance," *IEEE Trans. Commun.*, vol. 59, no. 11, pp. 2955–2963, Jul. 2011.

[23] D. Pham, K. R. Pattipati, P. K. Willett, and J. Luo, "A generalized probabilistic data association detector for multiple antenna systems," in *Proc. IEEE ICC*, vol. 6, 2004, pp. 3519–3522.

[24] P. Som, T. Datta, N Srinidhi, A. Chockalingam, and B. S. Rajan, "Low-complexity detection in large-dimension MIMO-ISI channels using graphical models," *IEEE J. Sel. Topics Signal Process.*, vol. 5, no. 8, pp. 1497–1511, 2011.

[25] A. Kumar, S. Chandrasekaran, A. Chockalingam, and B. S. Rajan, "Near-optimal large-MIMO detection using randomized MCMC and randomized search algorithms," in *Proc. IEEE ICC*, 2011, pp. 1–5.

[26] T. Datta, N. A. Kumar, A Chockalingam, and B. S. Rajan, "A novel Monte Carlo sampling based receiver for large-scale uplink multiuser MIMO systems," *IEEE Trans. Veh. Technol.*, vol. 7, no. 62, pp. 3019–3038, 2013.

[27] W. Ma, C. Su, J. Jalden, T. Chang, and C. Chi, "The equivalence of semidefinite relaxation MIMO detectors for higher-order QAM," *IEEE J. Sel. Topics Signal Process.*, vol. 3, no. 6, pp. 1038–1052, Dec. 2009.

[28] M. Seysen, "Simultaneous reduction of a lattice basis and its reciprocal basis," *Combinatorica*, vol. 13, no. 3, pp. 363–376, Sep. 1993.

[29] D. Seethaler, G. Matz, and F. Hlawatsch, "Low-complexity MIMO data detection using Seysen's lattice reduction algorithm," in *Proc. IEEE ICASSP*, Honolulu, HI, Apr. 2007, pp. 53–56.

[30] A. K. Lenstra, H. W. Lenstra, and L. Lovász, "Factoring polynomials with rational coefficients," *Mathematische Annalen*, vol. 261, no. 4, pp. 515–534, 1982.

[31] H. Yao and G. W. Wornell, "Lattice-reduction-aided detectors for MIMO communication systems," in *Proc. IEEE GLOBECOM*, Taipei, Taiwan, Nov. 2002, pp. 424–428.

[32] M. Taherzadeh, A. Mobasher, and A. Khandani, "LLL reduction achieves the receive diversity in MIMO decoding," *IEEE Trans. Inf. Theory*, vol. 53, no. 12, pp. 4801–4805, Dec. 2007.

[33] X. Ma and W. Zhang, "Performance analysis for MIMO systems with lattice-reduction aided linear equalization," *IEEE Trans. Commun.*, vol. 56, no. 2, pp. 309–318, Feb. 2008.

[34] Y. H. Gan, C. Ling, and W. H. Mow, "Complex lattice reduction algorithm for low-complexity full-diversity MIMO detection," *IEEE Trans. Signal Process.*, vol. 57, no. 7, pp. 2701–2710, Jul. 2009.

[35] C. Ling and N. Howgrave-Graham, "Effective LLL reduction for lattice decoding," in *Proc. IEEE ISIT*, 2007, pp. 196–200.

[36] J. Jaldén, D. Seethaler, and G. Matz, "Worst- and average-case complexity of LLL lattice reduction in MIMO wireless systems," in *Proc. IEEE ICASSP*, Las Vegas, Nevada, Mar. 2008, pp. 2685–2688.

[37] A. Burg, D. Seethaler, and G. Matz, "VLSI implementation of a lattice-reduction algorithm for multi-antenna broadcast precoding," in *Proc. IEEE ISCAS*, 2007, pp. 673–676.

[38] B. Gestner, W. Zhang, X. Ma, and D. V. Anderson, "VLSI implementation of a lattice reduction algorithm for low-complexity equalization," in *Proc. IEEE ICCSC*, 2008, pp. 643–647.

[39] Q. Zhou and X. Ma, "Hardware realizable lattice-reduction-aided detectors for large-scale MIMO systems," in *Proc. EUSIPCO*, 2014, pp. 91–95.

[40] Q. Wen and X. Ma, "Efficient greedy LLL algorithms for lattice decoding," *IEEE Trans. Wireless Commun.*, vol. 15, no. 5, pp. 3560–3572, May 2016.

[41] Q. Wen, Q. Zhou, and X. Ma, "An enhanced fixed-complexity LLL algorithm for MIMO detection," in *Proc. IEEE GLOBECOM*, 2014, pp. 3231–3236.

[42] Q. Wen and X. Ma, "VLSI implementation of incremental fixed-complexity LLL lattice reduction for MIMO detection," in *Proc. IEEE ISCAS*, 2016, pp. 1898–1901.

[43] Q. Zhou and X. Ma, "Element-based lattice reduction algorithms for large MIMO detection," *IEEE J. Sel. Areas Commun.*, vol. 31, no. 2, pp. 274–286, Feb. 2013.

[44] C.-J. Chen and L.-C. Wang, "On the performance of the zero-forcing receiver operating in the multiuser MIMO system with reduced noise enhancement effect," in *Proc. IEEE GLOBECOM*, St. Louis, MO, Nov. 2005, pp. 1294–1298.

[45] X. Ma and W. Zhang, "Fundamental limits of linear equalizers: Diversity, capacity, and complexity," *IEEE Trans. Inf. Theory*, vol. 54, no. 8, pp. 3442–3456, Aug. 2008.

[46] L. Zhao and V. K. Dubey, "Detection schemes for space-time block code and spatial multiplexing combined system," *IEEE Commun. Lett.*, vol. 9, no. 1, pp. 49–51, 2005.

[47] Y. Wu and C. Tellambura, "Low-complexity optimal detection for hybrid space-time block coding and spatial multiplexing," in *Proc. IEEE VTC*, 2006, pp. 1–4.

[48] X. N. Tran, H. C. Ho, T. Fujino, and Y. Karasawa, "Performance comparison of detection methods for combined STBC and SM systems," *IEICE Trans. Commun.*, vol. 91, no. 6, pp. 1734–1742, 2008.

[49] F. Riera-Palou and G. Femenias, "Improved linear group detection for combined spatial multiplexing/STBC systems," *IEEE Trans. Commun.*, vol. 57, no. 11, pp. 3252–3257, 2009.

[50] C.-h. An, T. Lee, J. Yang, and D. K. Kim, "Low complexity lattice reduction scheme for STBC two-user uplink MIMO systems," *EURASIP Journal on Wireless Communications and Networking*, vol. 1, no. 2011, pp. 1–10, 2011.

[51] G. Caire and S. Shamai, "On the achievable throughput of a multiantenna Gaussian broadcast channel," *IEEE Trans. Inf. Theory*, vol. 49, no. 7, pp. 1691–1706, Jul. 2003.

[52] K. Zu, R. C. De Lamare, and M. Haardt, "Multi-branch Tomlinson-Harashima precoding design for MU-MIMO systems: Theory and algorithms," *IEEE Trans. Commun.*, vol. 62, no. 3, pp. 939–951, 2014.

[53] B. Hochwald, C. Peel, and A. Swindlehurst, "A vector-perturbation technique for near-capacity multiantenna multiuser communication-part II: perturbation," *IEEE Trans. Commun.*, vol. 53, no. 3, pp. 537–544, 2005.

[54] C. Masouros, M. Sellathurai, and T. Ratnarajah, "Computationally efficient vector perturbation precoding using thresholded optimization," *IEEE Trans. Commun.*, vol. 61, no. 5, pp. 1880–1890, 2013.

[55] A. Tenenbaum and R. Adve, "Joint multiuser transmit-receive optimization using linear processing," in *Proc. IEEE ICC*, Paris, France, Jun. 2004, pp. 588–592.

[56] J. Zhang, Y. Wu, S. Zhou, and J. Wang, "Joint linear transmitter and receiver design for the downlink of multiuser MIMO systems," *IEEE Commun. Lett.*, vol. 9, no. 11, pp. 991–993, 2005.

[57] J. Joung and Y. H. Lee, "Regularized channel diagonalization for multiuser MIMO downlink using a modified MMSE criterion," *IEEE Trans. Signal Process.*, vol. 55, no. 4, pp. 1573–1579, 2007.

[58] H. Shen, B. Li, M. Tao, and X. Wang, "MSE-based transceiver designs for the MIMO interference channel," *IEEE Trans. Wireless Commun.*, vol. 9, no. 11, pp. 3480–3489, Nov. 2010.

[59] L.-U. Choi and R. Murch, "A transmit preprocessing technique for multiuser MIMO systems using a decomposition approach," *IEEE Trans. Wireless Commun.*, vol. 3, no. 1, pp. 20–24, Jan. 2004.

[60] Q. Spencer and M. Haardt, "Capacity and downlink transmission algorithms for a multi-user MIMO channel," in *Proc. 36th Asilomar Conf. Signals, Syst., Comput.*, Asilomar, CA, Nov. 2002, pp. 1384–1388.

[61] Q. Spencer, A. Swindlehurst, and M. Haardt, "Zero-forcing methods for downlink spatial multiplexing in multiuser MIMO channels," *IEEE Trans. Signal Process.*, vol. 52, no. 2, pp. 461–471, Feb. 2004.

[62] V. Stankovic and M. Haardt, "Multi-user MIMO downlink precoding for users with multiple antennas," in *Proc. WWRF*, Toronto, ON, Canada, Nov. 2004, pp. 12–14.

[63] ——, "Generalized design of multi-user MIMO precoding matrices," *IEEE Trans. Wireless Commun.*, vol. 7, no. 3, pp. 953–961, Mar. 2008.

[64] H. Sung, S.-R. Lee, and I. Lee, "Generalized channel inversion methods for multiuser MIMO systems," *IEEE Trans. Wireless Commun.*, vol. 57, no. 11, pp. 3489–3499, Nov. 2009.

[65] Q. Zhou and X. Ma, "Joint transceiver designs using lattice reduction algorithms," in *Proc. IEEE ChinaSIP*, Beijing, China, Jul. 2013, pp. 584–588.

[66] A. Bourdoux and N. Khaled, "Joint TX-RX optimisation for MIMO-SDMA based on a null-space constraint," in *Proc. IEEE VTC*, Vancouver, BC, Canada, Sep. 2002, pp. 171–174.

[67] K. Zu, R. C. de Lamare, and M. Haardt, "Generalized design of low-complexity block diagonalization type precoding algorithms for multiuser MIMO systems," *IEEE Trans. Commun.*, vol. 61, no. 10, pp. 4232–4242, 2013.

[68] X. Wang, X. Wang, and Y. Qi, "Low-complexity transceiver design for MIMO broadcast systems," *IEEE Commun. Lett.*, vol. 18, no. 9, pp. 1661–1664, 2014.

[69] T. O'Shea and J. Hoydis, "An introduction to deep learning for the physical layer," *IEEE Trans. on Cogn. Commun. Netw.*, vol. 3, no. 4, pp. 563–575, 2017.

[70] H. Ye, G. Y. Li, and B.-H. Juang, "Power of deep learning for channel estimation and signal detection in OFDM systems," *IEEE Wireless Commun. Lett.*, 2017.

[71] T. J. O'Shea, T. Erpek, and T. C. Clancy, "Deep learning based MIMO communications," *arxiv preprint:1707.07980*, 2017.

[72] N. Samuel, T. Diskin, and A. Wiesel, "Deep MIMO detection," *arxiv preprint: 1706.01151*, 2017.

[73] M. Imanishi, S. Takabe, and T. Wadayama, "Deep learning-aided iterative detector for massive overloaded MIMO channels," *arxiv preprint:1806.10827*, 2018.

[74] X. Tan, W. Xu, Y. Be'ery, Z. Zhang, X. You, and C. Zhang, "Improving massive MIMO belief propagation detector with deep neural network," *arxiv preprint:1804.01002*, 2018.

[75] H. Sun, Z. Zhao, X. Fu, and M. Hong, "Limited feedback double directional massive MIMO channel estimation: From low-rank modeling to deep learning," in *Proc. IEEE SPAWC*, 2018, pp. 1–5.

[76] H. He, C.-K. Wen, S. Jin, and G. Y. Li, "Deep learning-based channel estimation for beamspace mmWave massive MIMO systems," *arxiv preprint:1802.01290*, 2018.

[77] S. Yun and C. Caramanis, "Reinforcement learning for link adaptation in MIMO-OFDM wireless systems," in *Proc. IEEE GLOBECOM*, 2010, pp. 1–5.

[78] C. Wang, Z. Wang, W. Sun, and D. R. Fuhrmann, "Reinforcement learning-based adaptive transmission in time-varying underwater acoustic channels," *IEEE Access*, vol. 6, pp. 2541–2558, 2018.

[79] G. Durisi, T. Koch, and P. Popovski, "Toward massive, ultrareliable, and low-latency wireless communication with short packets," *Proceedings of the IEEE*, vol. 104, no. 9, pp. 1711–1726, Sep. 2016.

[80] H. Chen, R. Abbas, P. Cheng, M. Shirvanimoghaddam, W. Hardjawana, W. Bao, Y. Li, and B. Vucetic, "Ultra-reliable low latency cellular networks: Use cases, challenges and approaches," *IEEE Commun. Mag.*, vol. 56, no. 12, pp. 119–125, Dec. 2018.

[81] S. Lin and P. S. Yu, "A hybrid ARQ scheme with parity retransmission for error control of satellite channels," *IEEE Trans. Commun.*, vol. 30, no. 7, pp. 1701–1719, Jul. 1982.

[82] T. Kasami, T. Fujiwara, and S. Lin, "A concatenated coding scheme for error control," *IEEE Trans. Commun.*, vol. 34, no. 5, pp. 481–488, May 1986.

[83] A. Anand and G. de Veciana, "Resource allocation and HARQ optimization for URLLC traffic in 5G wireless networks," *IEEE J. Sel. Areas Commun.*, vol. 36, no. 11, pp. 2411–2421, Nov. 2018.

[84] E. Dosti, U. L. Wijewardhana, H. Alves, and M. Latva-aho, "Ultra reliable communication via optimum power allocation for Type-I ARQ in finite block-length," in *Proc. IEEE ICC*, Paris, France, May 2017, pp. 1–6.

[85] G. Berardinelli, S. R. Khosravirad, K. I. Pedersen, F. Frederiksen, and P. Mogensen, "Enabling early HARQ feedback in 5G networks," in *Proc. IEEE VTC (Spring)*, May 2016, pp. 1–5.

[86] B. Makki, T. Svensson, G. Caire, and M. Zorzi, "Fast HARQ over finite blocklength codes: A technique for low-latency reliable communication," *IEEE Trans. Wireless Commun.*, vol. 18, no. 1, pp. 194–209, Jan. 2019.

[87] E. G. Larsson, "MIMO detection methods: How they work [lecture notes]," *IEEE Signal Process. Mag.*, vol. 26, no. 3, pp. 91–95, May 2009.

[88] W. Zhang, G. Choi, and X. Ma, "Designing zero-forcing based MIMO relay networks with channel-controlled ARQ to achieve full diversity," in *Proc. IEEE Military Communications Conference*, Oct. 2010, pp. 363–368.

[89] Z. Wang and G. B. Giannakis, "Wireless multicarrier communications," *IEEE Signal Process. Mag.*, vol. 17, no. 3, pp. 29–48, May 2000.

[90] Z. Wang, X. Ma, and G. Giannakis, "OFDM or single-carrier block transmissions?" *IEEE Trans. Commun.*, vol. 52, no. 3, pp. 380–394, Mar. 2004.

[91] D. Tse and V. P., *Fundamentals of wireless communication*. Cambridge University Press, 2005.

[92] D. A. Gore, R. W. Heath Jr, and A. J. Paulraj, "Transmit selection in spatial multiplexing systems," *IEEE Commun. Lett.*, vol. 6, no. 11, pp. 491–493, 2002.

[93] Z. Wang and G. B. Giannakis, "Linearly precoded or coded OFDM against wireless channel fades?" In *Proc. IEEE Third Workshop on Signal Processing Advances in Wireless Communications*, 2001, pp. 267–270.

[94] J. G. Proakis, *Digital communications*, 5th ed. New York: McGraw-Hill, Inc., 2008.

[95] C. Gauss, *Untersuchungen über höhere arithmetik (german transl. of disquisitiones arithmeticae, h. maser)*, 1889.

[96] C. Ling, "Approximate lattice decoding: Primal versus dual basis reduction," in *Proc. IEEE ISIT*, Seattle, WA, Jul. 2006, pp. 1–5.

[97] B. LaMacchia, "Basis reduction algorithms and subset sum problems," Master's thesis, MIT, 1991.

[98] Y. Kong, X. Ma, and Y. Wang, "Applying lattice reduction technique to space-time coded multiplexing systems," in *Proc. ICNC*, Mar. 2018, pp. 275–279.

[99] Y. Kong, Q. Zhou, and X. Ma, "Lattice reduction aided transceiver design for multiuser MIMO downlink transmissions," in *Proc. IEEE MILCOM*, Oct. 2014, pp. 556–562.

[100] Y. Kong and X. Ma, "Lattice reduction techniques in MIMO systems with correlated channels," in *Proc. IEEE MILCOM*, Baltimore, MD, Oct. 2014, pp. 575–580.

[101] X. Ma and Y. Kong, "Capacity analysis of lattice reduction aided equalizers for MIMO systems," in *Proc. IEEE MILCOM*, Oct. 2015, pp. 866–871.

[102] D.-S. Shiu, G. J. Foschini, M. J. Gans, and J. M. Kahn, "Fading correlation and its effect on the capacity of multielement antenna systems," *IEEE Trans. Commun.*, vol. 48, no. 3, pp. 502–513, 2000.

[103] *IEEE P802.11 wireless LANs: TGn channel models*, May 2004.

[104] T.-H. Kim, "Low-complexity sorted QR decomposition for MIMO systems based on pairwise column symmetrization," *IEEE Trans. Wireless Commun.*, vol. 13, no. 3, pp. 1388–1396, 2014.

[105] G. H. Golub and C. F. Van Loan, *Matrix computations*, 3rd ed. The Johns Hopkins University Press, 1989.

[106] H. Sampath, P. Stoica, and A. Paulraj, "Generalized linear precoder and decoder design for MIMO channels using the weighted MMSE criterion," *IEEE Trans. Commun.*, vol. 49, no. 12, pp. 2198–2206, Dec. 2001.

[107] D. Wübben, R. Böhnke, V. Kühn, and K. D. Kammeyer, "Near-maximum-likelihood detection of MIMO systems using MMSE-based lattice reduction," in *Proc. IEEE ICC*, Paris, France, Jun. 2004, pp. 798–802.

[108] D. Silver, A. Huang, C. J. Maddison, A. Guez, L. Sifre, G. Van Den Driessche, J. Schrittwieser, I. Antonoglou, V. Panneershelvam, M. Lanctot, *et al.*, "Mastering the game of go with deep neural networks and tree search," *nature*, vol. 529, no. 7587, pp. 484–489, 2016.

[109] W. Li, F. Zhou, W. Meleis, and K. Chowdhury, "Learning-based and data-driven TCP design for memory-constrained iot," in *Proc. International Conference on Distributed Computing in Sensor Systems*, 2016, pp. 199–205.

[110] Y. Kong, H. Zang, and X. Ma, "Improving TCP congestion control with machine intelligence," in *Proc. ACM SIGCOMM Workshop on Network Meets AI & ML*, Budapest, Hungary, Aug. 2018.

[111] R. S. Sutton and A. G. Barto, *Reinforcement learning: An introduction*, 1. MIT press Cambridge, 1998, vol. 1.

[112] Y. Kong, X. Ma, and J. Lu, "Orthogonality deficiency of massive MIMO channels: Distribution and relationship with performance," *IEEE Signal Process. Lett.*, accepted.

[113] J.-C. Chen, "A low complexity data detection algorithm for uplink multiuser massive MIMO systems," *IEEE J. Sel. Areas Commun.*, vol. 35, no. 8, pp. 1701–1714, 2017.

[114] L. Dai, X. Gao, X. Su, S. Han, C. I, and Z. Wang, "Low-complexity soft-output signal detection based on Gauss–Seidel method for uplink multiuser large-scale MIMO systems," *IEEE Trans. Veh. Technol.*, vol. 64, no. 10, pp. 4839–4845, Oct. 2015.

[115] M. K. Simon and M.-S. Alouini, *Digital communication over fading channels*. John Wiley & Sons, 2005, vol. 95.

[116] N. C. Sagias and G. K. Karagiannidis, "Gaussian class multivariate Weibull distributions: Theory and applications in fading channels," *IEEE Trans. Inf. Theory*, vol. 51, no. 10, pp. 3608–3619, 2005.

[117] F. Babich and G. Lombardi, "Statistical analysis and characterization of the indoor propagation channel," *IEEE Trans. Commun.*, vol. 48, no. 3, pp. 455–464, 2000.

[118] G. Tzeremes and C. Christodoulou, "Use of Weibull distribution for describing outdoor multipath fading," in *Proc. IEEE APS*, vol. 1, 2002, pp. 232–235.

[119] J Reig, M.-T. Martínez-Inglés, L Rubio, V.-M. Rodrigo-Peñarrocha, and J.-M. Molina-García-Pardo, "Fading evaluation in the 60 GHz band in line-of-sight conditions," *International Journal of Antennas and Propagation*, 2014.

[120] H. Bateman, *Tables of integral transforms [Volumes I]*, 1954.

[121] J. M. Carrasco, S. L. Ferrari, and G. M. Cordeiro, "A new generalized Kumaraswamy distribution," *arxiv preprint:1004.0911*, 2010.

[122] G. Claeskens and N. L. Hjort, "Model selection and model averaging," *Cambridge Books*, 2008.

[123] H. Zheng, A. Lozano, and M. Haleem, "Multiple ARQ processes for MIMO systems," *EURASIP Journal on Applied Signal Processing*, vol. 2004, pp. 772–782, May 2004.

[124] Q. Liu, S. Zhou, and G. B. Giannakis, "Cross-layer combining of adaptive modulation and coding with truncated ARQ over wireless links," *IEEE Trans. Wireless Commun.*, vol. 3, no. 5, pp. 1746–1755, Sep. 2004.

[125] G. W. Stewart, "The efficient generation of random orthogonal matrices with an application to condition estimators," *SIAM Journal on Numerical Analysis*, vol. 17, no. 3, pp. 403–409, 1980.

[126] K.-L. Chung and W.-M. Yan, "The complex Householder transform," *IEEE Trans. Signal Process.*, vol. 45, no. 9, pp. 2374–2376, 1997.

[127] A Papoulis and U. Pillai, *Probability, random variables and stochastic processes*. McGraw-Hill, 2001.

[128] M. Springer and W. Thompson, "The distribution of products of Beta, Gamma and Gaussian random variables," *SIAM Journal on Applied Mathematics*, vol. 18, no. 4, pp. 721–737, 1970.

[129] P. R. Halmos, *Measure theory*. Springer, 2013, vol. 18.

VITA

Yiming Kong received the B.S. degree in Information and Communication Engineering from Zhejiang University, Hangzhou, P.R. China, in 2012, and the M.S. degree in Electrical and Computer Engineering from Georgia Institute of Technology, Atlanta, GA, in 2014. From Jan. 2016 to Dec. 2016, She was a research intern with FutureWei Technologies, Inc. at Santa Clara, CA. In summer 2017, she was a software intern with Intellipro, Inc. at Santa Clara, CA. She is now working towards the Ph.D. degree in the School of Electrical and Computer Engineering, Georgia Institute of Technology. Her current research interests include machine learning techniques for communication systems and networks, physical- and MAC-layer techniques for reliable low-latency communications, and high-performance receiver designs for large MIMO systems.